UC Berkeley
UC Berkeley Electronic Theses and Dissertations

Title
Structural Studies of the Yeast Dam1 Complex

Permalink
https://escholarship.org/uc/item/91p2374g

Author
Ramey, Vincent Harper

Publication Date
2011

Peer reviewed|Thesis/dissertation

eScholarship.org Powered by the California Digital Library
University of California

Structural Studies of the Yeast Dam1 Complex

By

Vincent Harper Ramey

A dissertation submitted in partial satisfaction of the

requirements for the degree of

Doctor of Philosophy

in

Biophysics

in the

Graduate Division

of the

University of California, Berkeley

Committee in charge:

Professor Eva Nogales, Chair
Professor Robert Glaeser
Professor Rebecca Heald
Professor Daniel Fletcher

Structural Studies of the Yeast Dam1 Complex

© 2011

by

Vincent Harper Ramey

Abstract

Structural Studies of the Yeast Dam1 Complex

by

Vincent Harper Ramey

Doctor of Philosophy in Biophysics

University of California, Berkeley

Professor Eva Nogales, Chair

All eukaryotic cells must equally segregate their chromosomes between two daughter cells each time they divide. This process must be extremely robust, as errors cause catastrophic losses or gains of genetic material. Chromosmes are attached to microtubules through an organelle called the kinetochore. Greek for *movement place*, the kinetochore serves as a platform both for generating the forces required to separate chromatids to opposite poles and a major site of regulation to ensure that all chromosomes are segregated properly. In the budding yeast S. *cerevisiae* a single microtubule attaches to each kinetochore, making this connection extremely precious. In the last decade a complete parts list of the yeast kinetochore, containing approximately 70 proteins arranged into roughly a dozen complexes, has been established. However, very little structural information exists for most of these components, and the mechanism by which the kinetochore remained attached to a dynamic microtubule plus-end. In the past five years the Dam1 complex emerged as an exciting component of the outer kinetochore that forms rings around microtubules and *in vitro* recapitulates much of the functionality of kinetochore-microtubule attachment, including remaining attached to ends and using the energy of the depolymerizing microtubule to do work on a load.

To understand Dam1 at the kinetochore we must know how it binds to microtubules, assembles into rings, and how its assembly is regulated by kinases at the kinetochore. In order to answer these questions I used electron microscopy to image Dam1 in various mutant forms both in the presence and absense of microtubules. Computational techniques allowed me to solve structures of the complex alone and bound to microtubules in three different assemblies. I also mapped 5 of the 10 proteins in the complex onto the structure. Integrating all this information I generated a structural model for Dam1 at the kinetochore that substantially advances our understanding of its function and will direct future experiments in the field.

This work is dedicated to my parents, Marta and Roger, and my brother, Phil. Without the fierce intelligence, curiosity, and imagination that they shared with me throughout my life none of this would have been possible.

Table of Contents

LIST OF ABBREVIATIONS ..... **II**

ACKNOWLEDGEMENTS ..... **III**

INTRODUCTION **1**

Chromosome Segregation During Cell Division 1
Microtubule Binding Proteins in the Kinetochore 1
Microtubule Attachment in budding yeast 4
Microtubule Attachment outside of Fungi 6
The Dam1 Complex *in vitro* 8
Motility and Force Generation 10
Interaction With Ndc80 12
Protein-Protein Interactions Within the Dam1 Complex 12
Rationale and Goals of This Project 15

CHAPTER 1 – ARCHITECTURE AND STRUCTURE OF THE DAM1 COMPLEX **16**

Motivation for Studying Unassembled Structure of the Dam1 Complex 16
Biological Electron Microscopy 16
Ab Initio Single Particle Reconstruction 17
Imaging of Wild-Type Dam1 Complex 18
Reconstruction and Segmentation of Dam1 Dimer 20
Dam1 Forms Rings in the Absence of Microtubules 22
Localization of Dam1 Subunits 24
Integration with Known Complex Interactions 30

CHAPTER 2 – RECONSTRUCTION OF POORLY ORDERED HELICAL SAMPLES AND DEALING WITH SYMMETRY MISMATCH **32**

Introduction to Helical Reconstruction and Dam1 Structure 32
Special Issues in Reconstructing Dam1 Spirals 35
Preprocessing - Removal of Microtubule and Boxing of Single Turns 35
Alignment and Classification Sort Segments Into Homogeneous Groups 38
Estimating Helical Symmetry 43
Real Space Helical Reconstruction of Dam1 46

CHAPTER 3 - STRUCTURE OF DAM1 COMPLEX ASSEMBLED AROUND MICROTUBULES **49**

Motivation 49
Structural Targets 49
Spirals *49*
Single Rings *52*
Stacked Rings *54*
Summary of Reconstructions 56
Docking of Unassembled and Assembled Structures 58
Rings Can Diffuse on Microtubules 62
Spacing of Rings on Microtubules 65
Ring is Insensitive to Microtubule Polarity 68

CONCLUSION AND FUTURE DIRECTIONS **69**

REFERENCES **71**

MATERIALS, METHODS AND PROTOCOLS **80**

List of Abbreviations

GMPCPP	Guanylyl-(alpha, beta)-methylene-diphosphonate
GTP	Guanosine Triphosphate
MT	Microtubule
EM	Electron Microscopy
NMR	Nuclear Magnetic Resonance
E-Hook	Acidic C-terminal tail of tubulin protein
NaCl	Sodium Chloride
MBP	Maltose Binding Protein

Acknowledgements

My time in graduate school has been wonderful and many people have contributed to my growth, both scientifically and personally. While we always strive for objectivity in our work, it's been driven home to me that being a successful scientist, a questioner of the world, requires both. We cannot, and should not, try to remove people from the equation. With that in mind, I would like to start by thanking Eva Nogales for being such a positive force in my life, on all fronts, and an outstanding mentor and friend for the last 6 years and hopefully for many more to come. A great part of my success has been due to her vision, pragmatism, optimism, and most importantly, her intense and infectious curiosity that makes her so good at what she does. I'd also like to thank my thesis committee: Robert Glaeser for his amazing knowledge of electron microscopy and his constant kindness, Dan Fletcher for keeping the elevator full of laughs, and Rebecca Heald for her good questions and empathy during our meetings. With their guidance I kept on track and stayed focused on the most important questions. I especially appreciated our talks about my next step. Your honesty and clear caring for my situation helped me live with the uncertainty the future always holds.

In an environment as intellectually and personally challenging as academic science it matters hugely who shows you the ropes, whether you have a good sounding board for ideas, and if you can tap into a waiting pool of experience when you run into problems. I was extremely lucky to work with the people I did. Thank you both past and present Nogales lab! Two people in particular, Hong-Wei Wang and Andres Leschziner, were foundational to getting me started on the right track. Both gave me invaluable advice and training. It's hard for me to imagine my graduate experience without them. Greg Alushin added immeasurably to my experience in the lab. Between friendship, shared lunchs and coffee, and the fact that his mind is an unstoppable laser, he always supported me in a great way. Two people who could never get enough praise in the lab are Jie Fang and Patricia Grob. Jie worked so hard to help the project with her biochemical experience, even when I sabotaged things. Much, much less would have been accomplished without her efforts. Patricia has been a great friend and always the source of both an insightful answer and a hearty chuckle. The folks in the MacroLab, Scott, Abbey, and Chris made everything possible with their wonderful preps. They are really amazing at what they do. Hugs! I'd like to thank Teresa Tucker for being an ever supportive lab mom. Her friendship, advice, and those peanut M+Ms saved my life more than once. This section wouldn't be complete without giving my heartfelt thanks to Evan Fletcher who gave me my start in research science. His kindness and intelligence gave me a wonderful role model from the beginning.

I'd also like to thank the friends I've had in my life during this journey. Both new and old, they kept life interesting, exciting, fresh, crazy, and reminded me constantly of the world outside of the lab. Through sitting around telling old jokes to traveling together in far flung places and everything in between I've learned and grown and laughed so much. It's been the greatest and I'm hoping it never ends.

Lastly, I'd like to thank my family. They have been an essential source of support and stability through all the changes in my life. I love you!

Introduction

Chromosome Segregation During Cell Division

The accurate segregation of genetic material between daughter cells is an essential step in cell division. Errors in this process lead to aneuploidy and can result in cell transformation (King, 2008). The kinetochore is a network of protein complexes that assembles on centromeric chromatin. It acts as the connection point between chromatids and the microtubules that segregate them into daughter cells (Cheeseman and Desai, 2008; Westermann et al., 2007). Kinetochores can sense that sister chromatids are attached to microtubules from the same spindle pole and can correct such attachments through a mechanism that has been proposed to be mediated by physical tension, in which pulling forces of the spindle puts strain on the centromeric region of chromosomes (Li and Nicklas, 1995; Maresca and Salmon, 2009; Uchida et al., 2009). The stable engagement of a kinetochore is regulated by the Aurora B kinase, the activity of which has been shown to reduce the affinity of several kinetochore proteins for microtubules (Cheeseman et al., 2002; Ruchaud et al., 2007). A single unattached or incorrectly attached kinetochore is sufficient to trigger the spindle assembly checkpoint and halt progress into anaphase, thereby preventing cell division.

An essential function of the kinetochore is to couple chromosome movement to microtubule depolymerization. Once all of the chromosomes in a cell preparing to divide are correctly bi-oriented, they must be pulled apart into daughter cells. After the spindle assembly checkpoint has been satisfied, the anaphase-promoting complex triggers the destruction of the cohesin complexes that tether sister chromatids together (Cheeseman and Desai, 2008; Westermann et al., 2007). Kinetochores are then able to track microtubule ends as they depolymerize and, in a process that does not require motor activity, harness the energy released during microtubule depolymerization to move chromosomes to the two opposite spindle poles (Koshland et al., 1988).

The molecular mechanisms by which chromosomes attach to kinetochores have remained a great mystery since the mitotic process was first visualized using live movies. In budding yeast, where there is a single microtubule attachment per kinetochore, a complete component list of kinetochore proteins has recently been determined.

Microtubule Binding Proteins in the Kinetochore

Each sister chromatid is connected to spindle microtubules via a complex protein machinery called the kinetochore. Robust and correct attachment of kinetochores to microtubules is essential to prevent incorrect chromosome segregation and aneuploidy. This attachment generates the force necessary to pull the entire chromosome into the proper daughter cell (Koshland et al., 1988). However, the spindle microtubule is a dynamic polymer and the mechanism by which a stable connection to its depolymerizing

end could be maintained is unclear. Recently, the heterodecameric Dam1 complex has been shown to be a component of the yeast outer kinetochore and form closed rings around microtubules (Cheeseman et al., 2001a; Miranda et al., 2005; Westermann et al., 2005). Additionally, Dam1 complex follows the depolymerizing ends of microtubules *in vitro* and has the ability to transduce the force released during microtubule depolymerization into carrying cargoes (Asbury et al., 2006; Westermann et al., 2006). Taken together, these observations strongly point to a model in which the ring form of Dam1 complex is used as a topological constraint to "surf" along the depolymerizing end of the microtubule as the protofilaments peel back (Figure 1) (Hill, 1985; Miranda et al., 2005; Westermann et al., 2005). Its attachment to other kinetochore proteins could then stably tether the chromosome to the end of the spindle microtubule.

Kinetochores of sister chromatids frequently attach to microtubules from the same spindle poles, a condition known as syntelic attachment (Westermann et al., 2007). It is thought that this incorrect attachment is sensed through the lack of tension generated by this arrangement and in response Dam1 is phosphorylated by a checkpoint kinase along with several other kinetochore complexes (Kang et al., 2001; Nezi and Musacchio, 2009; Pinsky et al., 2006; Shannon et al., 2002). This signal causes the release of the current microtubule and primes the kinetochore to capture another microtubule. This process is repeated until correct connections are established.

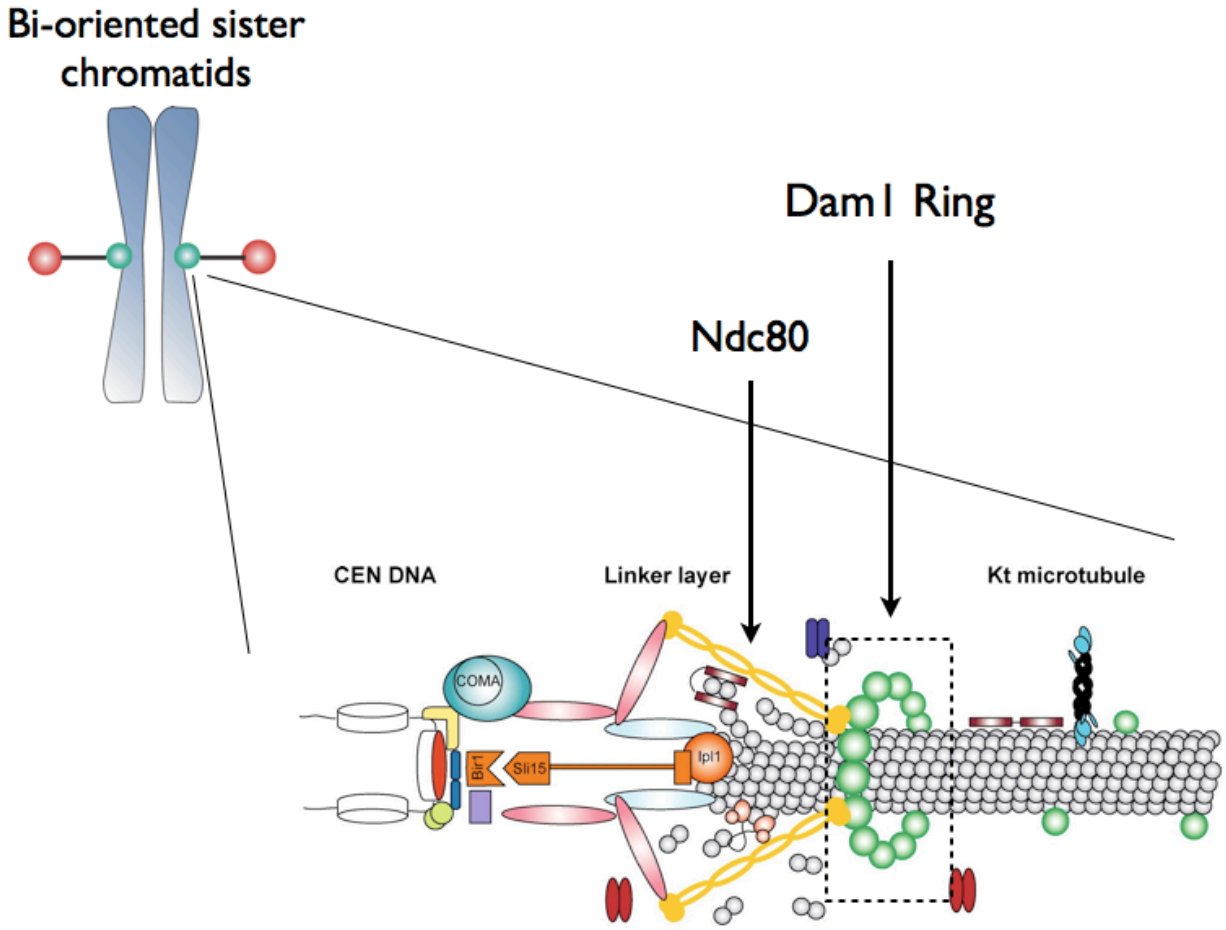

Figure 1 - Model of the budding yeast kinetochore. Protein complexes assemble into a three layered structure. The Dam1 complex works with other microtubule binding proteins, including the Ndc80 complex, to keep the kinetochore attached to the dynamic spindle microtubule plus-end. Figure adapted from Westermann et al. 2007 *Ann Rev Biochem.*

Microtubule Attachment in budding yeast

In budding yeast, where there is a single microtubule attachment per kinetochore, a complete component list of kinetochore proteins has recently been determined (Westermann et al., 2007; Wong et al., 2007). The first report on Dam1 complex subunits and their requirement for a functional mitotic spindle was published over a decade ago. In this report, Drubin, Barnes and coworkers identified Duo1p as a protein that contributed to aspects of spindle function sensed by the spindle assembly checkpoint (Hofmann et al., 1998). Furthermore, a yeast two-hybrid approach was used to identify Dam1p as a Duo1p-interacting protein that was shown to bind directly to microtubules. Soon after these discoveries, Winey and colleagues (Jones et al., 1999) identified the *Dam1* gene in a genetic screen, and showed that the protein it encoded was involved in spindle integrity, and that it localized to spindle microtubules and probably to the kinetochore. Major breakthroughs in the next few years included the characterization of the remaining Dam1-complex components (Cheeseman et al., 2001a; Cheeseman et al., 2001b; Enquist-Newman et al., 2001; Janke et al., 2002) and the identification of the functional interaction between the Dam1 complex and the checkpoint kinase Ipl1 (Cheeseman et al., 2002; Jung-seog Kang, 2001; Shang et al., 2003).

These initial genetic and biochemical studies showed that the ten-subunit Dam1 complex (Fig 2) was essential for regulated microtubule-kinetochore attachment. However, only in the last five years has a structural and biophysical description of the interaction between the Dam1 complex and microtubules become available. The expression of the ten Dam1 complex subunits in bacteria by the Harrison lab (Miranda et al., 2005) made it possible to purify a functional, recombinant full complex and therefore to explore the structural bases for the interaction of the complex with microtubules. The first electron microscopy (EM) studies of the complex proved to be illuminating and exciting, as they showed the microtubule-induced assembly of Dam1 complexes into rings and spirals (Miranda et al., 2005; Westermann et al., 2005). A ring was thought to be an ideal structure to allow coupling of the energy released during microtubule depolymerization, when GDP-tubulin relaxes into its low energy state by protofilament peeling. Although these data and the concepts they inspired have captivated the minds of both structural and cell biologists (Salmon, 2005), the molecular mechanism behind Dam1 complex function remains highly controversial. The character of the interaction between the Dam1 complex and tubulin is under discussion, as is whether ring formation is required for the tracking and functionality of the complex. Finally, although rings have yet to be visualized in vivo, and the Dam1 complex initially appeared to be unique to fungi, a potential alternative complex with similar properties has recently been proposed for metazoans.

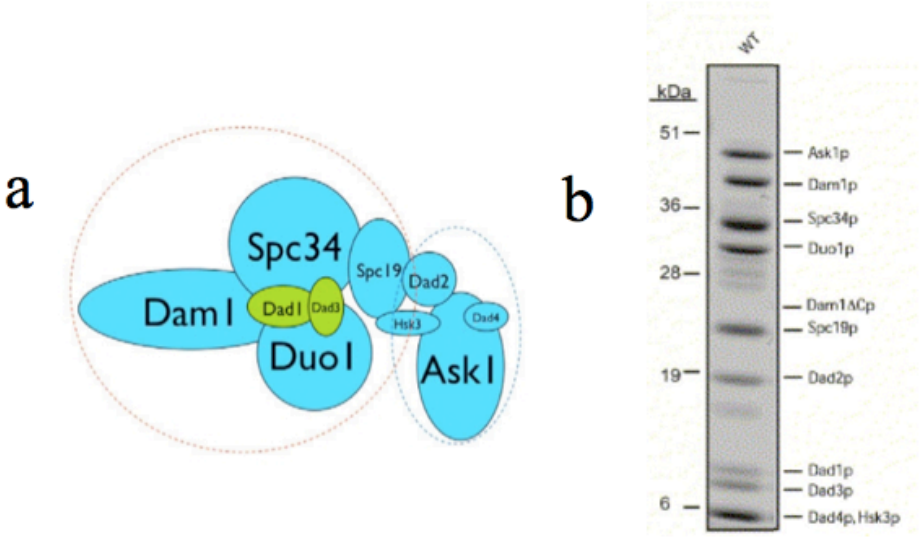

Figure 2 - The Dam1 complex is a heterodecamer. a) Model of protein-protein interactions within the complex based on published data in the uniprot database (http://www.uniprot.org/) and Miranda et al. 2007. b) The complex can be expressed and purified through a 6xHis tag on the Hsk3p subunit, followed by gel filtration. This results in a 210 kDa complex which appears to contain one copy each of 10 proteins.

Microtubule Attachment outside of Fungi

Unlike most other outer kinetochore components, which are conserved across the tree of life, the Dam1 complex is unique to Fungi. The Dam1-complex ring could be the perfect coupler in budding yeast cells, in which the attachment of a single microtubule per kinetochore requires constant molecular engagement at the microtubule end to avoid kinetochore release. In systems where more than one microtubule engages each chromatid, one or more microtubules might disengage without release, the requirements for each microtubule-kinetochore interaction might be less stringent and allow a different, non-encircling attachment (Fig 3) (Joglekar et al., 2010). The number of budding yeast Dam1 complexes per kinetochore is compatible with the size of the ring observed in vitro, but fission yeast appears to express the Dam1 complex at a lower copy number per kinetochore, which is insufficient for ring closure. Interestingly, the Dam1 complex is not essential in fission yeast (Sanchez-Perez et al., 2005).

Conversely, the NDC80 complex is another crucial site of kinetochore-microtubule attachment in yeast that appears to be conserved and is essential in all eukaryotes. This four-protein complex has a long coiled-coil with globular domains at each end for microtubule and kinetochore binding, respectively. Importantly, it has recently been shown that NDC80 is a member of a conserved network of protein complexes known as the KMN network (Cheeseman et al., 2006) that also includes the KNL-1 protein, which is reported to have microtubule-binding activity of its own, and the MIS12 complex, which appears to acts as a coordination hub that tethers the network to the inner kinetochore. Recently, an electron tomography study of PtK_1 cells suggests that there are fibrils associated with the inside surface of microtubule ends at the site of kinetochore attachment (McIntosh et al., 2008). The authors suggested that these filamentous proteins could couple shortening microtubules to cargo movement and, furthermore, that they could be NDC80 complexes. In support of this idea, in vitro studies have shown that this complex can track microtubule ends (McIntosh et al., 2008; Powers et al., 2009). However there is no direct evidence for whether these filaments form part of the KMN complex or whether they correspond to a yet-unidentified component of the kinetochore.

A newly identified molecular player is the Ska1 complex (Gaitanos et al., 2009; Hanisch et al., 2006). This three-protein kinetochore complex is present in all eukaryotes except yeast, and therefore in all species that lack the Dam1 complex. Interestingly, the Ska1 complex appears to share a number of properties with the Dam1 complex, such as its direct binding to microtubules via the Ska1 protein, and its microtubule-induced oligomerization (Welburn et al., 2009). It is currently difficult to judge whether the mechanistic details of the attachment of the Ska1 and Dam1 complexes to spindle microtubules will define them as functional homologs.

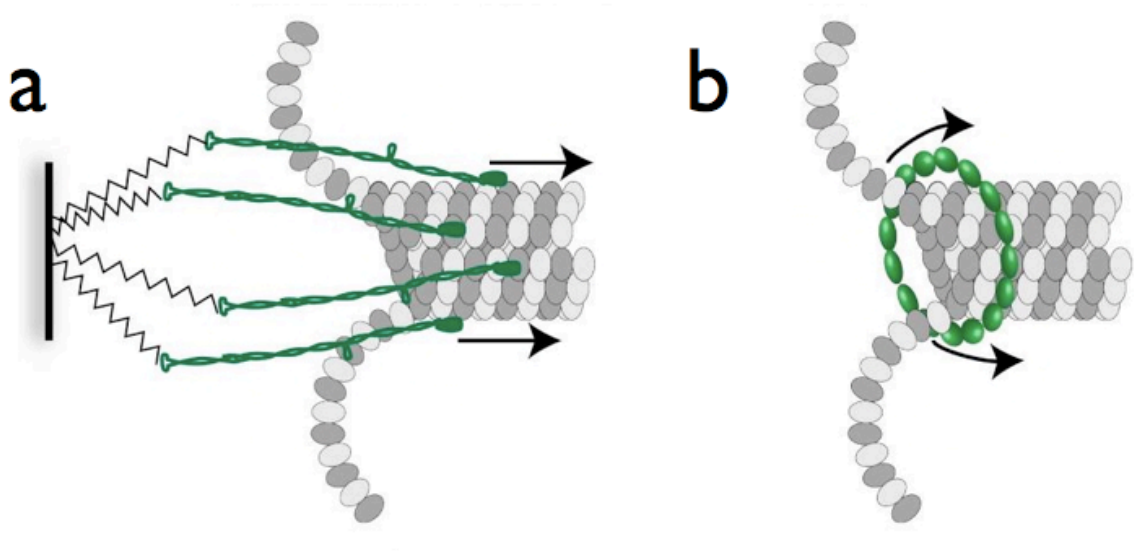

Figure 3 - Models of attachment at the microtubule plus-end. a) Biased diffusion of many, independent attachments, such as the multiple Ndc80 molecules at the kinetchore, would keep a kinetochore attached to a dynamic microtubule. b) An encircling coupler could either harness the force released by peeling protofilaments or follow a biased diffusion walk to maintain attachment.

Adapted from Joglekar et al. 2010

The Dam1 Complex *in vitro*

In vitro reconstitution of the ten-protein Dam1 complex made it possible to carry out electron microscopy (EM) studies of the complex bound to microtubules, which revealed an assembly of rings and spirals interacting in a novel manner with the underlying tubulin (Fig 4) (Miranda et al., 2005; Westermann et al., 2005). Fourier analysis of images of microtubules covered with double spirals showed that the axial repeats of tubulin and Dam1 complex subunits are different from one another (Westermann et al., 2005), and end-on views suggested that thirteen-protofilament microtubules are surrounded by sixteen repeats of the Dam1 complex oligomerized into a ring (Westermann et al., 2006). Furthermore, initial analysis of frozen hydrated samples by cryo-EM showed that the mass of the Dam1 complex is positioned approximately 20 Å away from the ordered microtubule lattice that underlies it (Westermann et al., 2005). This hinted at the possibility that the ring-microtubule interaction is mediated by the C-terminal tails of a- and/or b-tubulin – these unstructured and highly extended segments of about 15 amino acids are also known as E-hooks due to their abundance of glutamic acids. This C-terminal region of each tubulin molecule can be selectively cleaved by the serine protease subtilisin. In the original experiments by Westerman et al., subtilisin cleavage of tubulin abrogated the binding of the Dam1 complex, supporting the idea that the C-terminal regions of tubulin molecules were involved in the ring-microtubule interaction (Westermann et al., 2005). In contrast, however, a later study by Harrison and coworkers reported a negligible effect of subtilisin cleavage on binding of the Dam1 complex to microtubules or on ring formation(Miranda et al., 2007). The disparity of results concerning the effect of subtilisin may have been caused by the different experimental conditions – in particular, the relative ratios of Dam1 complex to tubulin. At concentrations of Dam1 complex that saturate the lattice of native microtubules, little or no Dam1 is observed to bind to subtilisin-cleaved microtubules. Only when Dam1 complex is present in excess, at levels that cause it to accumulate in solution, do the subtilisin-cleaved microtubules become significantly bound by with Dam1 complex rings (Ramey et al., 2011). This result suggests that the C-terminal tails of tubulin are relevant for Dam1 complex interaction under physiological conditions.

Proteolysis experiments carried out by Miranda et al. (Miranda et al., 2007) showed that the treatment of the Dam1 complex with elastase, which causes cleavage of the complex components Ask1p, Dam1p and Duo1p, abrogates the capacity of the complex to bind to microtubules. Interestingly, the outcome of elastase treatment is the same when the Dam1 complex is in the assembled ring form around microtubules during treatment. The fact that the cleavage sites are accessible in this assembled form supports the notion that there is a loose interaction between the oligomeric ring and the microtubule. The alternative possibility is that individual Dam1 complexes have a short dwell time within a dynamic ring assembly; however, this idea conflicts with experimental results showing that there is no turnover once the ring is formed (Westermann et al., 2006).

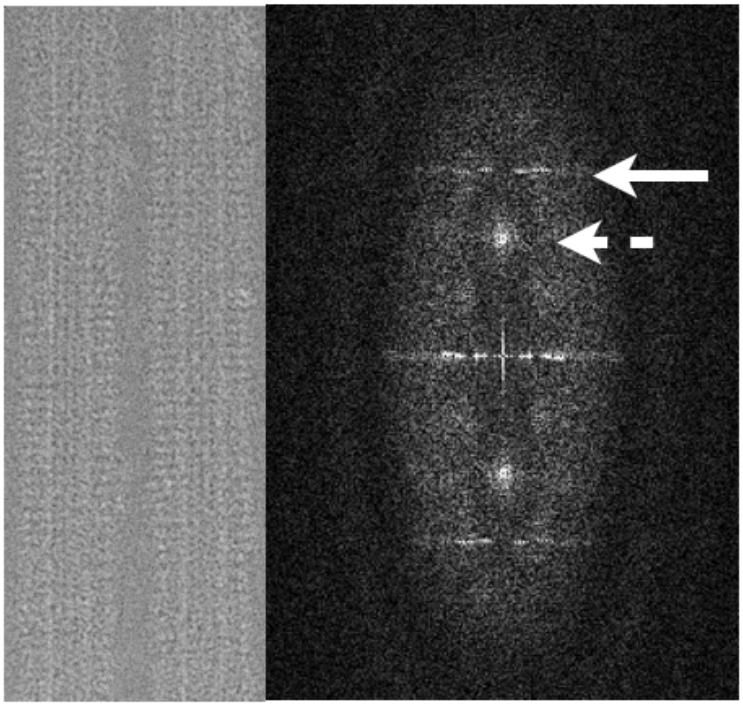

Figure 4 - Dam1 complexes assemble around microtubules with an independent repeat. Cryo-EM micrograph of closely packed Dam1 rings assembled around microtubules (left) and its power spectrum (right). Solid arrow shows the strong 4 nm layer line describing the monomer repeat of tubulin. Dashed arrow highlights the ~6.4 nm spacing between adjacent rings. Rings bind approximately every 1.6 tubulin monomers.

Motility and Force Generation

The flexible electrostatic interaction between the mismatched symmetries of the Dam1-complex ring and the microtubule suggested that the Dam1-complex ring would be able to diffuse along the microtubule lattice by switching stochastically from one E-hook to another. The implications of this idea for kinetochore function were considerable and led to experiments showing that rings were capable not only of one-dimensional diffusion on the microtubule lattice but also of tracking depolymerizing microtubule ends, with high processivity and without energy consumption of their own (Westermann et al., 2006). In the model put forward, it was proposed that Dam1-complex ring structures interact with the microtubule via flexible elements and lack a footprint on the microtubule lattice, which would allow for diffusion that becomes biased and unidirectional when the microtubule depolymerizes (Nogales and Wang, 2006; Westermann et al., 2006).

A number of microtubule-binding proteins, including the Dam1 complex, have been reported to engage in 1-dimensional diffusion on the microtubule lattice (Gestaut et al., 2008; Grishchuk et al., 2008b; Powers et al., 2009; Westermann et al., 2006). The fact that these proteins share this common property attests to both the minimal physical requirements for microtubule-based gliding and its potential usefulness. To diffuse on the microtubule lattice, a protein must bind to assembled tubulin with an affinity that allows robust attachment but that is not so tightly bound that the energetic barrier for jumping between adjacent binding sites becomes prohibitive. Processivity of diffusion can be enhanced by the cooperation of multiple copies of the binding protein, as was demonstrated recently for NDC80 (Powers et al., 2009) – either through oligomerization, as for the Dam1-complex ring, or by being associated with a scaffold, or both. Regulation of a microtubule binder's affinity for the microtubule, or its assembly state, could therefore produce a wide range of effects in vivo. Consequently, many recent biophysical studies of the Dam1 complex have been and are still being aimed at determining the effects of phosphorylation, mutation and oligomerization on these binding properties.

Robust connection of the depolymerizing spindle microtubule to the kinetochore requires a highly processive and mobile attachment. There is currently disagreement about whether this is accomplished by the Dam1 complex through a biased diffusion or a 'forced-walk' mechanism (Grishchuk et al., 2008b; Westermann et al., 2006). The Dam1-complex ring has been proposed to harness an impressive amount of force (Efremov et al., 2007) – up to the 70 pN calculated to be generated at depolymerizing microtubule ends from single molecule studies (Grishchuk et al., 2005). On the other hand, experiments using laser-trapped beads have reported the force harnessed by the Dam1 complex to be up to a more modest 3 pN (Asbury et al., 2006). Forces in this range have been, however, interpreted as an underestimation due to the geometry of the experimental setup by McIntosh and coworkers. These authors proposed a geometrical correction due to the lateral attachment of the bead to the ring, which gives an estimate of the force that the Dam1 ring experiences from bending protofilaments of an average ≈30 pN (Grishchuk et al., 2008a). This disagreement has made it difficult to decide, unambiguously, which of two distinct models, biased diffusion versus force-walk,

is more appropriate. Thus, the mechanism of Dam1 motility on the microtubule remains an area of heated controversy. (Gestaut et al., 2008; Grishchuk et al., 2008a; Liu and Onuchic, 2006; Westermann et al., 2005). In an effort to discriminate between the competing models of Dam1 function we have recently focused on experimental disagreements in the literature. Retesting the affinity of Dam1 for the microtubule, observing Dam1 bound to microtubules lacking their E-hooks, and performing a statistical mechanics analysis of the angles of rings bound to microtubules has, we hope, argued strongly for a model where Dam1 binds strongly to the E-hook and is capable of diffusion. These results are discussed in detail in Chapter 3.

An encircling ring is clearly an attractive model for processivity and has been an evolutionary solution for tracking another linear substrate – DNA by processive clamps like PCNA (Indiani and O'Donnell, 2006). However, some of the required properties of the Dam1 complex at the kinetochore have been recapitulated in vitro by non-encircling oligomers or single complexes, suggesting that a ring may not be necessary for function (Gestaut et al., 2008; Grishchuk et al., 2008b). Fluorescence data has put the number of Dam1 complexes at the budding yeast kinetochore at 16-20 during metaphase (Joglekar et al., 2006), which is in agreement with the number seen in a single ring. Recent studies of the yeast mitotic spindle by electron tomography have identified ring-like structures near the plus ends of kinetochore microtubules. (Richard McIntosh, personal communication).

Using Dam1-complex-coated beads, Asbury et al. (Asbury et al., 2006) showed that the complex could follow both growing and shrinking microtubule ends. The attachments made between the beads and the microtubule were load-bearing, and sliding experiments suggested that Dam1 complexes were forming a ring that sensed growing and shrinking ends as barriers. However, Asbury and coworkers went on to show that applying tension to the bead against the direction of microtubule depolymerization decreased catastrophe frequency (switch from growth to shrinkage), slowed microtubule shortening and increased rescue frequency (switch from shrinkage to growth) (Franck et al., 2007). The authors noted the compatibility of a ring model with the force-dependent changes in dynamic parameters they observed: the ring would transmit tension to the peels at the end of depolymerizing microtubules and tend to straighten them, resulting in a microtubule-stabilizing effect. The dependency of microtubule stabilization on tension also agrees well with the idea of multiple weak binding sites for the ring: weak attachments would allow for diffusion and by themselves have little effect on disassembly parameters. However, the ring would be able to affect the stability of the microtubule when force was exerted through it against the depolymerizing direction. However, at the time these concepts were proposed, they had already been put into question. Davis and coworkers developed a high sensitivity fluorescence-based assay to measure the affinity of the Dam1 complex for microtubules at extremely low concentrations of tubulin (Gestaut et al., 2008). They reported values in the nanomolar range that were 30 fold greater than previously described. Furthermore, single molecule experiments showed that, at low concentrations of the Dam1 complex when only short oligomers of one to four copies in size are formed, this oligomeric complex can follow disassembling microtubule ends, although with reduced procesivity.

The issue of the oligomerization state of Dam1 and its functional relevance has been further analyzed by McIntosh and coworkers (Grishchuk et al., 2008b). On the basis of fluorescence assays, they proposed that ring oligomers of the Dam1 complex are unable to diffuse but able to track depolymerizing ends. Smaller oligomers diffuse with rates that are inversely proportional to their sizes. Interestingly, they also found that single rings can track microtubule ends, but not larger assemblies. The presence of one tracking ring reduces the depolymerization rate, whereas a second ring results in halting of the depolymerization process until one of the rings disassembles, most likely the one that is in contact with the microtubule edge. These results resemble the effect of force on depolymerization speed and rescue rates in the bead experiments of Asbury and coworkers. Experiments by McIntosh and coworkers using Dam1-complex-coated beads show two different behaviors depending on whether soluble Dam1 complexes were also available in solution. Without soluble Dam1 complexes, the beads bound only to the GMPCCP section of microtubules (a region that would mimic the stabilizing GTP cap at growing microtubule ends). The beads increased the depolymerization rate as the amount of Dam1 complex on the beads increased. The authors also proposed that these beads tracked depolymerizing ends by rolling over the microtubule, rather than sliding, based on experiments with unevenly fluorescent beads. The authors interpreted these results as a lack of ring formation and thus postulated that there are two distinct mechanisms for end tracking by rings and small oligomers (Grishchuk et al., 2008b).

Interaction With Ndc80

Two reports have recently explored the interaction of Ndc80 and Dam1 *in vitro* (Lampert et al., 2010; Tien et al., 2010). Their interaction *in vivo* is critical to correct chromosome segregation through a robust kinetochore attachment to the spindle microtubule (Maure et al., 2011). In these reconstituted studies it was observed that Ndc80's dwell time and processivity on microtubules increased when Dam1 was added, and that the two complexes co-localized on the microtubule. Their binding to each other was also disrupted when the checkpoint kinase Ipl1 was added to the system, an effect that had been observed in phosphomemetic mutants of Dam1p previously and could be part of the mechanism that resets incorrect chromosome attachments *in vivo* (Shang et al., 2003). These exciting results come as the field is taking its first steps from studying kinetochore components individually to building up a functional kinetochore *in vitro* to more fully understand the synergy of these complexes.

Protein-Protein Interactions Within the Dam1 Complex

Several groups have worked to map the protein interactions within the Dam1 complex. Since much is known from genetic and biochemical studies about phosphorylation sites and binding partners in the kinetochore, an organizational map of the complex produced the first models of Dam1 function.

The first study utilized a two-hybrid and targeted binding assay approach to identify pairwise binding partners in the complex and binding partners of Dam1p in the

rest of the kinetochore (Shang et al., 2003). Their results showed Dam1p, Duo1p, and Spc34p to be central interaction hubs in the complex.

A mutational and selective expression approach, presumably to both map the complex and generate samples for x-ray crystallographic studies, was undertaken by Miranda and coworkers (Miranda et al., 2007). Deletion of specific subunits from coexpression vectors resulted in the formation of a number of subcomplexes that have shed light on how the complex is organized. Removal of Hsk3 results in two subcomplexes – Ask1p-Dad2p-Dad4p (which does not bind to microtubules) and Dam1p-Duo1p-Spc34p-Spc19p-Dad1p-Dad3p (which binds to microtubules but does not form rings). In the absence of Dam1p the complex that forms is also missing Duo1 and the Dad1-Dad3 dimer (which can be expressed and purified independently and is a stable structural module). Thus, Dam1p and Duo1p have been proposed to form a structural unit. This paper also supported the previously reported role of Dam1p and Duo1p as the microtubule binding elements of the complex (Hofmann et al., 1998).

Most recently a Japanese group approached the Dam1 complex as a proof of concept sample for a high throughput domain interaction mapping technique they had developed, generating the most detailed map of protein-protein interactions within the complex to date (Ikeuchi et al., 2010). In this study two-hybrid interactions between proteins were monitored after generating many truncations of each protein through a selective PCR step. The process favors the minimal PCR product, and therefore the smallest protein fragment, that still supports binding between the two proteins. Using this powerful tool they were able to map the minimal domains needed for binding in complete map of the complex (Fig 5). This detailed interaction map was indispensible for making a model of how the ten proteins in the complex are arranged once I had generated both the wild-type structure and had labeled five of the proteins. These results will be discussed in Chapter 1.

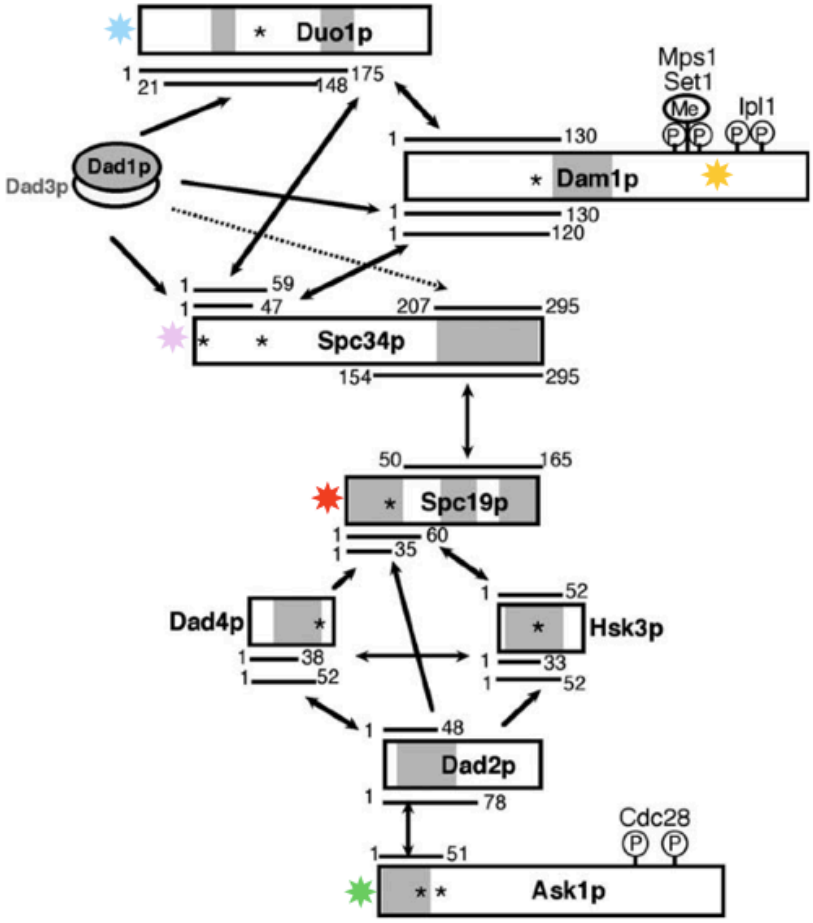

Figure 5 - Interaction map of the ten proteins of the yeast Dam1 complex. Arrows show connections between numbered domains. Grey shading denotes regions predicted to be coiled-coils. Conserved cystines shown as *. Regulatory post-translational modifications are shown on Dam1p and Ask1p. Colored stars indicate the N or C terminal regions of the 5 proteins localized during this thesis project. Figure adapted from Ikeuchi et al 2010.

Rationale and Goals of This Project

At the start of this project essentially nothing was known about the Dam1 complex structurally except that it formed rings around microtubules. The full complement of proteins had only recently been discovered and purified stably. It was an exciting sample to study because we knew that it was important to kinetochore function and had many novel properties. We knew some of what it did but not how. My 6 years studying the Dam1 complex aimed to close that gap through structure. We felt that if we could see the complex in detail both on and off the microtubule and relate the structures to the increasing amount of genetics and biochemistry known about Dam1 there would be an exciting story to tell.

The first goal, which I describe in Chapter 1, was to uncover what the complex looked like in the absence of microtubules and how the 10 proteins were arranged in the complex. This 'unassembled' structure came fairly quickly while attempts to map the architecture of the complex through genetically encoded tagging took considerably longer due to a combination of priorities and bad luck. A post-doctoral researcher in the lab, Hong-Wei Wang, had, just as I joined the lab, computed the structure of the complex assembled into spirals around microtubules. Our initial attempts to dock the unassembled structure into it to visualize Dam1 oligomerization were at best ambiguous and at the least both structures, assembled and unassembled, were low resolution – we lacked detail.

Much effort was then spent trying to improve the structure of the assembled form of Dam1 around microtubules. In the initial attempts to get a structure my co-worker was limited greatly by the lack of order in the sample. Because Dam1 does not follow the microtubule symmetry and can diffuse along the microtubule lattice the spirals were always loose. He and I both tried greatly to correct this biochemically, but I also approached it computationally and in the process developed a general method for the helical reconstruction of poorly ordered samples. This method is presented in Chapter 2.

Finally, with this method in hand I pursued a high-resolution structure of Dam1 around microtubules. Under differing buffer conditions and protein concentrations the Dam1 complex forms a range of assemblies around the microtubule. I explored all of these as structural targets, each having their own advantages and disadvantages. First the spiral form, then the ring (which we consider the most likely physiological form), and finally a stacked ring helical crystal that forms under low pH. While none of the reconstructions reached high resolution, the ring showed the densities of the repeating unit clearly in a way that allowed for a satisfying docking of the unassembled structure. This docking is further supported by rings formed in the absence of microtubules. Relating the assembled and unassembled forms unambiguously has allowed us to 'paint' the assembled form with the subunit labels, identifying protein-protein interactions responsible for assembly and perhaps interaction with other kinetochore components. This work is presented in Chapter 3.

Chapter 1 – Architecture and Structure of the Dam1 Complex

Motivation for Studying Unassembled Structure of the Dam1 Complex

Throughout this thesis I will refer to 'unassembled' Dam1 complex and 'assembled' Dam1 complex. I use these terms to describe its oligomerization state, usually with the 'assembled' state referring to its assembly around microtubules. The Dam1 complex is thought to exist in both states *in vivo* and current models suggest that phosphorylation regulates its transition between them (Cheeseman et al., 2002; Gardner and Odde, 2008; Gestaut et al., 2008; Grishchuk et al., 2008b; Wang et al., 2007; Westermann et al., 2005). Under physiological conditions Dam1 complex assembles into rings around microtubules *in vitro*. However, at high concentrations both rings in the absence of microtubules and other structures around microtubules, such as spirals, are possible. These are discussed in detail in Chapter 3.

Defining the architecture of the Dam1 complex and its self-assembly into a ring structure is essential for understanding the mechanisms by which rings may contribute to the end-on attachment of spindle microtubules to chromosomes (Shimogawa et al., 2006; Tanaka et al., 2007), and how the complex couples microtubule disassembly to processive chromosome movement. It is also crucial for determining how the assembly of the ring could be regulated and how the ring could attach to other components of the kinetochore. To understand the assembly of Dam1 into the rings that appear so critical for its function it is essential we understand the other state, the unassembled state. How do they fit together when they oligomerize and how are the ten proteins that make up each complex laid out? Those are the two aims that I approached this part of the project with.

Biological Electron Microscopy

At the beginning of this project the biggest missing piece of information about the Dam1 complex was the total lack of structural information about the complex. Because of its large size, (over 200 kDa), its tendency to assemble into curved oligomers at high concentrations, and the need to study it bound to microtubules, both NMR and x-ray crystallographic approaches to structure were not possible. Electron Microscopy is uniquely suited to image both large complexes and assemblies around microtubules and so became the technique of choice for much of the work in my project.

I will briefly describe the technique, however, anyone wishing to understand EM in depth should read one of several good reviews or books on the subject (Glaeser et al., 2007; Jensen, 2010). An electron microscope shares many of the basic fundamental principles of a light microscope. Illumination, (in the EM case this is an element that emits electrons), is directed down the optical axis of the microscope. This beam is condensed, focused, and magnified using electro-magnetic 'lenses' and the

resulting image of the sample at high magnification is recorded either on a film plate or a digital camera. Electrons are used as the probe to image molecular-scale objects because at the acceleration voltages used in the microscope they have an extremely small wavelength, < 0.1 nm, and therefore can provide images of the sample with atomic detail. However, the engineering necessities of the EM, namely that the entire internal chamber, including the region surrounding the sample, must be kept under high vacuum and that the high energy electrons necessary for imaging severely damage biological specimens complicate the collection of high quality images.

To preserve the protein sample to be studied, both against the vacuum of the column and damage by the electron beam, it is either embedded in a heavy metal stain and dried or flash frozen (vitrified) and kept at cryogenic temperatures throughout the experiment. Further, imaging protocols have been developed to generate 'low dose' exposures. To minimize the electron dose absorbed by the sample, and therefore the amount of radiation damage, all focusing is done on a region of the sample adjacent to the one illuminated for the final exposure.

Ab Initio Single Particle Reconstruction

To determine the three-dimensional structure of a macromolecule we must have images of the sample viewed from many angles and know how those images relate to each other. Since biological samples are radiation sensitive we may only image a particular molecule once with the sizable dose needed for high resolution data before it is damaged. We must therefore image many copies of the molecule as they sit in different, hopefully random, orientations on the sample support. With these images we can now attempt to assign, a posteriori, which view each image came from and thereby integrate them into a coherent, 3-D structure. The field of *ab initio* reconstruction, the generation of a 3-D structure of an object where no previous information about its shape exists, has been an intense area of research. Several methods have been developed and are suitable for different samples, usually depending on the type and amount of symmetry in the molecule: symmetrical (Van Heel, 1987), helical (Egelman, 2000; Radermacher et al., 1987; Ramey et al., 2009), or asymmetrical (Leschziner and Nogales, 2006; Radermacher et al., 1987).

I used two of these methods during my analysis of Dam1. I determined the structure of Dam1 complex alone preserved in negative stain using the Random Conical Tilt method (Radermacher et al., 1987) and the structure of Dam1 assembled around microtubules by helical reconstruction (Egelman, 2000; Ramey et al., 2009). Random Conical Tilt, and the more recent Orthogonal Tilt Reconstruction (Leschziner and Nogales, 2006), both generate an initial structure by taking pairs of images of the same sample area, one image tilted with respect to the other. Tilted and untilted views of each particle are picked from these images. The untilted particles are then separated into homogeneous groups based on which view of the molecule they represent. With like views clustered this way, the tilted mates of each particle in this group can be related to each other since we know what the tilt angle was between then. Each group of particles then generates a low resolution 3-D reconstruction based on their tilted mates. These volumes are then aligned and averaged to generate an initial model of

the molecule. This model can be refined to a high-resolution structure using projection matching methodology (Frank et al., 1996). I discuss the *ab initio* helical reconstruction of Dam1 in depth in Chapter 2.

Imaging of Wild-Type Dam1 Complex

The Dam1 complex is composed of 10 subunits, has a predicted molecular weight of 210 kDa, and assembles into rings and related curved oligomers at high protein concentration and low salt (<= 150 mM NaCl). I used EM-based single-particle analyses to obtain the first structure of the Dam1 complex in the absence of microtubules. Dilute protein sample, (~10 nM), was added to a thin carbon support and stained with a heavy metal solution of 2% Uranyl Formate and allowed to dry. Contrast in EM images is generated by differences in electron density. As the proteins are much less dense than the stain they will be readily visible in images. This sample was introduced into an electron microscope and imaged using Random Conical Tilt methodology. 50 tilted pairs of images were collected. With a further 50 untilted micrographs collected for later projection matching.

A range of differently sized particles were observed in each field of view (Fig 6a). After processing the roughly 3,000 particles into homogeneous classes by their features using reference-free 2-D alignment and classification it became clear that under the 500 mM NaCl 'high salt' condition the complex existed in monomer, dimer, and trimer states (Fig 6b)(Wang et al., 2007). Single Dam1 complexes appeared as elongated rods about 15 nm long with an arm hooking out of an enlarged central density. A Dam1 dimer is formed by translating one monomer relative to the other: they are not related by a symmetry operator. Monomers assembled in this way interact at two sites (Fig 6b). Trimers appeared to follow the same pattern, with a Dam1 monomer attached to a dimer at the same two interfaces. This head-to-tail assembly could be continued indefinitely until either it forms a closed structure like a ring or a long, curved oligomer. Later observation of closed rings of Dam1 in the absence of microtubules confirmed that these two interfaces seen in the dimer structure of 'unassembled' Dam1 are the same seen in 'assembled' Dam1 around microtubules. This structure therefore showed the structure of the complex alone but also how it assembles into higher order structures to track microtubule plus ends.

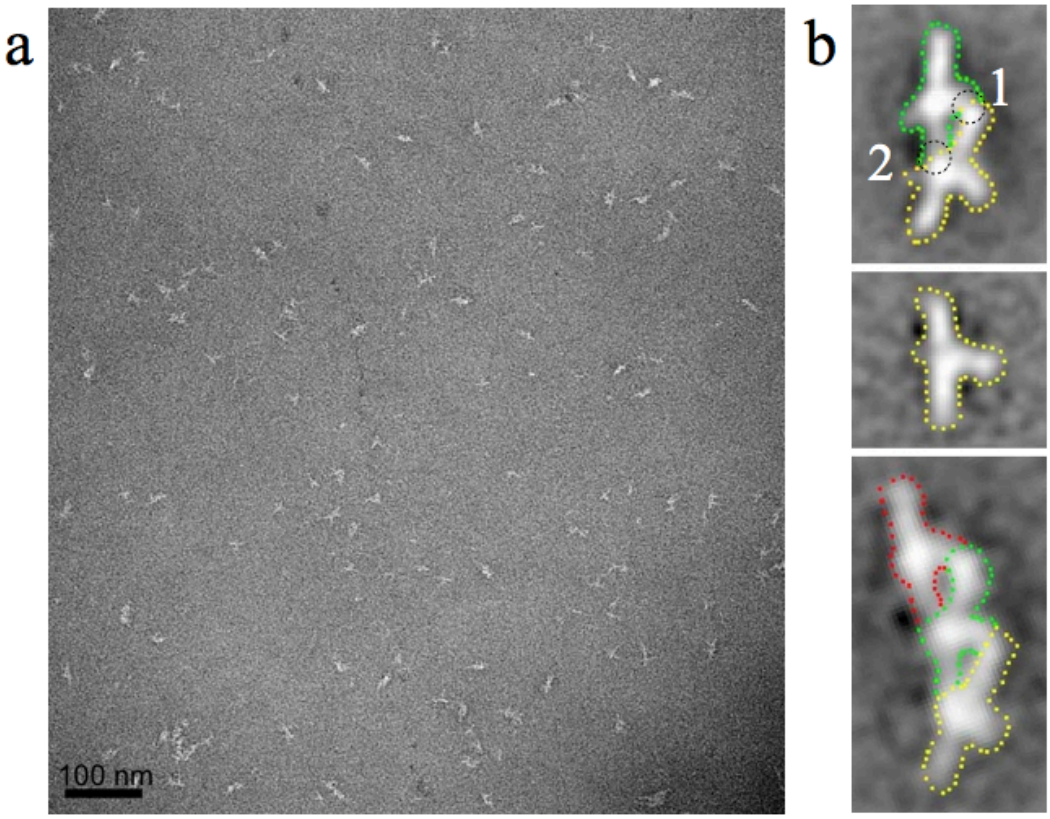

Figure 6 - Negative stain EM analysis of wild-type Dam1 complex. a) Representative untilted micrograph of negatively stained Dam1 complexes. b) Class averages of Dam1 complexes showing, from top to bottom: dimers, monomers, and trimers. Monomers are outlined with dotted colors. Two interfaces exist between monomers as they oligomerize, circled and labeled in the top, dimer, panel.

Reconstruction and Segmentation of Dam1 Dimer

It was clear from reference-free alignment and classification that the majority of the particles had a doubly repeated shape with some having a single copy of this motif and others having three (Fig 6b). Approximately 80% of particles observed were of this 'double' type. Classes showing this doubly repeating unit were selected for 3-D reconstruction. Tilted pair particles were back-projected to generate initial class volumes. Five class volumes judged by eye to agree best with each other were computationally aligned and averaged (Fig 7a). This initial model was sufficiently accurate that when the separate, untilted particles were used to refine this structure it converged to a structure that matched all reference-free class averages (Fig 7b,c). That a structure has views that match all reference-free class averages is a major quality control check. Only correct reconstructions are expected to account for all views observed in the sample.

Inspection of this reconstruction made it clear that the sample was a dimer of Dam1 complexes. The volume of the whole structure corresponded to a protein mass of approximately 400 kDa (a predicted dimer) and the repeated shape could be aligned and averaged together with almost perfect agreement (Fig 7d). This repeated shape matches well to the motif seen in both single and triple-motif class averages, reinforcing the idea that this fundamental unit is a single copy of the complex. The structure of the Dam1 dimer has been deposited in the EMDataBank (http://emsearch.rutgers.edu/, accession #1372).

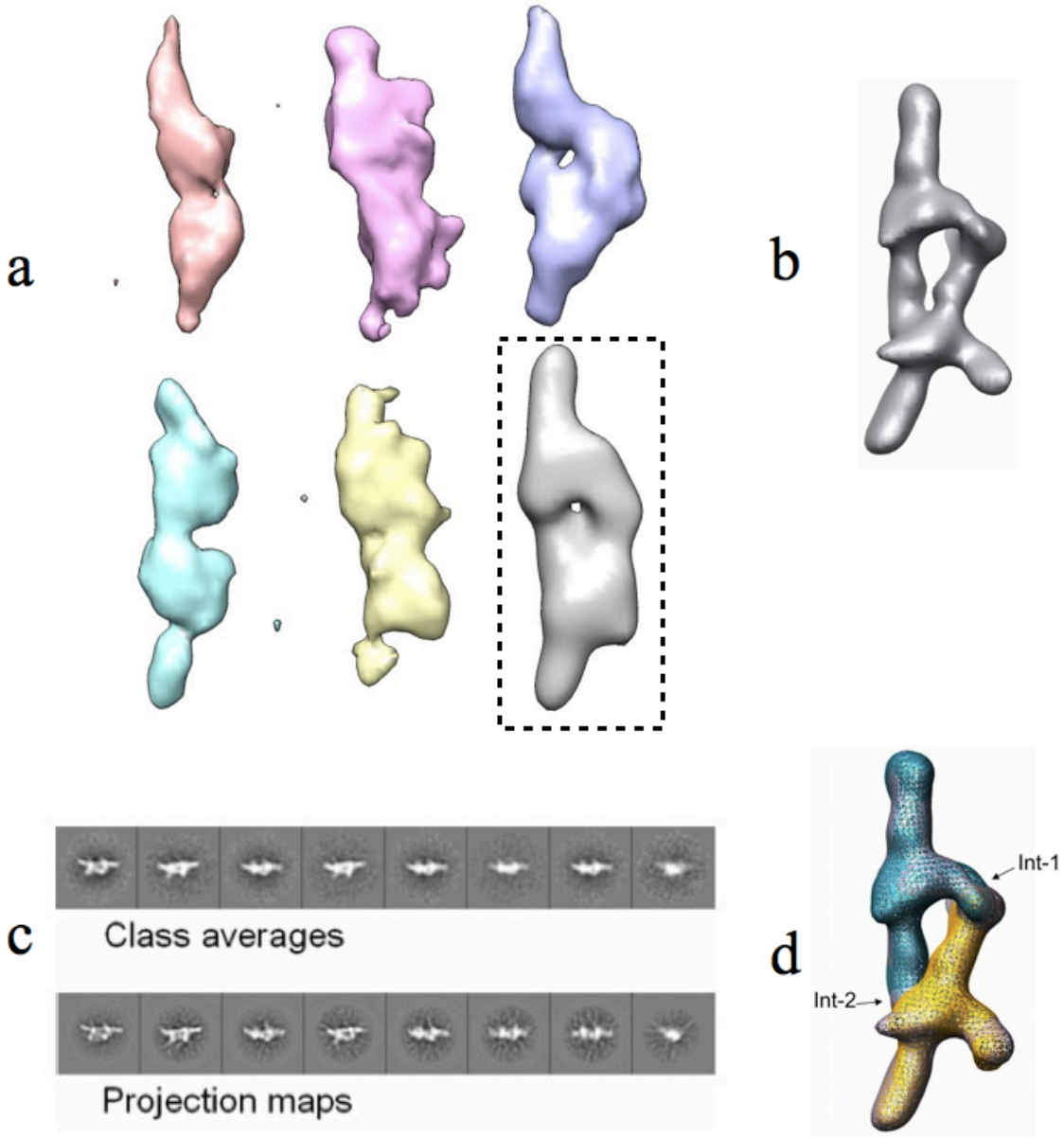

Figure 7 - Reconstruction of wild-type Dam1 dimer. a) Initial class volumes generated from Random Conical Tilt processing. Volume in dashed box is the average of the other five after alignment. b) Final structure after projection matching refinement against averaged model in (a). c) Comparison between reference-free class averages and reprojections of the model in (b), showing good agreement. d) Segmented and averaged monomers from the reconstruction in (b), docked into the dimer structure.

Dam1 Forms Rings in the Absence of Microtubules

To this point all structural studies I had carried out on the Dam1 complex in the absence of microtubules had been done using negative stain EM. This was due to the small size of the complex and the relative ease of that technique. To improve any comparison of the assembled and unassembled structures I attempted to reconstruct the Dam1 complex from cryo-EM images of the complex. While this was ultimately unsuccessful, the observation of Dam1 rings in the absence of microtubules in these experiments suggested that Dam1 does not undergo a large conformational change upon binding the microtubule that facilitates oligomerization, which had previously been our model for microtubule-induced ring formation (Fig 8) (Wang et al., 2007). This clue informed the docking of the two models and resulted in the structural model I present in Chapter 3. These microtubule-free Dam1 rings were observable in cryo-EM conditions because the concentration of complex used on the sample grid is approximately 1000-fold higher than what can be used for negative stain. At these higher concentrations, and with a low salt buffer with 150 mM NaCl, Dam1 can oligomerize into closed rings.

a

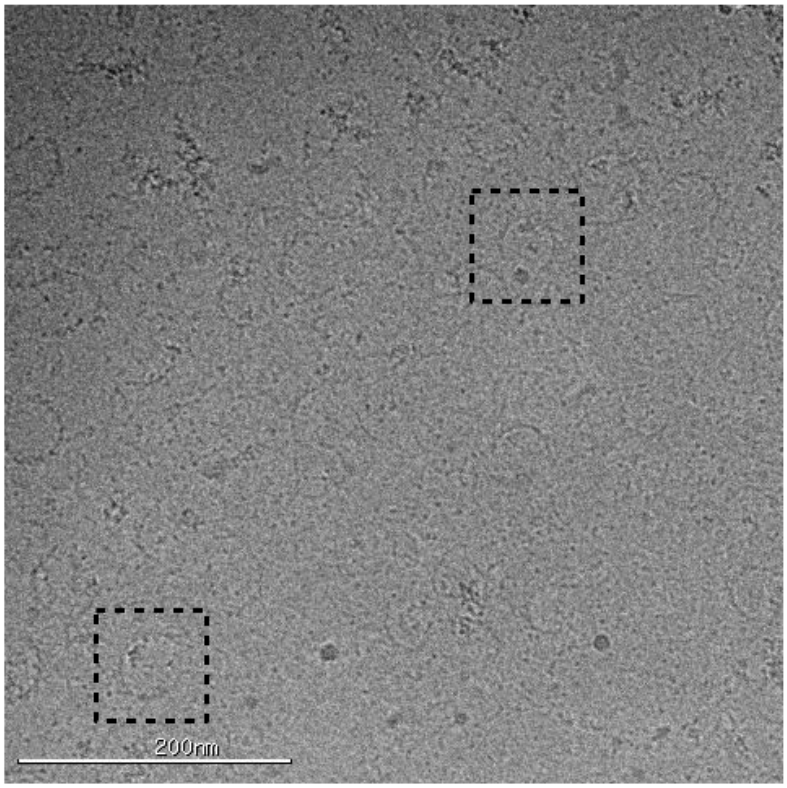

b

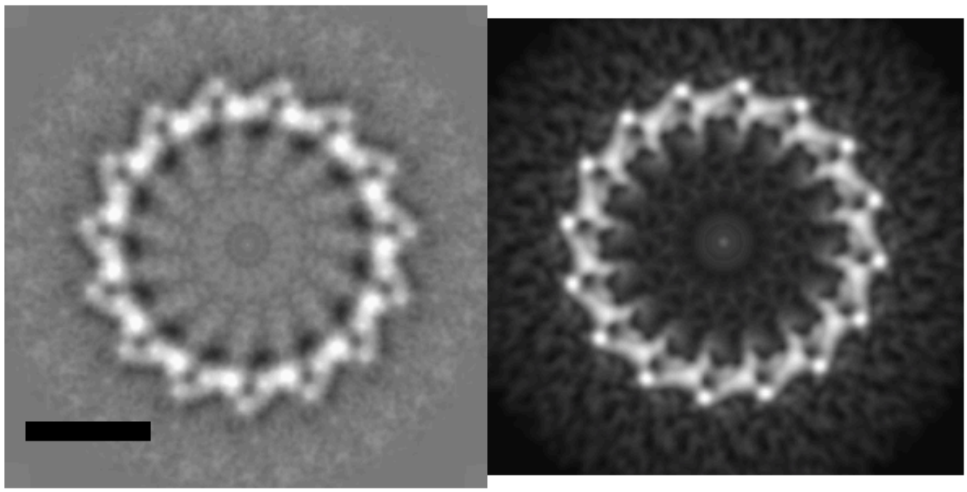

Figure 8 - Dam1 forms rings and curved oligomers at high concentration in the absence of microtubules. a) Cryo-EM micrograph of wild-type Dam1 complex over open holes at a concentration of 0.5 mg/ml. Two rings are highlighted by dashed boxes. b) Left: selection, averaging, and symmeterization of 52 rings produced this image of rings in the absence of microtubules. When compared to a reprojection of the structure of the Dam1 ring assembled around microtubules, right, it is clear that no major conformational change is induced by the microtubule. The two rings are very similar. Scale bar is 20 nm.

Localization of Dam1 Subunits

While a wealth of information had been generated by our collaborators and others about the connectivity between the proteins within the complex, there were no structural markers to 'paint' this interaction map onto the structure of the complex. Several regions are of special interest. For instance, the complex interacts at two sites to oligomerize into spirals and rings and this assembly appears to be important for *in vivo* function. Knowing what proteins sit at these interfaces could direct further genetic and biochemical experiments to further our understanding of Dam1's assembly regulation. Also, identifying proteins at the Dam1-microtubule interface or exposed surfaces for connection with other elements of the kinetochore is vital to understanding Dam1.

Structural analysis of the Dam1 complex containing a truncated form of Dam1p lacking its C-terminus revealed that the C-terminus of Dam1p is located in an "arm" of the unassembled complex (Fig 9) (Wang et al., 2007). Dam1p is a major target of the spindle check point kinase Ipl1 and phosphorylation of the Dam1 complex promotes detachment of kinetochores, therefore 'resetting' the kinetochore for another try at a correct bioriented spindle attachment (Cheeseman et al., 2002). Interestingly a phosphomimetic mutant of the Ipl1 sites in Dam1p, (three out of four of which are at the Dam1p C-terminus) shows little effect on the binding of the Dam1 complex to the microtubule but causes a reduction in ring assembly (Westermann et al., 2005). Therefore, one role of Ipl1 might be to regulate the formation of the Dam1 ring and cause the kinetochore to lose this processive attachement to the spindle (Wang et al., 2007).

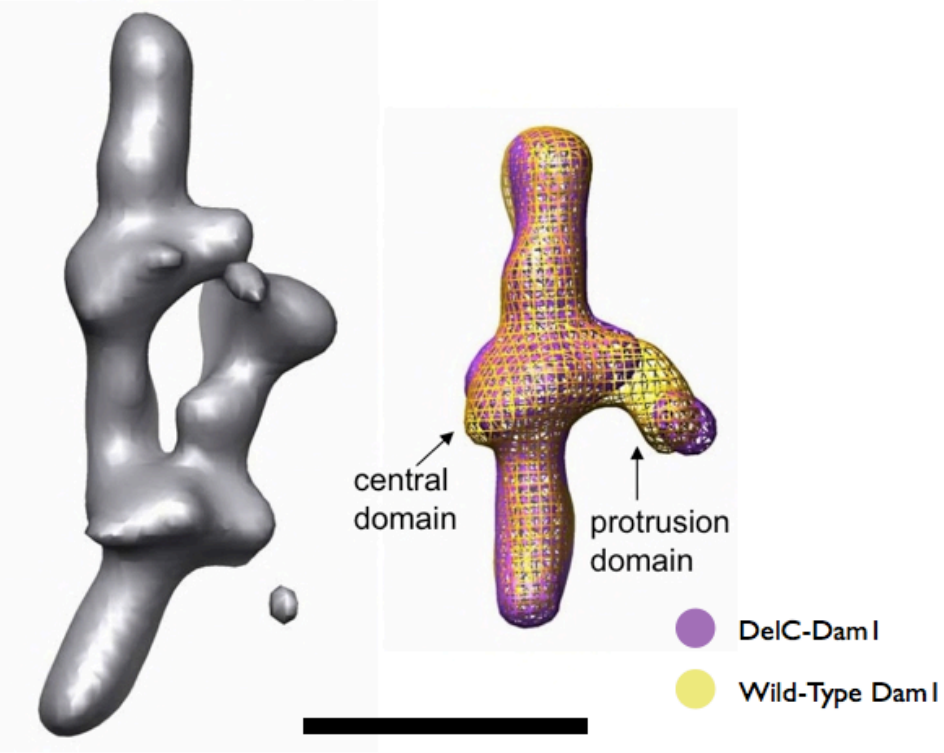

Figure 9 - Reconstruction of the DelC-Dam1 complex. The mutant complex forms dimers, left, similarly to wild-type Dam1. The C-terminus of Dam1p is therefore not required for inter-complex interaction. Averaging of monomers and comparison with the wild-type Dam1 structure, right, shows the disappearance of the 13 kDa density in one of the protruding domains. Scale bar is 10 nm.

To further locate individual proteins within the complex my collaborators in the MacroLab, a user facility on the UC Berkeley campus for high throughput molecular biology (http://qb3.berkeley.edu/qb3/macrolab/), cloned, expressed, and purified N-terminal MBP fusions of each of the ten proteins in the context of otherwise wild-type complex. Ten different complexes were expressed, each with one tagged subunit and nine wild-type subunits. Each was purified through a 6xHis tag on the MBP using Nickel bead chromatography followed by gel filtration. Surprisingly, all expressed and purified as complete complexes except for the MBP-Dam1p construct (Fig 10a). This is perhaps due to the rather long 22 amino acid unstructured linker region between the MBP and start of each protein. This was not tested however; these were the only constructs studied. Further, each complex was also competent to bind to microtubules and oligomerize into rings or spirals (Fig 10b). This suggests that the minority of the surface of each protein is buried in protein-protein interfaces, as one would expect an insertion to disrupt the interface and cause either subcomplexes or disrupt oligomerization.

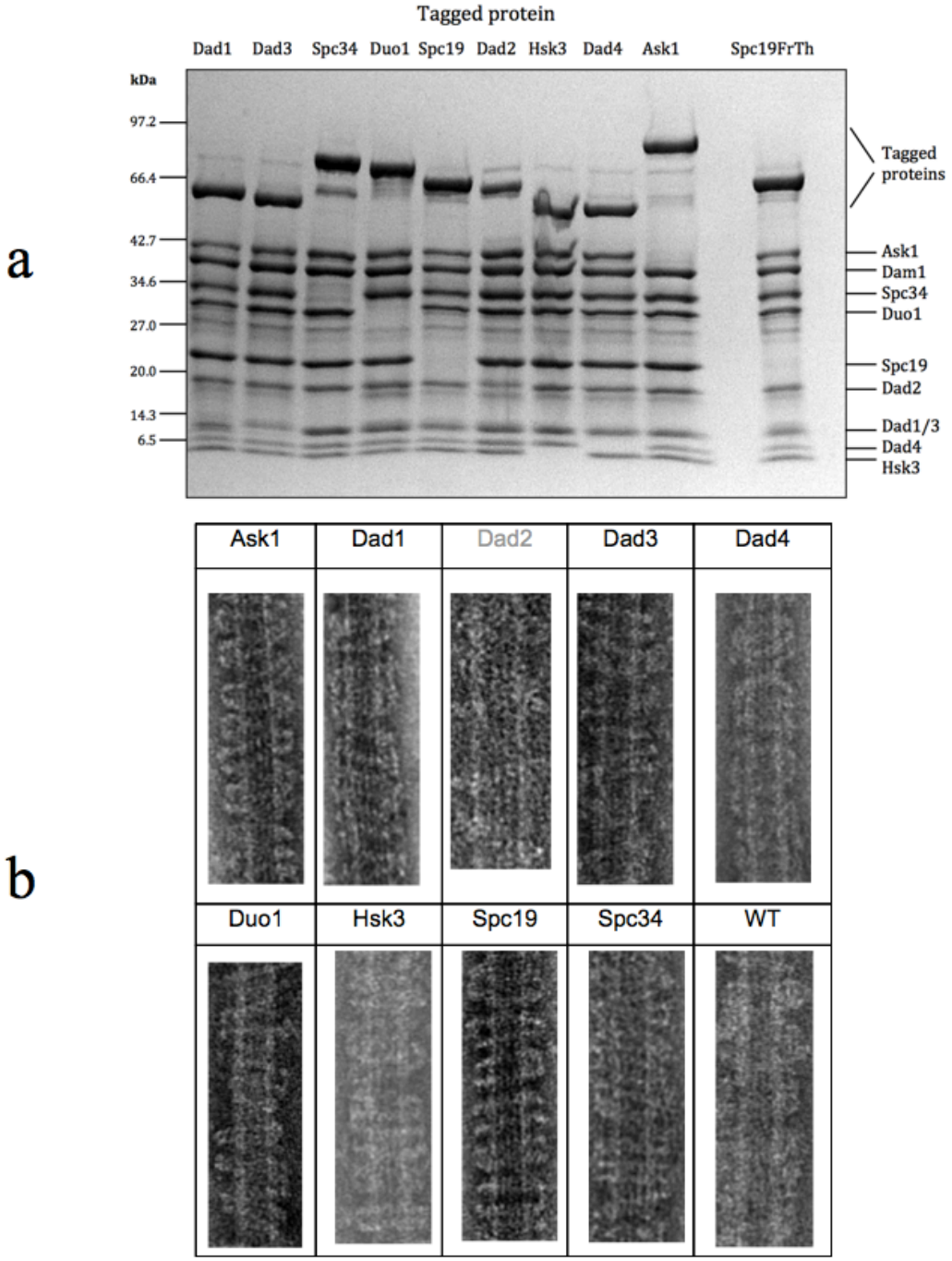

Figure 10 - Characterization of N-terminal MBP fusion complexes. a) Gel of the final, purified, tagged complexes. All 9 complexes, (every protein except Dam1p), formed intact complexes. The Dad2 construct showed partial cleavage of its tag and therefore was not used. b) Binding and assembly of complexes on microtubules was investigated by negative stain EM. All labeled complexes are competent to bind and form rings or spirals around microtubules.

I structurally mapped the locations of the 5 largest of the 10 subunits in the Dam1 complex using either N-terminal MBP-tagging experiments or domain deletions. The total mass of the labeled proteins accounts for almost three quarters of the complex. These experiments rely on the fact that the readout in an EM image is a map of electron density. If you add mass, through non-intrusive genetic tagging, or remove mass, through a domain deletion, the location of the appearance of disappearance of mass in the resulting images of those samples compared to Wild-Type Dam1 Complex will point to the location of that tagged subunit (Fig 11a). DelC-Dam1 complex was obtained from our collaborators in the Drubin-Barnes lab at UC Berkeley and expressed and purified by Jie Fang in the Nogales Lab (Westermann et al., 2005). The DelC-Dam1p complex removed a 13 kDa domain that contains 3 of 4 known Ipl1 phosophorylation sites on Dam1 that appear to modulate ring assembly (Wang et al., 2007).

These mutants were prepared for negative stain EM as described for the wild-type complex, except that the samples were prepared without the extra 'sandwich' layer of carbon (De Carlo and Stark, 2010). Each complex was imaged on a Tecnai 12 microscope with either film plates or a 4k x 4k digital CMOS Tietz camera (Tietz Video and Image Processing Systems GmbH, www.tvips.com). Data from both sources were treated by the same computational techniques. Images were assessed visually for good stain and to be free of imaging artifacts. Particles were then manually selected without regard for whether they appeared to be monomers or dimers, which together made up the vast majority of particles. Reference-free class averages were then generated using an iterative alignment and classification script using the IMAGIC (van Heel et al., 1996) and CAN (Ogura et al., 2003; Ramey et al., 2009) software packages. Dimer class averages showing either either loss, in the deletion case, or gain, for MBP labels, of density in the same location in each monomer were found and used to localize subunits (Fig 11b). Observing changes in two equivalent locations within each dimer class average provides an internal control that the changes seen are in fact due to the known mutation.

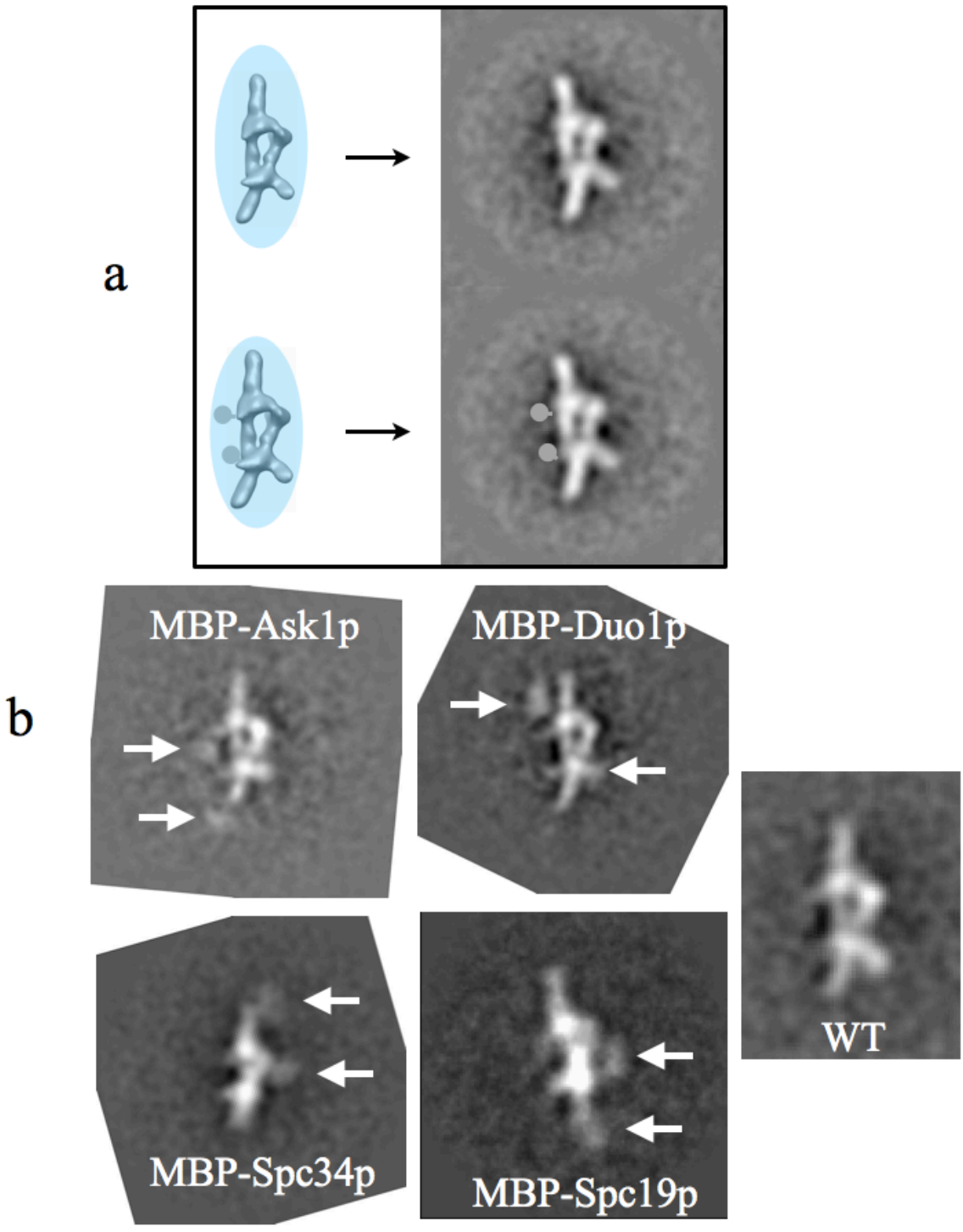

Figure 11 - Mapping the locations of MBPs in labeled complexes. a) Schematic of the design of this experiment. WT, top, or labeled, bottom, complexes are imaged and processed through reference-free alignment and classification, generating class averages. Additional density in a labeled class average compared to WT indicated the location of that labeled protein. b) Class averages of 4 MBP labeled constructs with WT for comparison. Arrows point to extra, MBP densities

Integration with Known Complex Interactions

With half the proteins, and the great majority of the mass, of the Dam1 complex now localized within the wild-type structure through EM imaging I was able to generate a model of the structural organization of the entire complex by adding constraints from known biochemical interactions. All three reports of protein interactions within the complex agree with each other but contain differing amounts of detail. Because the most recent study contained the highest resolution interaction map I used their results to guide my model (Ikeuchi et al., 2010) (Fig 12).

Each of the four largest proteins in the complex: Dam1p, Duo1p, Ask1p, and Spc34p, appear to occupy either an arm of the complex or the central domain and would account for most of the mass seen in its region. Interestingly, the C-terminal domains of both Dam1p and Ask1p have been shown to not participate in intra-complex interactions and are post-translationally modified by mitotic regulatory proteins (Cheeseman et al., 2002; Li and Elledge, 2003; Shimogawa et al., 2006; Zhang et al., 2005). These regions are both positioned at interfaces between complexes, suggesting that these C-terminal domains may be important interfaces for inter-complex binding and oligomerization, and that their modification by other factors may regulate their assembly and therefore their function *in vivo*. Phospho-memetic mutants of both Dam1p and Spc34p have been shown to specifically decrease binding between those two proteins. EM analysis of phospho-memetic Dam1p complexes showed decreased dimer formation but no obvious separation within the complex, suggesting that the Spc34p-Dam1p interaction modulated by phosphorylation is between complexes (not shown – included as supplementary material in (Wang et al., 2007)). According to my structural model, phosphorylation of either Dam1p, Spc34p or both would weaken this outer interface and therefore reduce oligomerization.

Ask1p appears to form the bulk of the 'lower' leg of the Dam1 complex monomer (Fig 12). The bottom of this leg joins with the central domain of the next monomer,forming the other oligomerization interface. The N-terminal domain of Ask1p that has been localized using MBP tagging is also the region found to interact with the rest of the complex (Ikeuchi et al., 2010). It is interesting to notice that in the study of Ikeuchi et al. the vast majority of Ask1p does not appear to participate in binding interactions with the rest of the complex. This large C-terminal region also contains two cdc28 phosphosites. It is the tip of this bottom leg that touches the central domain of the adjacent monomer. If this interface does contain the cdc28 phosphosites it may be another mechanism for the regulation of Dam1 assembly. Additionally, we may wonder if interactions found in this study, which were studied as pairwise interactions, represent intra- or inter-complex interactions.

a

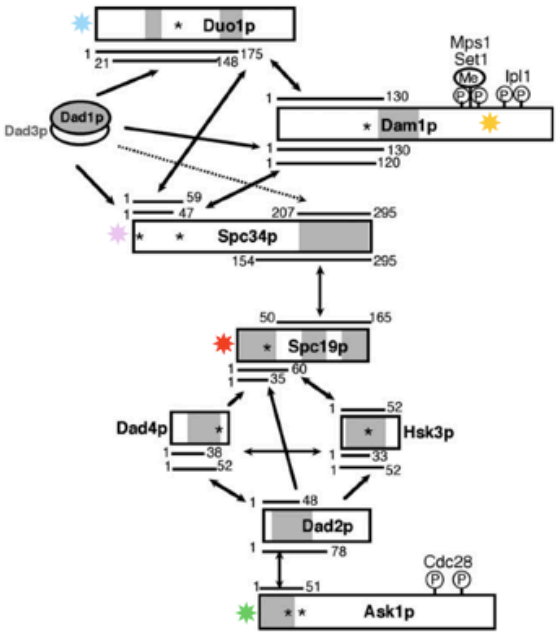

b

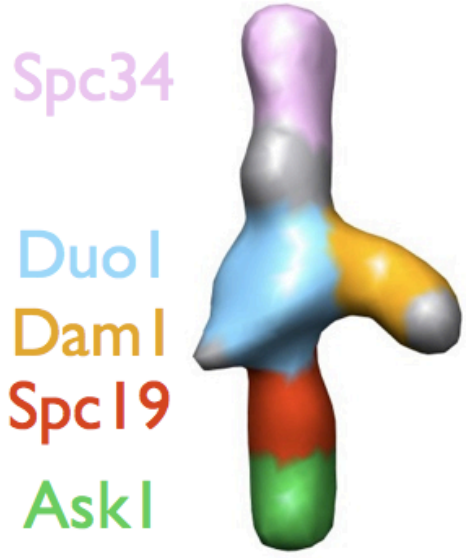

Figure 12 - Localization of subunits within the Dam1 complex. a) Interaction map of proteins in the complex as determined by Ikeuchi et al 2010. Colored stars correspond to the subunits labeled in this thesis and the locations of those labels, N or C terminal. b) Locations of subunits inferred from labeling experiments mapped onto the structure of the Dam1 monomer.

Chapter 2 – Reconstruction of Poorly Ordered Helical Samples and Dealing with Symmetry Mismatch

Introduction to Helical Reconstruction and Dam1 Structure

The first three-dimensional (3-D) structures of biological macromolecules ever to be obtained by electron microscopy were those of samples with helical symmetry (DeRosier and Klug, 1968). The 3-D structure of an object arranged in a helix can be reconstructed from a single two-dimensional (2-D) projection image, whose Fourier transform is composed of a series of layer lines. These layer lines are Bessel functions of different orders defined by the helical symmetry (DeRosier and Klug, 1968; DeRosier and Moore, 1970). Application of Fourier-Bessel helical reconstruction methods have led in recent years to close to atomic resolution for a number of important biological macromolecules (Miyazawa et al., 2003; Yonekura et al., 2003). However, these classical helical reconstruction methods are limited by the requirement of robust, long-range, helical order in the sample to be studied. This condition can sometimes be extremely difficult to attain, if not impossible. In the past decade, new computational methods combining single particle image processing techniques with conventional helical reconstruction have been successfully implemented to address a number of problems in helical assemblies (Egelman, 2000, 2007; Holmes et al., 2003; Li et al., 2002; Pomfret et al., 2007; Sachse et al., 2007). For the use of these algorithms, images of several helical filaments are chopped into small fragments, each containing a few to tens of turns of the helix. Analogously to single particle analysis of asymmetric molecules, the fragments can be sorted based on their features to reduce heterogeneity and a reconstruction of the experimental filament can be calculated by situating each segment in 3-D space according to its relative orientation and applying the correct helical symmetry.

The need to effectively deal with the heterogeneity observed in many helical assemblies was the original impetus for the development of single particle helical methods by Egelman and co-workers. Our work here seeks to expand on the method to routinely deal with short range order on the scale of single turns and competing symmetries during the *ab initio* reconstruction of these assemblies. The single most important step of helical reconstruction is finding the correct symmetry for each helical segment in the dataset. This is confirmed by the observation that refinement of helical particles against a featureless cylinder using the correct symmetry recovers the correct structure. The estimation of this symmetry for highly heterogeneous assemblies is difficult as each turn of the helix may differ from its neighbors. Therefore our addition to the single particle method is especially aimed at this problem in systems where it is impractical to assign symmetries by other means, namely: the limited amount of known structural information prevents sorting of heterogeneity by using models of different helical states and order is too rare and short-ranged to calculate helical symmetry from inspection of layer lines of averaged segments. A reference-free 2-D classification and alignment step has been added to sort the data into homogeneous classes of helical segments based on features and symmetry without prior knowledge or manual user

intervention. The class averages from these groups can then be used for symmetry estimation, initial 3-D model generation and projection matching refinement to achieve higher resolution following the established single particle methods of Egelman. In collaboration with Dr. Hong-Wei Wang, this approach was successfully applied it to the Dam1 complex, a kinetochore component required for the robust connection of the mitotic chromosome to the spindle microtubule.

At saturating concentrations the Dam1 complex forms tightly packed spirals around microtubules, with each turn corresponding very closely to a slightly skewed ring (or lock-washer). This helical arrangement has the potential to aid structural analysis, by both concentrating the complexes and aligning them. However, the Dam1 spirals formed around microtubules almost never sustain the type of long-range helical order required for conventional helical reconstruction methodology. This is opposed to the well-ordered assembly that is commonly seen for other microtubule-interacting proteins as they bind tightly to the microtubule lattice and thus "reproduce" the helical arrangement of tubulin, (e.g. kinesin)(Amos and Hirose, 1997; Hirose et al., 1997; Metoz et al., 1997; Sosa and Milligan, 1996). Furthermore, because of the flexible character of the attachment of Dam1, as well as its much larger size, the Dam1 assembly has a different, unrelated helical symmetry from that of the underlying microtubule, an interesting property for its biological function that, however, adds technical challenges to using single particle approaches for its study.

The microtubule itself is a well-studied helical structure made of repeating αβ tubulin heterodimers. The dimers assemble head to tail to form protofilaments, about thirteen of which interact laterally to create a hollow tube approximately 250 Å in diameter. About 16 Dam1 complexes assemble into a single turn of the spiral around the microtubule based on our previous structural studies, (Wang et al., 2007; Westermann et al., 2006). The inner diameter of this arrangement is 320 Å with a helical pitch of 150 Å (compared to the 40 Å pitch of microtubules). The difference in helical symmetries between the Dam1 complex and the microtubule would makes it easy, in principle, to use conventional Fourier-Bessel helical reconstruction methods to study this system, as the two components are separable in Fourier space. In other words, there is no layer line overlap. Thus, the information corresponding to each structure could be extracted independently and each reconstructed with their appropriate symmetries. However, during our cryo-EM studies of Dam1 spirals on microtubules, out of hundreds of filaments examined, only two showed clear helical diffraction to a resolution better than 40 Å (Wang et al., 2007). Most spirals appear ordered by visual inspection but do not display more than one blurred layer line due to a loss of registry between adjacent turns, (Fig 13). Ideally we would like to utilize the helical order retained on the level of single turns to avoid this limitation and robustly study this sample. Since conventional Fourier-Bessel methods cannot operate on such short helical stretches, due to extreme layer line broadening and lack of signal, the structural information of the microtubule and Dam1 helix must be separated in a different way and an alternative reconstruction method used to gain structural information.

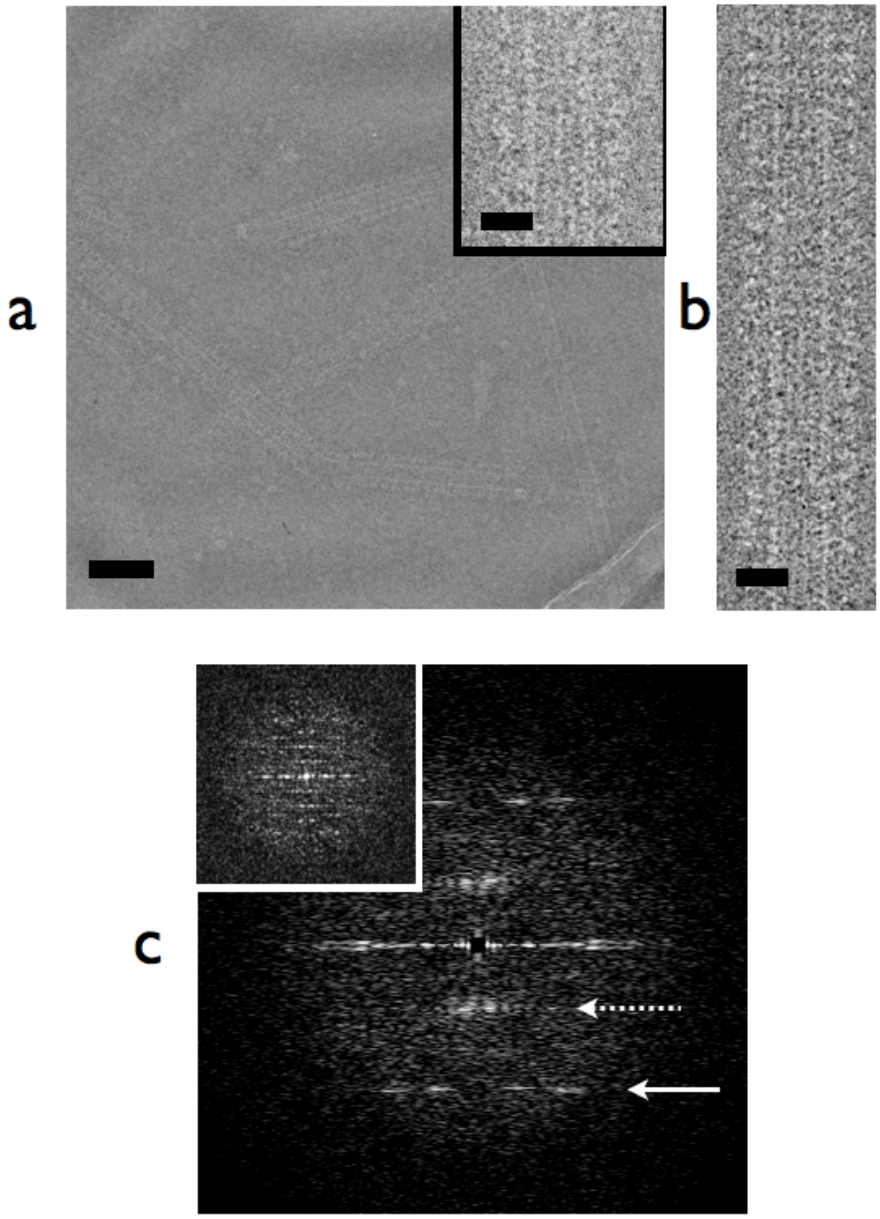

Figure 13 - a) Micrograph containing several Dam1 decorated microtubules. Scale bar 1000 Å. Inset shows the short helical crystal used in our previous studies. It was one of only a few found after screening hundreds of assembled segments and only sustained order over ~7 turns. Scale bar 200 Å for this inset. b) CryoEM image of a typical microtubule fully decorated with a Dam1 spiral. Scale bar 200 Å. c) Power spectrum of image in (b). The 40 Å layer line corresponding to the repeat of tubulin in the microtubule is clearly visible (solid white arrow) while only one blurred layer line is visible for the Dam1 spiral (white dashed arrow). This layer line corresponds to the ~100Å pitch of this variable Dam1 helical assembly. Inset shows power spectrum of crystal from (a).

The approach presented here overcomes these difficulties in studying Dam1 structure by removing the microtubule from each short segment and then applying 2-D image alignment and classification techniques to sort the assembly turn by turn into homogeneous classes, with no assumptions made about the symmetries present or amount of disorder. Inspection of class averages then provides information about the number of symmetries present and allows an estimation of what helical parameters to use in their reconstruction.

Special Issues in Reconstructing Dam1 Spirals

The character of the Dam1 complex assembly around the microtubule makes it extremely challenging for studies using either conventional helical methods or single particle approaches. In order to overcome these challenges we have implemented the automated removal of the microtubule structure from the images, generating 'microtubule-edited' segments, which then made it possible to take on a single particle approach using short helical stretches along the spiral. Additionally, we successfully applied image classification techniques commonly used in single particle methods to address the problem of extreme disorder and symmetry heterogeneity in the Dam1 assembly, opening the door for structural studies of this complex that have been hampered by lack of long-range helical order.

Preprocessing - Removal of Microtubule and Boxing of Single Turns

When averaging single particles during 3-D EM reconstruction, as we are doing here by treating a small number of helical turns as a 'single particle', it is commonly assumed that the objects being analyzed are identical biochemically and that each image being averaged corresponds the same orientation. When mismatched symmetries co-exist in the sample, as for the Dam1 helix assembled around a microtubule, this is almost never the case, because the specific arrangement between the two assemblies in each segment will only rarely be repeated elsewhere, (i.e. they are two hollow helical tubes that are free to rotate and slide past each other within the scale of individual subunits). Therefore, each image of a Dam1 helical turn has several million Daltons worth of randomly rotated and translated microtubule signal in it. This corrupting signal must be removed to prevent it from biasing the alignment and classification steps of single particle processing and therefore blurring structural features after averaging.

We remove the microtubule signal using an automatic approach, in which each small segment, rather than the entire long filament, is processed, thus avoiding the time consuming, manual step of filament straightening. Two main structural features of the underlying microtubule lattice interfere with attempts to align, classify and average Dam1 helices. They are: the head-to-tail protofilament pattern of the wall and the 40 Å axial repeat of tubulin in the lattice. The preprocessing steps taken for removal of this unwanted microtubule signal are outlined in Figure 2. In order to remove the pattern of protofilaments, which for these short segment lengths can be treated as a circular arrangement of vertical cylinders, the raw image of the Dam1-surrounded microtubule

(Fig 14a bottom) is projected along their shared helical axis to generate a one-dimensional (1-D) density profile, (Fig 14a top). This profile is "trimmed" to contain only the central density corresponding to the microtubule, (Fig 14b top). This is based on the fact that the Dam1 spiral sits at a significant distance from the microtubule wall and therefore their radial density distributions are easily separated. Then a 2-D protofilament mask (Fig 14b bottom) is generated by backprojecting this truncated 1-D profile along the helical axis. Now the protofilament signal can be removed by simply subtracting this mask from the raw image in real space, resulting in the corrected image shown in Figure 14c. Its corresponding 1-D profile (Fig 14c top) confirms the removal of this central protofilament density. This real-space procedure is mathematically equivalent to a Fourier-space operation on the equatorial layer line, which contains information about radial density distribution. Power spectra of the raw, masked, and corrected images are shown in Figures 14d,e and f respectively. After masking, the microtubule contribution is removed and the overall shape of the microtubule disappears from the image. This method for microtubule removal is conceptually similar but procedurally different from one presented recently, (Narita et al., 2007). In that study it was necessary to remove the microtubule because it interfered with identifying points of sparse decoration on its lattice. They removed the protofilament pattern by zeroing out the entire equator in the Fourier transform of longer stretches of microtubule, removing the moire pattern and density corresponding to the microtubule wall. Our method also removes the microtubule contribution from the equator but it is done in real space rather than Fourier space and this allows us to simultaneously preserve the signal from other lattices while removing the microtubule specifically.

The major remaining contaminating signal from the microtubule comes from the axial repeat of tubulin along the protofilament. In Fourier space this is mainly located in the 40 Å layer line, (higher orders were neglected for this low resolution implementation of the process involving a limited number of segments). There is no layer line overlap between the two helices since they have unrelated symmetry. Taking advantage of this independence, the 40 Å microtubule layer line was zeroed out in each short helical segment using a mask width of 4 pixels, (Fig 14g). Dam1 helical segments that had been treated to completely remove the microtubule contribution to the image were then boxed to single turns of the helix with a soft rectangle to allow the algorithm to sort heterogeneity turn by turn (Pomfret et al., 2007).

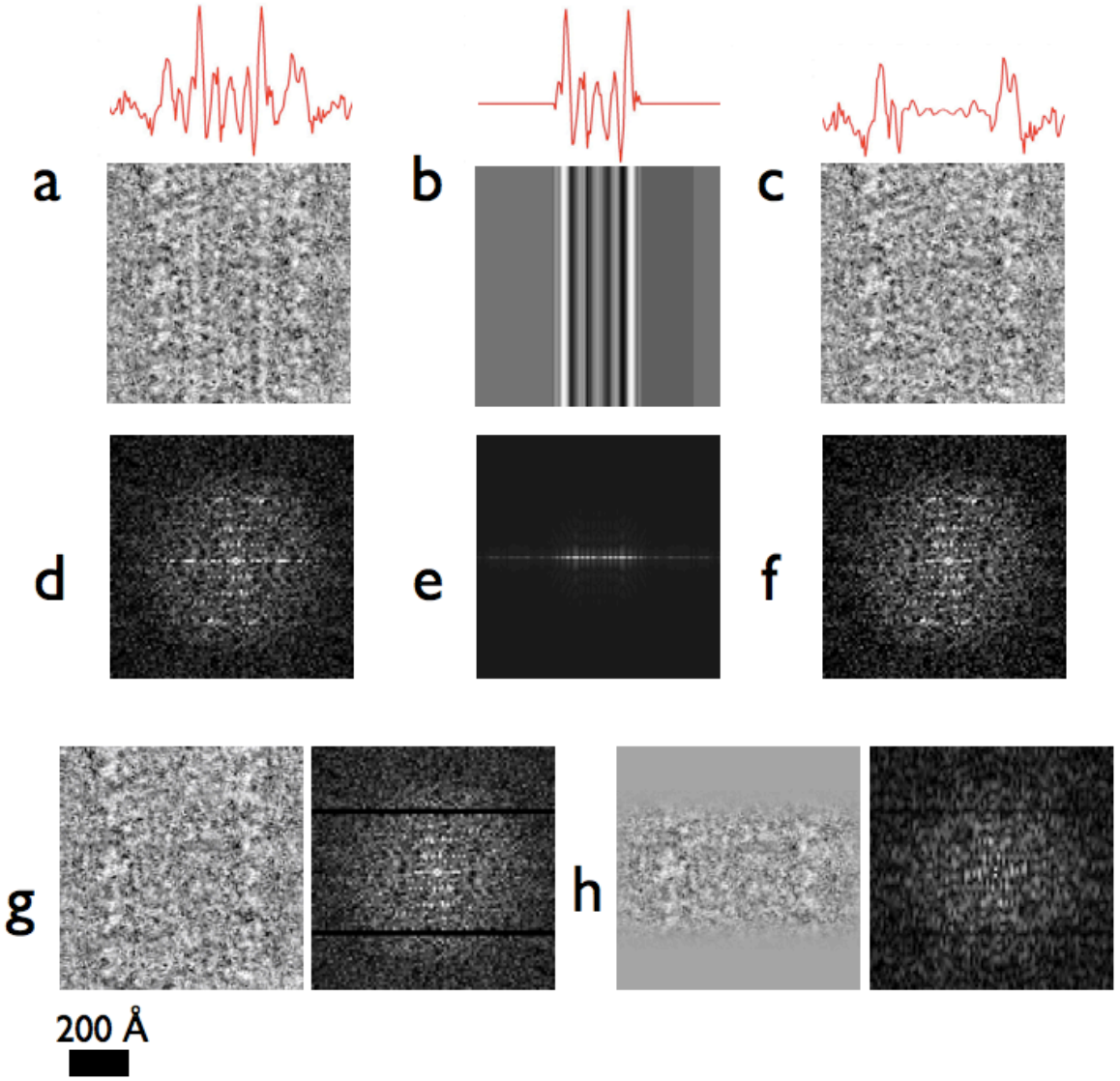

Figure 14 - Preprocessing of images by removing microtubule and boxing single turns. a) Raw segment of Dam1 assembled around microtubule. The 1D density profile for this image is shown above. b) Central portion of 1D density profile in (a) corresponding to the microtubule protofilaments has been projected in 2D to make this mask. Compare 1D profile above with profile from (a). c) Resulting image and 1D profile after real space subtraction of image in (b) from image in (a). Both the image and the 1D profile show the complete removal of the central microtubule density. d), e) and f) Power spectra of images in (a), (b), and (c) respectively. These illustrate how the masking, which is performed entirely in real space, is equivalent to masking the microtubule's contribution to the equator in Fourier space. g) Masking of the microtubule's 40 Å layer line in Fourier space (right) removes the signal from the tubulin repeat in the image (left). h) Segment from (g) that has had all but one to two turns of Dam1 helix masked out with a soft mask (left). Power spectrum of this small stretch (right) shows that at the size of helical fragment that is required to treat extreme disorder traditional Fourier space methods of reconstruction fail due to extensive layer line broadening and overlap. The image in (h) is then carried over for 2D processing.

Alignment and Classification Sort Segments Into Homogeneous Groups

Heterogeneity has been successfully resolved in previous studies using single particle helical methods by comparing segments against 3-D models of different states of the assembly having varying symmetry or conformation, (Egelman, 2007; Frost et al., 2008; Galkin et al., 2008a; Galkin et al., 2008b; Orlova et al., 2007; Trachtenberg et al., 2005). Models have been generated in different ways, including: low resolution Fourier-Bessel reconstruction (Frost et al., 2008), application of various symmetries to an 'average' model derived from heterogeneous data (Trachtenberg et al., 2005), and making simulated structures based on the symmetries seen in the averaged power spectra of particles (Wang et al., 2008). By matching each segment to reprojections of these models they can be put into homogeneous groups of known symmetries and reconstructed separately. While we were able to generate a 30 Å reconstruction of the Dam1 complex assembled around microtubules from two rare ordered stretches we were unable to sort the rest of the data using this model due to the extreme short-ranged order of the sample. Frequently helical segments seemed to not maintain a unique symmetry even for a single turn and this made it difficult to apply the existing methods to create homogeneous groups. The Dam1 complex then is a case where the reconstruction of this assembly requires a different mechanism of sorting heterogeneity.

Our approach is to create groups of segments with homogeneous pitch and diameter by aligning and classifying them in 2-D, (Fig 15a,b). By making the common assumption that the size of the asymmetric unit along the spiral is constant in each particle this implies that segments with homogeneous pitch and diameter all represent a single helical symmetry. There are a small number of cases where this is not true and these degenerate arrangements must be disambiguated by further experiments (Chen et al., 2004; Egelman, 2007; Zhang and Hinshaw, 2001). Because this sorting is reference-free it requires no *a priori* knowledge about the number of states or symmetries of the assembly. The classification algorithm will group segments based on their features alone, deriving the distribution of symmetries directly from the data. This is an important point because existing methods for sorting require a model to be generated for each symmetry in the data. Since Dam1 spirals contain many disordered turns (turns without a constant helical symmetry), we failed to generate models that could sort our data to homogeneity. Reference-free alignment and classification avoids this difficulty. Class averages and their power spectra quickly make it clear which groups are characterized by disorder or have a specific helical symmetry. This type of iterative, reference-free alignment and classification of images has been used very successfully to reduce heterogeneity and reconstruct samples during single particle analysis of asymmetric samples (Frank et al., 1996; Ludtke et al., 1999; van Heel and Frank, 1981; van Heel et al., 1996). When confronted with a large degree of heterogeneity, as caused by the highly variable symmetries in the Dam1 helix, we must isolate one or a few well ordered turns from a mostly disordered filament of tens of turns. This sparseness of order makes any type of 'ensemble' image processing, (i.e. averaged power spectra), impossible. In fact, during our analysis approximately 80% of

segments were classified into groups without constant, well defined pitch and diameter, indicating that these segments did not preserve even short range helical order, (Fig 3b). This is unsurprising given the large amount of disorder in filaments seen as the single broad layer line in Figure 13. This initial step dedicated to finding the segments that belong to the same type of helical symmetry, while excluding disorder, is a key step in single particle helical reconstruction.

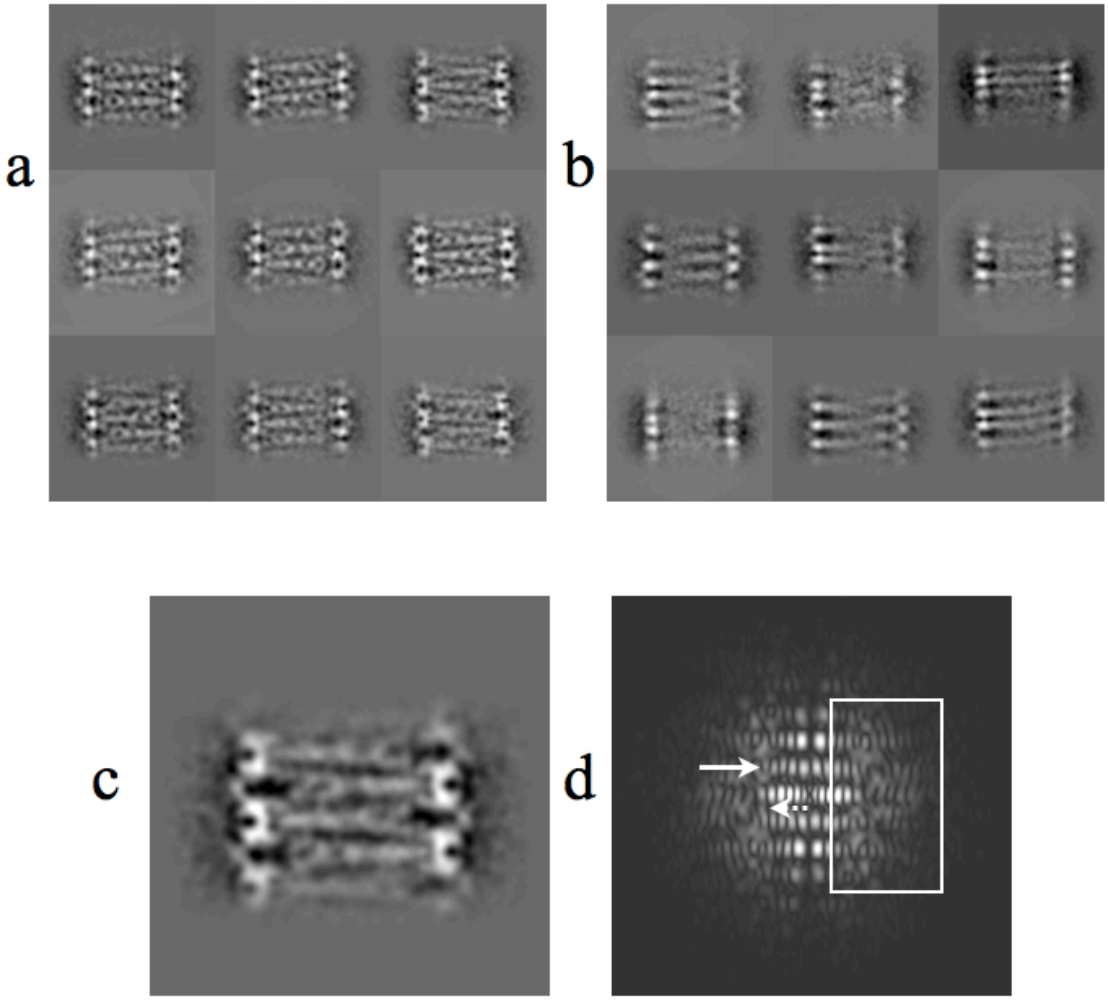

Figure 15 - a) Class averages that represent well ordered particles of homogeneous symmetry based on a visual assessment of their features. Averages with sharply defined edges and a clear repeat along the spiral were said to be 'well ordered'. b) Averages from the same classification whose features are blurred and represent disordered segments or minority groups such as the small number of particles that have a specific out of plane tilt. c) Class average used to generate the initial model for refinement. While there are clear features along the length of the spiral they cannot be interpreted directly to give helical parameters. d) Power spectrum of the image in (c). Layer lines corresponding to the pitch of the helix (white arrow) are strong and clear while those describing the number of subunits per turn (area inside white box) are broad and overlapping. This overlap, stemming from the small number of turns in the average, prevents indexing by conventional methods. However, their distance from the meridian, (dashed arrow), gives an estimate of the number of subunits per turn. Further, from the image this is clearly a 1-start helix with a 2-fold axial symmetry. Taken together these narrow the range of helical parameters sufficiently to test them by convergence during refinement.

During 2D processing, classification separates helical particles based on several features, which are, in decreasing order of scale in their effect on the image: diameter, pitch, out of plane tilt, and azimuthal angle. Changes in these parameters dominate other characteristics and help us separate segments primarily based on these properties. Eigen images generated during Multivariate Statistical Analysis (MSA) classification have been a powerful tool for visualizing and sorting size differences during single particle processing, (White et al., 2004). This can be seen clearly in Figure 16. The major eigen images, (Fig 16a), contribute heavily to the separation of images into classes and describe the features of varying pitch/diameter or amount of disorder but have essentially no features from the repeating unit. Later eigen images, (Fig 16b), contributing less, show the repeat of Dam1 along the helical lattice very strongly. MSA analysis based on symmetry can be clearly shown in eigen images and this implies that the sorting techniques used for other single particle samples with symmetry and size heterogeneity are effective for helical samples as well, (Orlova et al., 2000; White et al., 2004).

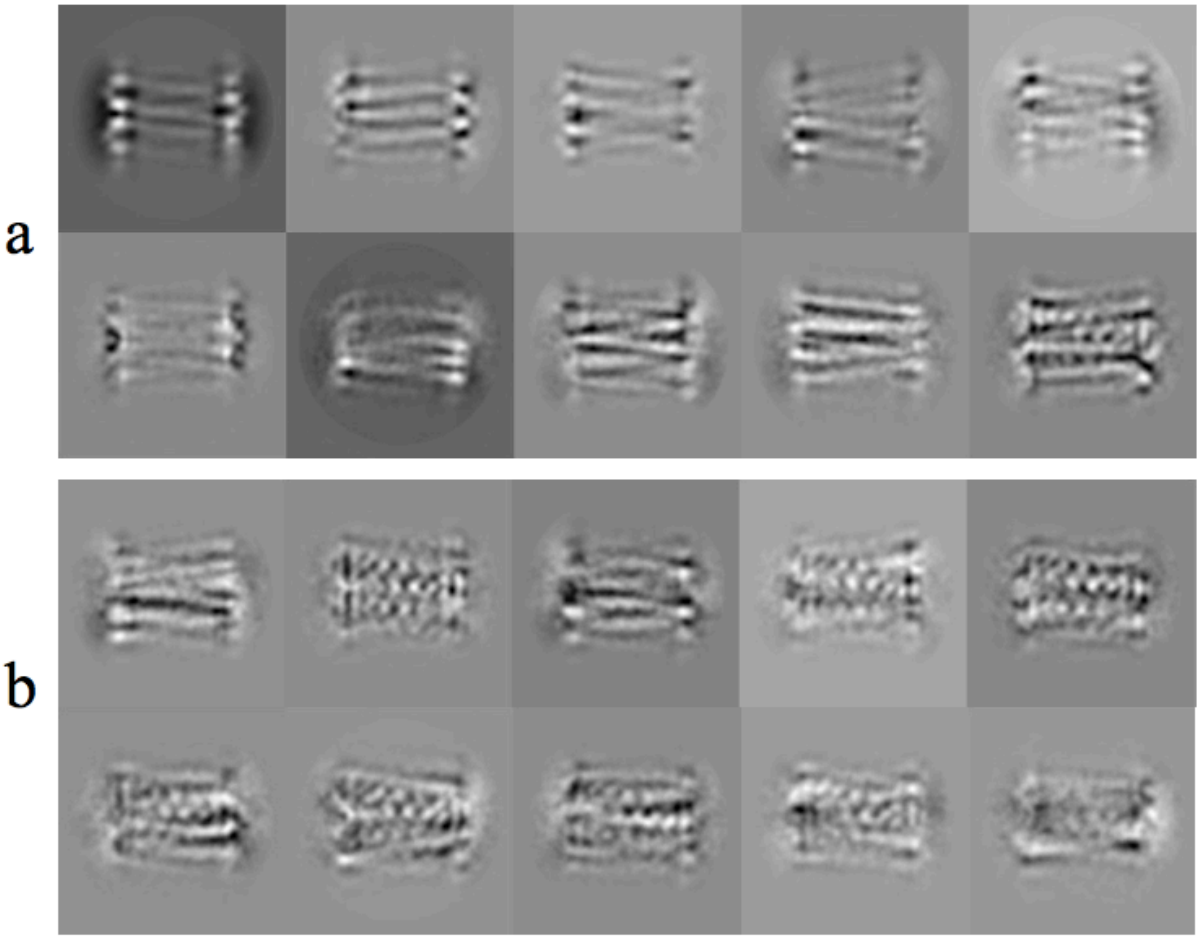

Figure 16 - Eigen images generated during reference-free 2D alignment and classification using MSA. Eigen images are ordered with respect to their contribution to sorting (i.e. those with biggest effect first) a) First ten eigen images. These describe large, strong features in the spirals. Except for image number ten these all describe the positions, pitch, and diameter of spirals and lack features corresponding to the repeating unit. b) Eigen images 11-20 which mainly contain the repeating pattern of the complex around the spiral. Taken together these 20 eigen images efficiently sort helical segments based on their pitch, diameter, and view into classes characterized by homogeneous symmetry or disorder.

Estimating Helical Symmetry

Once a class average of helical segments with homogeneous symmetry is obtained it can be used to estimate initial helical parameters for that group, but also, due to its unique symmetry, to generate a 3-D reconstruction (Fig 17). Helical symmetry has the special property that all of the information needed for a 3-D reconstruction exists in a projection that is perpendicular to the helical axis, assuming that there are a large number of subunits per turn or helical repeat. Correct helical parameters, the twist (°) and rise (Å) per repeating unit that defines the helical arrangement, are essential to accurately determine a structure. The second key step of reconstruction after calculating homogeneous classes is therefore assigning symmetry values to those classes with a visually well-defined pitch and diameter. A huge number of symmetries are possible for any given assembly but these can be narrowed down to only a few by careful inspection of the power spectrum of class averages and knowledge of the size of the repeating unit. By including later eigen images in the classification, or using a large number of classes, averages show the features of the asymmetric unit, (Fig 15a). The high amount of signal and homogeneity of symmetry make power spectra of averages very strong so that the positions of layer lines can be determined. Indexing the Fourier transform of such averages using conventional helical methods can help define its lattice and therefore its symmetry in terms of twist and rise. In cases where a single turn per segment is needed to sort extreme heterogeneity, such as for the Dam1 complex, exact indexing is impossible due to layer line broadening. However, the possible symmetries of the sample can still be greatly reduced, (Fig 15d). First, visual appearance of the average and the meridional distance of the layer line describing the 150 Å pitch confirms it is a one-start helix. Second, the distance of the broad lines from the meridian, (dashed arrow in Fig 15d), points to an asymmetric unit size of ~100 Å along the spiral, very close to the final value of 107 Å. Calculation of the path length of the spiral in one turn,

$$L^2 = C^2 + P^2$$

Where C is the circumference of a circle with the diameter of the helix, P is the pitch, and L is the path length leads to a value of ~1,570 Å for Dam1 spirals of the dominant symmetry. An asymmetric unit length of 100 Å implies ~15.7 subunits per turn and a twist 1.6° different from the correct value found after refinement.

Classification and alignment generates averages that can be used for finding symmetry and making an initial model by applying that symmetry. But just as importantly the procedure groups segments based on their features. After 2-D processing we have, for each class: an initial model, symmetry parameters, and the homogeneous group of raw segments from which these came. We can therefore follow a projection matching scheme identical to those used in other single particle helical reconstruction approaches, but for each class separately (Egelman, 2000). During each individual refinement, every segment from that class is matched against reprojections of that class reference volume. It is assigned Euler angles, which define its orientation in 3-D space, based on its best matching view and this information is used to reconstruct a new 3-D model without applying symmetry. Using programs developed by Egelman, we

search for the intrinsic symmetry of this volume to gain more accurate helical parameters. These are then applied to segments to create a helically symmetric reconstruction that will more faithfully reflect the data. This model in turn can be used for another cycle of projection matching, and the process is iterated until it converges to a final, stable structure. Underlying the importance of accurate estimation of the helical parmeters, we have observed that beginning the refinement for the Dam1 assembly with an estimate of the twist per subunit that was off more than 2˚ from the correct 24.6˚, invariably diverged into an incorrect structure, which we could discriminate based on its dissimilarity in projection to the reference-free class average from which it was derived.

It has been shown that an initial model resembling the sample is not required to correctly refine a helical structure as a cylinder has been used successfully in many cases, (Egelman, 2000, 2007; Galkin et al., 2006). While this is also true of the Dam1 complex we observed a shorter convergence time when starting with a model generated from class averages. The extra constraint of starting with a model with the correct pitch, diameter, and low-resolution features seemed to confine segments to roughly their correct angles from the beginning. Whether this would make the refinement converge from a wider range of symmetry values was not exhaustively tested and is still an open question.

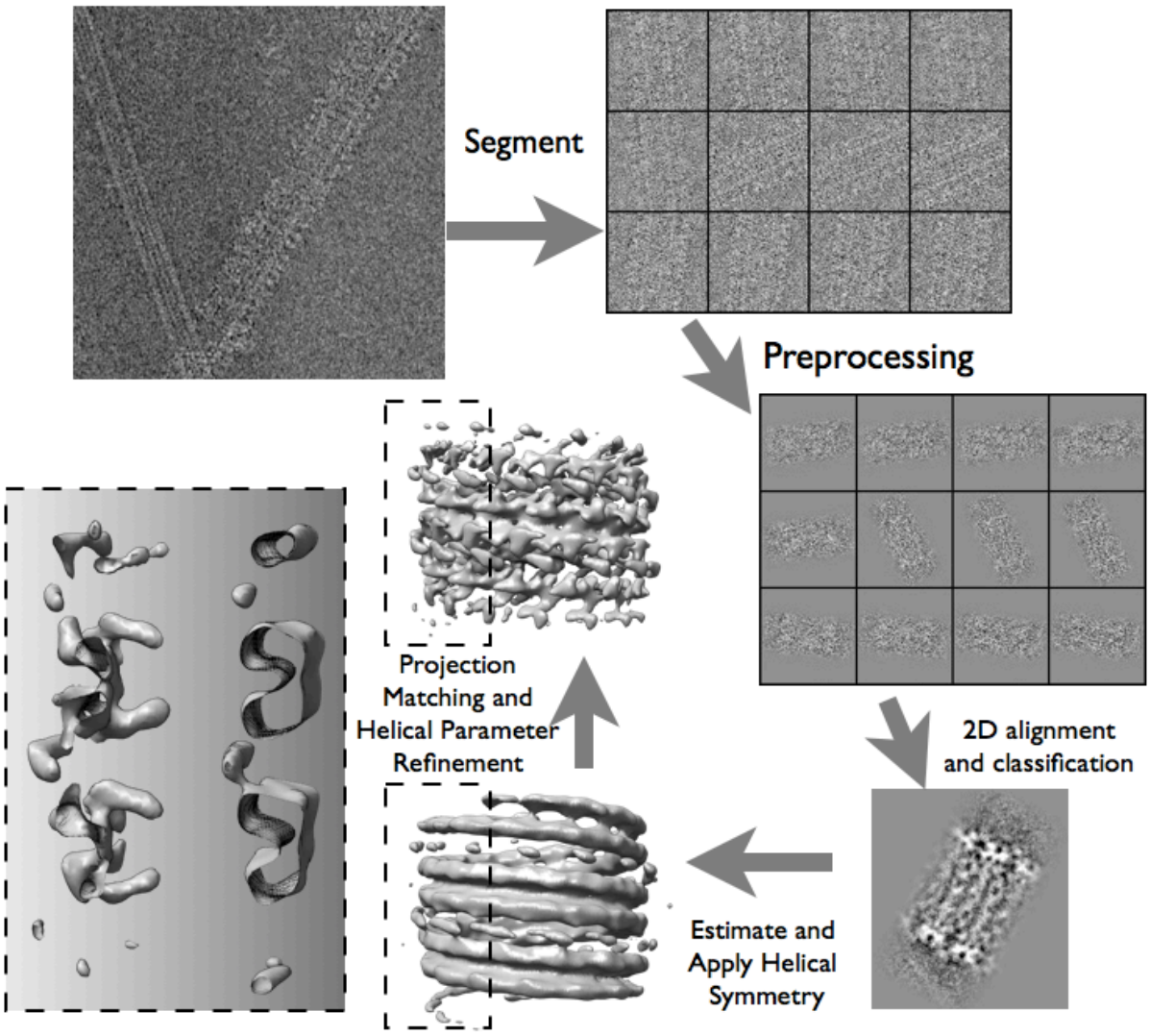

Figure 17 - Visual overview of the reconstruction process. Helical segments are boxed, processed to remove the microtubule, and then aligned and classified to reduce heterogeneity. 2-D averages can then be used to estimate helical symmetry and create an initial model for refinement by single particle methods. Inset at left compares a central slab from one side of the initial model (right) with the refined structure (left). This area is indicated on the full structures by transparent boxes. The two have the same general morphology but fine features are gained as refinement progresses. This comparison is a quality control step to ensure refinement progresses smoothly to the correct structure.

Real Space Helical Reconstruction of Dam1

The application of our algorithm to Dam1 spirals proceeded as shown visually in Figure 17. Overlapping segments are selected from digitized cryo-EM micrographs of Dam1 decorated microtubules. The approximate in-plane angle of each segment is estimated based on its orientation and used to process each particle. Specifically, this angle was used to project the segment along its axis for microtubule protofilament removal and 40 Å layer line editing. Both of these masks were created with a temporary, vertical version of the segment and then were applied to the raw image to prevent losing accuracy by interpolation. Each segment was then boxed with a small, soft rectangular mask of fixed size, leaving between one and two turns of the helix per segment. This was done to make the classification as fine grained as possible and thus take advantage of data that was only ordered on the small scale of one or a few turns. After this preprocessing was completed, segments were subjected to automated, iterative 2D alignment and classification. Class averages showing the sharp features of a well-ordered assembly were then carried forward for 3D processing.

One predominant, helical symmetry became clear from the class averages. Its parameters were estimated by measuring its pitch, the off meridional distance of layer lines, and the known size of the complex from images of unassembled Dam1, (Wang et al., 2007). A range of symmetries were applied to a representative, ordered class average, (Fig 15c), with values ranging from 20˚ to 27˚ twist, or 13 to 18 subunits per turn, and an 8 to 11.5 Å rise selected to preserve the known pitch. Each was then used a starting model for projection matching refinement using that symmetry as the initial estimate and the members of that single representative class as raw particles. This class included 286 segments for a total of ~8500 asymmetric units. Volumes refined with a twist of 24˚ ± 2˚ converged to a common solution whose projection matched both its reference-free class average and the existing structure. The final helical parameters of 24.6˚ and 10.2 Å are very similar to 24.7˚ and 10.24 Å determined by conventional methods during our previous studies, though different data were used, (Wang et al., 2007). This shows that we found turns of the same symmetry that had previously generated multi-turn helical crystals.

The major features in this new, real space reconstruction are in good agreement with our previous structure from conventional helical reconstruction methods, (Fig 18) (Wang et al., 2007). The maps superimpose well, with the protrusion from the Dam1 spiral towards the microtubule, the bridge between adjacent turns, and the main body of the spiral all strongly showing the same morphology. As before, this assembly is a one-start helix made of two anti-parallel head-to-tail arrangements of the complex. To quantitate the similarity of the two structures, a Fourier Shell Correlation (FSC) (Fig 18c) of the asymmetric unit and a phase residual over their corresponding layer lines was computed. The 0.5 FSC cutoff at 30 Å coincides with the resolution of both maps, confirming that they are nearly identical over all features. The phase residual over all layer lines within 30 Å was 43°, however, several of the layer lines were barely over the noise level in the power spectrum of the previous helical structure. The phase residual

calculated over the strong layer lines in both structures yielded a value of 30°, with 47˚ for the 30 Å layer line, which indicate good agreement all the way to this resolution.

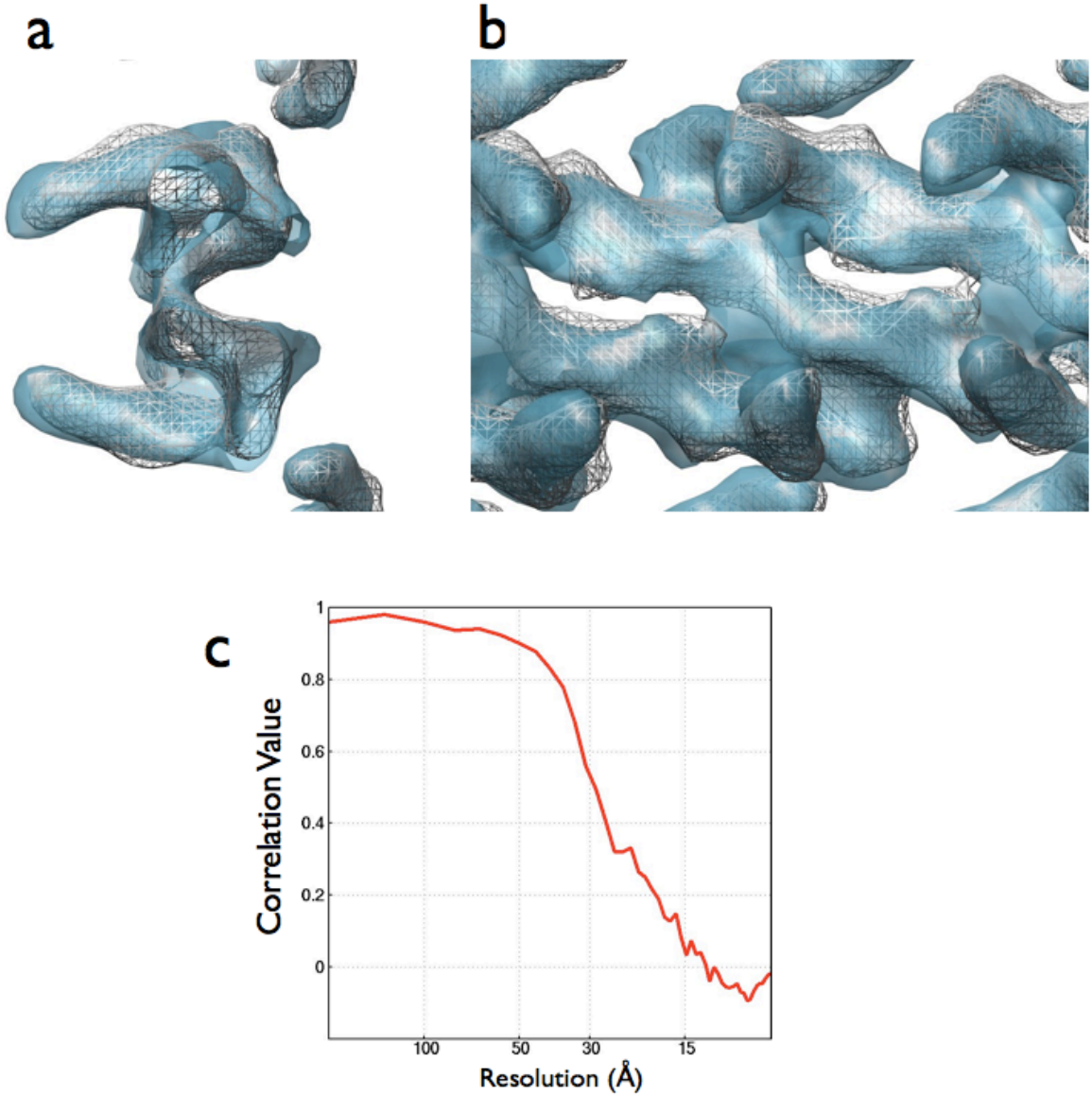

Figure 18 - Superposition of structures of the assembled state of Dam1 by traditional methods (gray mesh) and currently presented single particle methods (solid blue). a) Slice of a side view of the volume. The microtubule wall would be to the left. b) Inner surface view. This view is from the microtubule looking outwards. The good agreement in (a) and (b) is quantitated in c) the Fourier Shell Correlation curve for the two structures. The 0.5 cutoff occurs just above 30 Å, which is the resolution of both reconstructions.

Chapter 3 - Structure of Dam1 Complex Assembled around Microtubules

Motivation

Dam1 acts as an essential piece of the bridge between the spindle microtubule and the inner kinetochore (Westermann et al., 2007). *In vitro* it can recapitulate essential properties of the kinetochore: plus-end tracking and carrying a load poleward along depolymerizing microtuble ends (Asbury et al., 2006; Franck et al., 2007). The first EM images showed the complex assembling into rings around microtubules, a geometry that has obvious appeal as a processive coupler. Since its oligomerization is so critical to its function *in vivo* and modifying its ability to assemble is the mechanism by which Ipl1 phosphorylation appears to regulate its function (Kang et al., 2001; Shang et al., 2003; Wang et al., 2007), the structure of the complex assembled around microtubules is a key piece of information needed to understand the Dam1 complex.

Structural Targets

At the beginning of my project a low-resolution structure of helical Dam1 around microtubules had been solved (Wang et al., 2007). The resolution was limited by the sample's disorder. But it was unclear if there was sufficient order on a smaller scale that could not be taken advantage of by the classical methods. As discussed in the previous Chapter, I created a set of computational tools to overcome any methodological hurdles to determining a high-resolution structure. Therefore it remained to find the optimal sample for imaging and reconstruction, the main criteria being robust order.

Order is the most important criterion for this sample because it is the limiting factor in getting to high resolution. With the size of each assembly ranging into the several Mega-Dalton, alignment and classification of each segment is nearly perfect. There is a huge amount of signal. The step that degrades resolution is the application of symmetry when the imaged particles are not perfectly symmetrical.

See Protocols section for descriptions of the conditions needed to generate each of these assemblies of Dam1 around microtubules.

Spirals

At high, non-physiological concentrations, Dam1 assembles around microtubules in spirals. This has been seen robustly for WT, DelC, and Ask1p-MBP Dam1 complexes (Fig 19). They are always 1-start, double (anti-parallel) spirals and do not follow the symmetry of the microtubule. There are approximately 15.5 complexes per turn and one turn approximates an open, lock-washer ring. The densest part of the complex sits back approximately 10 nm from the microtubule lattice, reinforcing the idea that flexible connections are involved in their binding. Further underscoring that idea is

the measurement of the distance between spirals. At 21 nm per turn the spiral helical pitch does not match any integer repeat of the microtubule lattice, which is either 4 or 8 nm depending on whether you consider a tubulin monomer or dimer. A flexible linker must bridge this gap and may not have any specific binding site on the microtubule lattice.

The main drawback of this assembly state for helical reconstruction is that they exist with a continuous distribution of helical symmetry parameters even within a single spiral. Each subunit has a slightly different twist and rise relative to its neighbors and therefore coherent averaging of spiral images is not possible. If this distribution of symmetries is not widely spread we may still achieve fairly high resolution as the error in averaging is still rather small. However, no conditions were found that trapped a highly ordered helix. As a further hurdle the helical symmetry must be computed during the calculation of the structure, making the reconstruction of the helical objects somewhat more technically demanding.

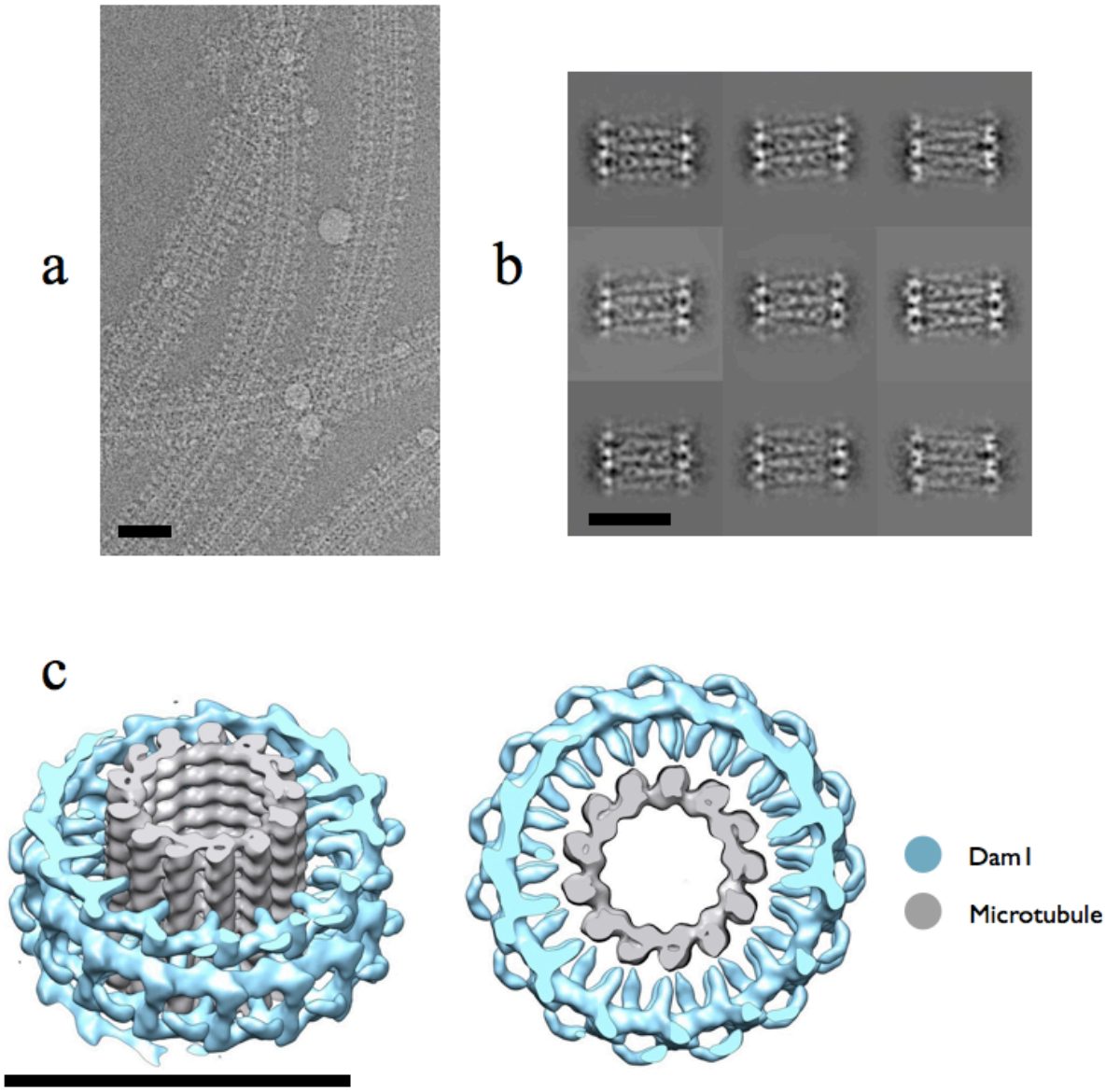

Figure 19 - Reconstruction of wild-type Dam1 spirals. a) Cryo-EM micrograph of 5 microtubules fully decorated by Dam1 spirals. b) Class averages showing groups of well ordered segments used for further processing. c) Tilted and top down renderings of the final structure. A long arm stretches out from each repeating Dam1 monomer to contact different points on the microtubule surface. The resolution of this reconstruction is ~3 nm. Scale bars are 50 nm.

Single Rings

Single rings are the most readily formed oligomer of Dam1 around microtubules (Fig 20). They appear with nanomolar concentrations of Dam1 and saturate the microtubule lattice as more is added. A protocol for making a dense but not packed decoration of Dam1 rings is included in the Materials, Methods, and Protocols Section.

Rings are an ideal target for reconstruction as they are proposed to be the physiological form of Dam1 at the kinetochore. They are also good samples of EM due to their high amount of rotational symmetry. Rotational symmetry is qualitatively different from helical symmetry in that it is discrete. There are an integer number of Dam1 complexes per ring. This small number of possible symmetries, further constrained by knowledge of the complex size and previous images of rings, simplifies the task of reconstruction further.

Likely because of these advantages, the ring reconstruction has the most detail and affords the best docking of the unassembled dimer structure (Figs 20, 23). However, attempts to push the resolution further through additional data collection were unsuccessful. In fact, aside from the single microscopy session that yielded the high-quality ring structure shown in Fig 20, no other imaging sessions produced data that would refine correctly to a low-resolution structure. Close observation of micrographs revealed qualitative differences between some rings: Some had high constrast ‘strands’ extending out, perhaps denatured proteins. Others were dense, compact disks and some contained internal details without having ‘strands’. These ring phenotypes co-existed in single micrographs and were uniform within a single microtubule. This suggests that different environments inside the reaction tube or just prior to blotting may drastically affect the structure of the ring. My untested opinion is that neither of these first two types of rings is suitable for reconstruction and that only 'detailed' but not 'exploded' rings yield anything meaningful. However, what causes each type of ring to appear in the images and what they represent is unknown. This heterogeneity prevented collection of a high-resolution set of ring images.

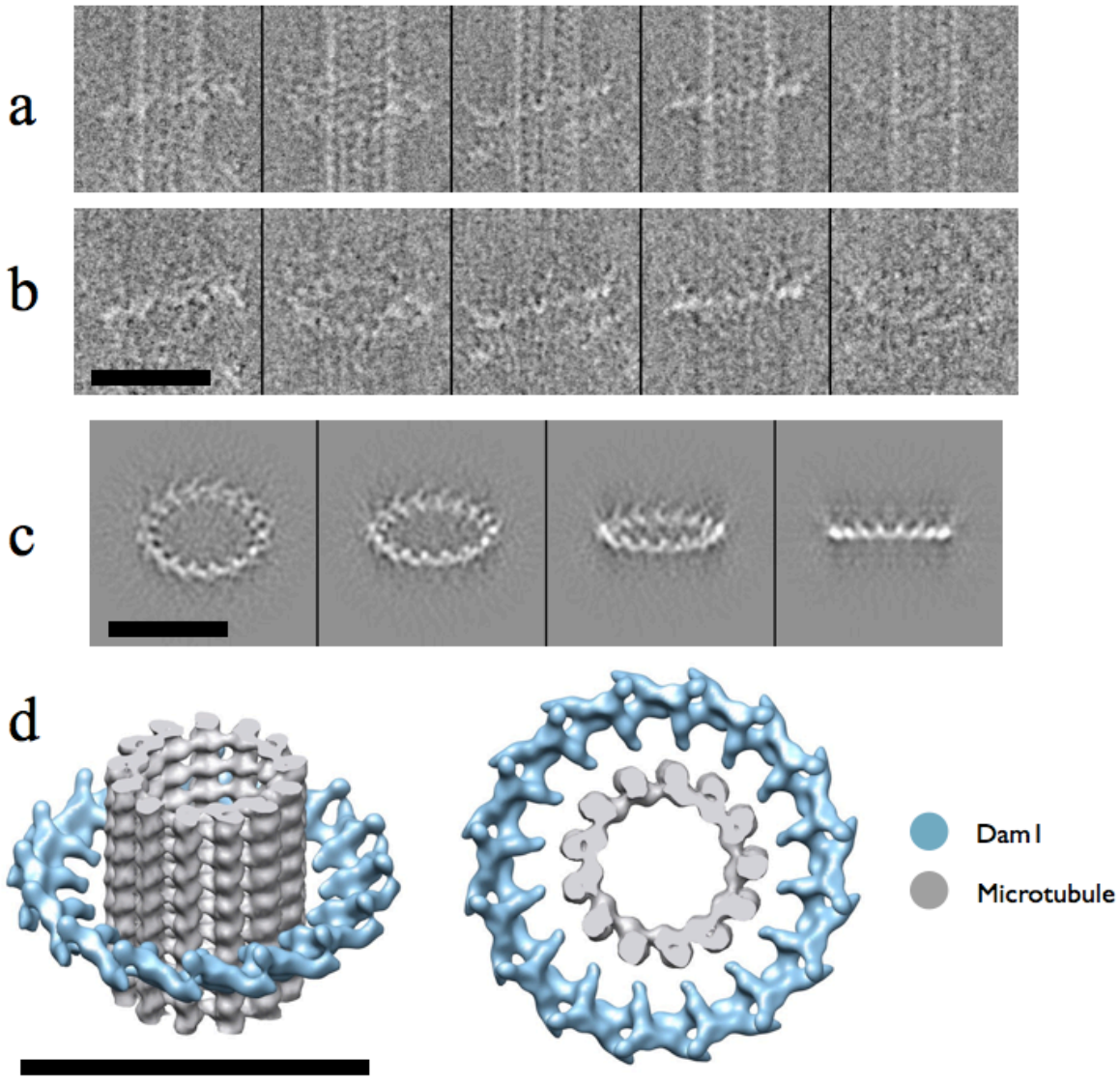

Figure 20 - Reconstruction of the Dam1 ring assembled around microtubules. a) Gallery of 5 rings from the dataset. b) Images from (a) after microtubule has been computationally removed to allow for further processing. This step is expained in detail in Figure 14. c) Reprojections of the final structure. d) Tilted and top down renderings of the Dam1 ring structure assembled around a microtubule. Each monomer connects to its neighbor at two points and extends an arm towards the microtubule. Scale bars are 50 nm.

Stacked Rings

While searching for conditions that would tighten the packing of the spiral form of Dam1 I discovered a low pH buffer condition that promotes the packing of rings on microtubules (Fig 21). At pH 5.8, the calculated pI of the complex based on sequence, rings pack head-to-tail along the microtubule and lock together forming a helical tube. This is an exciting structural target because it combines the best characteristics of rings and spirals. The repeating unit is a physiologically-relevant ring, while the geometry of the assembly could perhaps lock in a high amount of order and prevent whatever was degrading the resolution in images of single rings.

Initial reconstructions were again limited by the disorder of the sample (Fig 21a). This prompted a screen for conditions that could lock the rings together. It seemed that if changing the pH could have such a dramatic effect on ring packing, perhaps another change in the buffer could further improve packing. To test this I tried approximately 30 conditions that included changes in temperature, incubation time, salts, metals, and organics taken from the crystallization additive screen from Hampton Bioscience (hamptonresearch.com). My assay was the qualitative assessment of order in the stacked rings in negative stain, which limited throughput. While some conditions appeared marginally better to the eye, none obviously had the large change to robust order that I was seeking.

The final structure, at 3 nm resolution, agrees extremely well with the other reconstructions of WT Dam1. The reconstruction of the single ring is superimposable on one ring of the stack. Each ring is rotated 11.25 degrees from the next, exactly half the amount between one subunit and the next within a ring. A protruding arm, predicted to be Spc34p from dockings, is the only point of contact between rings and this lack of a large amount of buried area is perhaps the cause of the disorder seen regularly in this assembly. The repeat distance between rings, 6.8 nm, again underscores the mismatch between the Dam1 and microtubule symmetries and the idea of a flexible, electrostatic attachment.

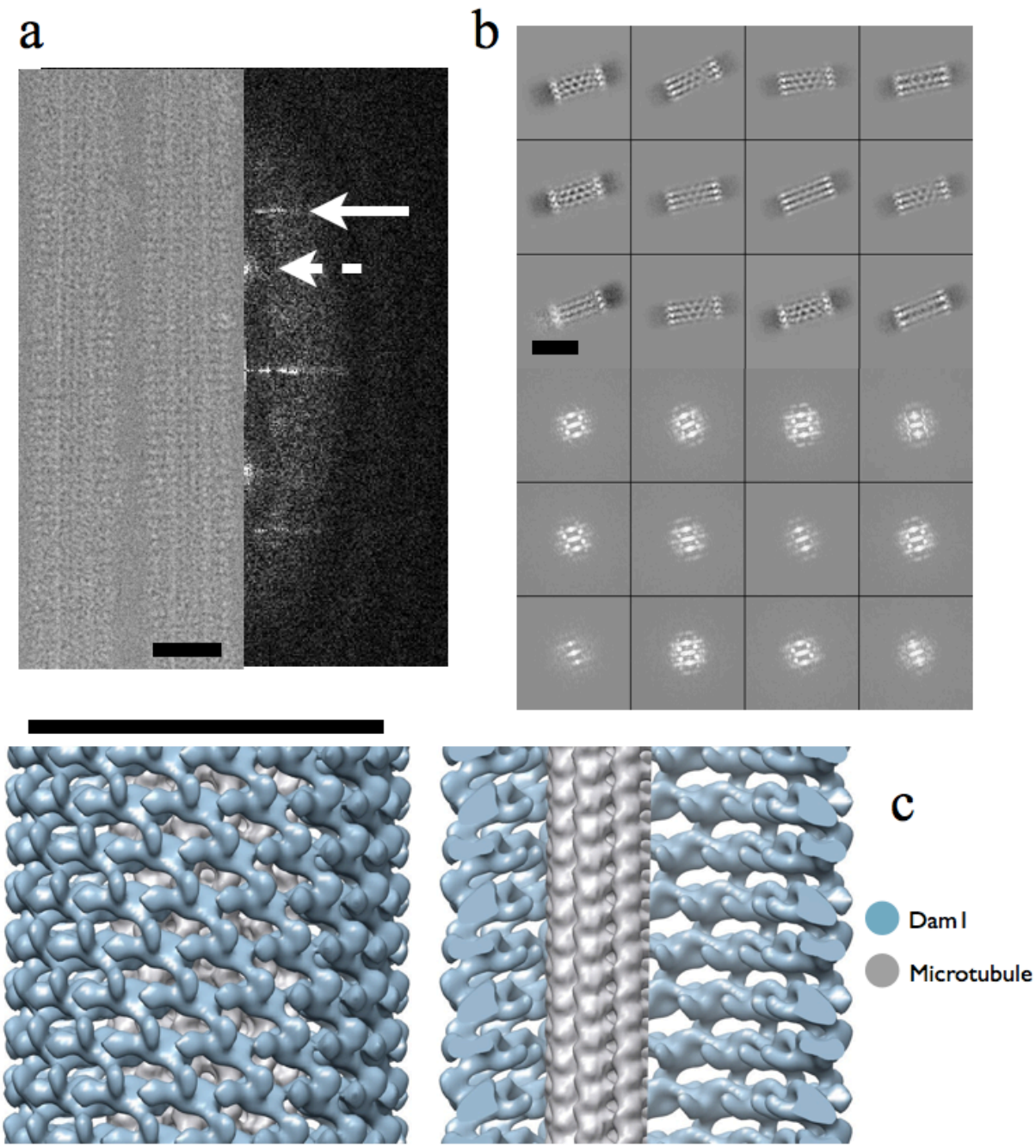

Figure 21 - Reconstruction of stacked Dam1 rings around microtubules. a) Micrograph showing two stacked ring decorated microtubules, left, and its power spectrum, right. The diffuse reflection highlighted by the dashed arrow shows a high amount of disorder between rings. b) Class averages of stacked ring segments, top, and their power spectra, bottom. Reference-free alignment and classification has made homogeneous populations with much improved order, as evidenced by the increased number of visible layer lines in their power spectra. c) Side and side cut-away views of the final structure. Each ring in the stack contains 16 monomers and is at this resolution essentially identical to the structure of the single ring. Like that structure, each monomer contacts its neighbors at two interfaces and directs an arm inward towards the microtubule.

Summary of Reconstructions

All three samples were approached similarly for their reconstruction. Each assembly did not follow the symmetry of the microtubule and so the contribution of the microtubule in each segment was removed as discussed in Chapter 2. Classification, followed by symmetry estimation was performed for the spiral and stacked ring structures. For the single rings there weren't enough particles for reliable classification and so symmetry heterogeneity was sorted in 3D with multiple models. Each of the three samples yielded reconstructions to ~30 Å resolution. The helical samples never yielded class averages showing layer lines to higher resolution than 30 Å, pointing to disorder as the culprit. Removing 50% of the data from each reconstruction and recalculating the map did not result in noticeable degradation of resolution, (not shown), suggesting that they were not limited in resolution by signal.

Each of the three reconstructions resulted in the same shape for the repeating unit and can be aligned easily against each other (Fig 22). The most striking common feature is the protrusion bridging the main density of the Dam1 complex and the microtubule wall, (a distance of ~100 Å). This was initially thought to correspond to the hooked arm coming out of the central bulb in images of the unassembled structure and images of rings that had fallen off of microtubules, due to their similar size. This argued for a docking and a model where a large conformational change occurred in the Dam1 complex upon microtubule binding.

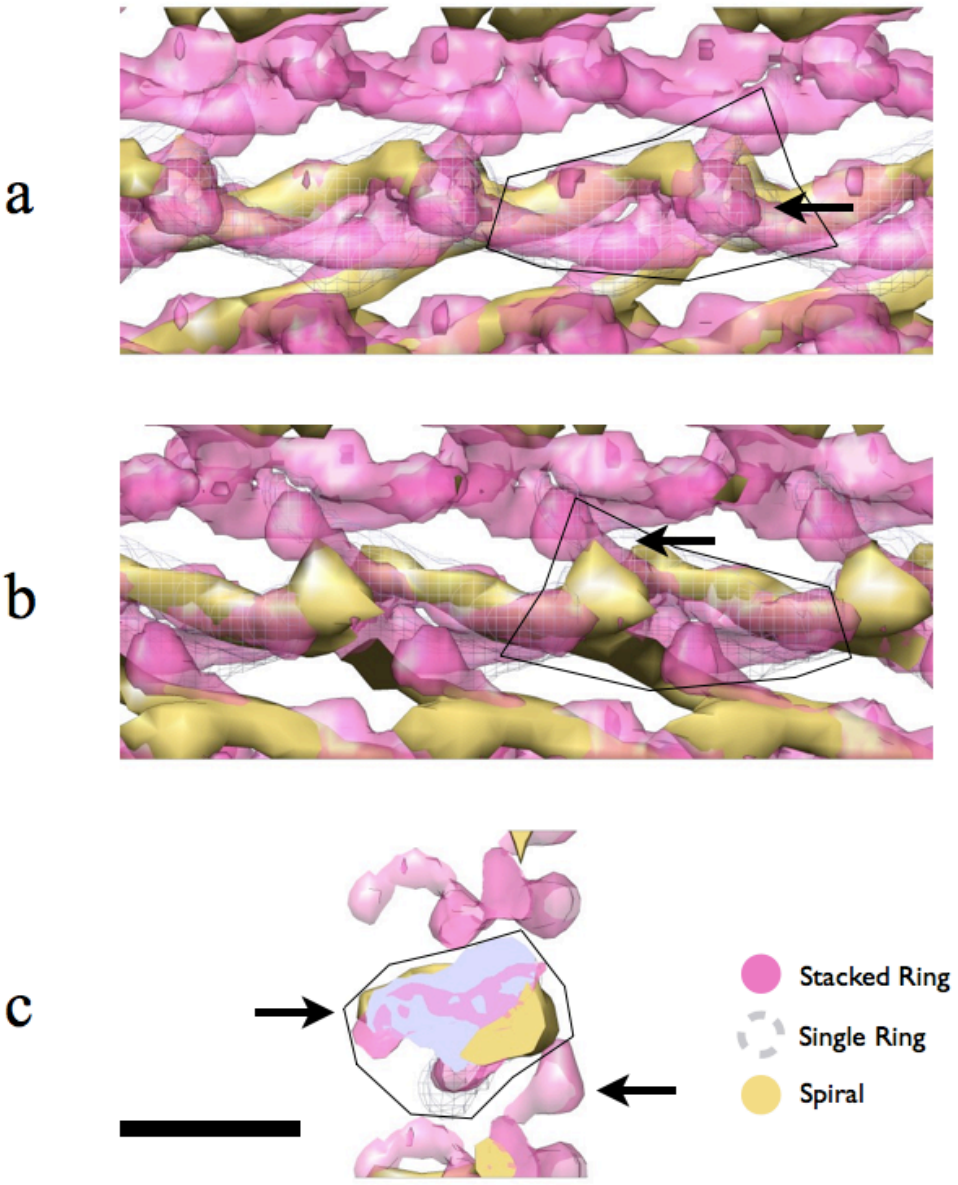

Figure 22 - Aligned views of stacked ring, single ring, and spiral reconstructions of wild-type Dam1 complex. In each panel the volumes have been rendered as translucent pink, blue mesh, and gold surface, respectively. The repeating unit, a monomer of Dam1 complex, used to align the assemblies is outlined in black. Each reconstruction shows a central angled bar with two arms extending out towards opposite directions. Angled bar highlighted as dotted line, arms highlighted with arrows. a) Inner view of these assemblies as would be seen from the microtubule, looking out. Arrow highlights the protruding arm that contacts the microtubule. b) Outer view. Arrow highlights opposite arm which extends from the top surface of the ring, perhaps to interact with other kinetochore complexes. C) Side view rendering a thin slice to generate a clear profile. Microtubule would be on left side. Scale bar is 10 nm.

Docking of Unassembled and Assembled Structures

While imaging Dam1 complex alone at high concentrations under cryo-EM conditions to improve the unassembled structure I observed closed rings (Fig 8). This was the first time we had seen closed rings in the absence of microtubules and it suggested that a large conformational change induced by the microtubule was not necessary for ring formation. With this new suggestive result in hand I revisited the docking, this time to the ring structure which did not exist during our first attempts at explaining assembly. Eight Dam1 dimers clearly fit into the ring with no observable conformational rearrangement if the arm coming from the central density was allowed to point outward instead of in, as previously inferred (Fig 23) (Wang et al., 2007). My attempts at independently verifying this arrangement through labeling have been unsuccessful, with both an Ask1-MBP helical reconstruction, showing extra density on the inner face of the spiral, but other labeling experiments, including a MBP-Spc34p assembly and the DelC-Dam1 helical reconstruction are either contradictory or unclear (Fig 24). The idea that the connections between Dam1 and the microtubule were flexible 'arms' has been proposed (Miranda et al., 2007), which would explain the absence of these domains in the unassembled structure – they only become stabilized and therefore visible after averaging when bound to microtubules.

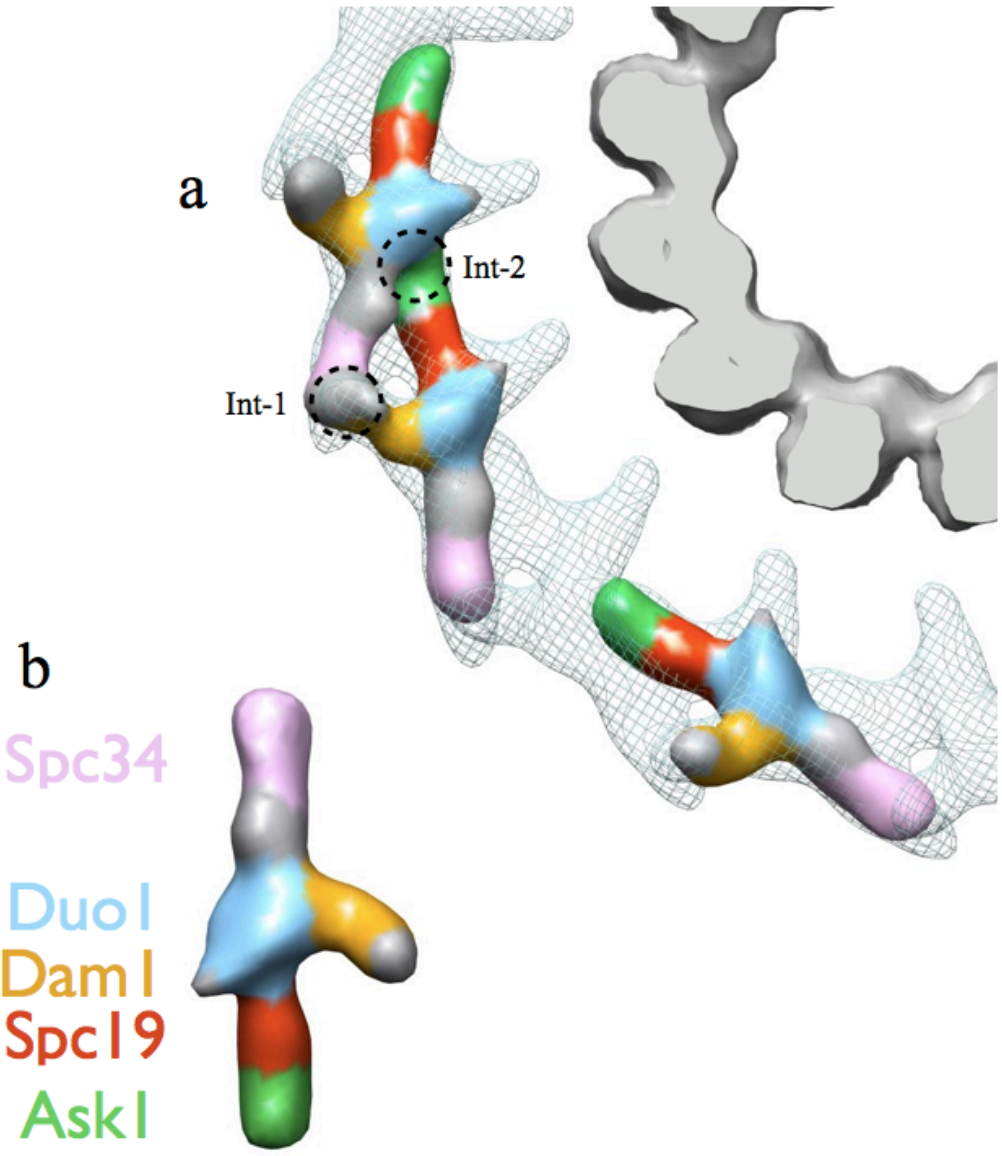

Figure 23 - Docking of subunit-'painted' monomer and dimer structures into the single ring assembled structure. a) Top down view of the docking. Only one quarter of the ring is shown for size reasons and to show detail. Microtubule is in the upper right rendered as solid grey. Dam1 ring is a blue mesh. Both dimer and monomer structures, each colored based on the localizations of MBP labeled subunits, are docked into the ring. The excellent agreement of the densities for both dimer and monomer proves that no large conformational changes occur during ring polymerization, and that the two interaction sites between monomers within the dimer are the same sites used for oligomerization into rings *in vivo*. Interaction sites 1 and 2 are labeled as in Fig 7. b) Dam1 monomer colored the same as (a), based on MBP labeling with the names of the localized subunits.

This updated docking now allows me to 'paint' the assembled structure with the mapped subunits of the complex, generating a model for the interaction sites in the assembled complex around microtubules (Fig 23). The Dam1 ring appears as a fiberous scaffold with two points of interaction between adjacent subunits. Distal from the microtubule the arm coming from the central density interacts with the long domain labeled by Spc34-MBP (Interaction 1). The central density of this arm, shown in gold in Fig 23, is greatly reduced in the unassembled structure of DelC-Dam1, indicating that it is formed at least in part by the C-terminus of Dam1p. Interestingly, a phosphomemetic mutant of Dam1p in which 3 of the 4 phospho-sites sit in this C-terminal region shows greatly reduced oligomerization but unchanged binding affinity for microtubules. In light of the 'painted' docking this makes sense, and would suggest a model where phosphorylation weakens this distal interface and disrupts oligomerization, causing ring breakdown, while leaving the flexible domain that is responsible for microtubule binding unchanged.

The second interface, labeled 2 in Fig 23, is formed by the interaction between the Ask1-MBP lobe and the large, central domain of the next complex. This central domain contains several proteins. From interaction maps and labeling it is predicted to be made of Duo1p and Dam1p, the small proteins Dad1p and Dad3p, and possibly pieces of Spc34p and Spc19p. Therefore it is unclear what exactly constitutes this second interface. Again, like in interface A, this second interface B, may contain phospho-sites that modulate it. Both Dam1p and Ask1p are post-translationally modified. Dam1p is methylated by Set1 and phosphorylated by Ipl1 and Mps1. Mutating these regulatory sites causes spindle defects *in vivo* (Cheeseman et al., 2002; Zhang et al., 2005). Ask1p is phosphorylated at two sites on its C-terminus by Cdc28. Abolishing phosphorylation at these sites *in vivo* sickens temperature-sensitive ask1 mutant yeast (Li and Elledge, 2003).

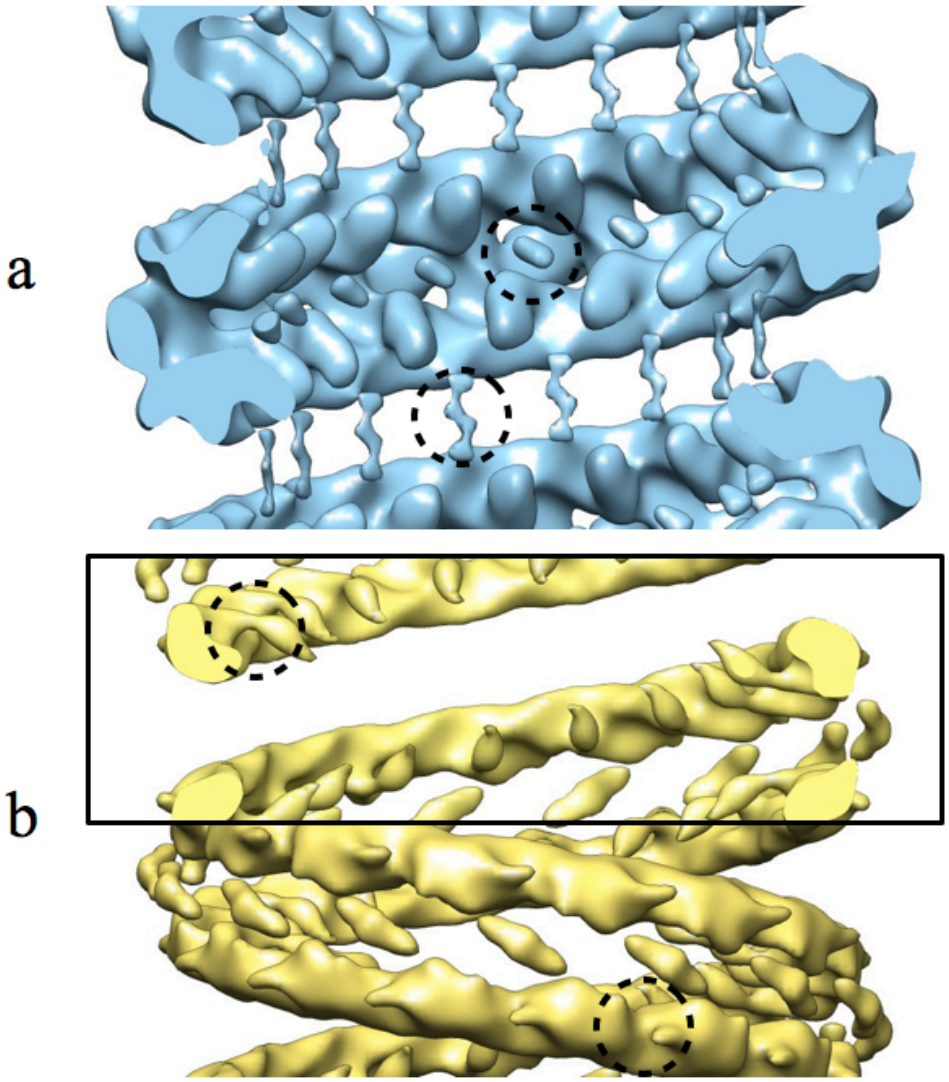

Figure 24 - Reconstructions of mutant Dam1 complexes assembled as spirals around microtubules. a) MBP-Ask1p complex spiral with the front half cut away. Dashed circles highlight two densities not observed in wild-type Dam1 spiral reconstructions as shown in Fig 18a,b and Fig 19. These extra densities are consistent with the prediction from the docking of unassembled Dam1 into the ring that Ask1p would be on the internal surface of the spiral. However, the two densities are too diffuse to accurately localize Ask1p. b) DelC-Dam1p complex spiral. Region inside solid box showing spiral with the front cut away, while the bottom shows full spiral. The two dashed circles highlight regions of lessened density relative to wild-type. The inner missing density (top) is predicted by a previously published docking (Wang et al. 2007) while the outer density is consistent with the current docking shown in Fig 23.

Rings Can Diffuse on Microtubules

In the process of generating the Dam1 ring reconstruction using microtubule-edited segments, each image of a single ring was assigned a tilt angle to bring it into register with its corresponding model projection (Fig 25). By combining this information with the previously measured microtubule angle, we obtained the angle of each ring relative to the microtubule axis (Fig 25c). These correspond to the angle Θ in the work of Efremov et al., however we expect our current measurements to be more faithful representations of the position of the ring since the previous study used images of rings that were dried and stained, a procedure that frequently distorts the sample (Efremov et al., 2007). Applying the maximum tilt angle seen in the distribution, 26 degrees, to the model shown in Figure 3, brings the protrusion of the Dam1 ring to within <1 nm of the microtubule wall (Fig 25b). Further tilt is thus prevented by steric clash between the protrusion and microtubule wall. The histogram of these angles follows an exponential distribution. This shows that the ring does not have a preference for any angles that maximize the number of contacts between the planar ring and the helical pattern of the microtubule. This distribution is most easily explained by a simple spring-like restoring force acting on the ring that increases with larger tilt, perhaps through the increasing steric clash of flexible elements from both sides.

Assuming that the rings we observed are at equilibrium with their surroundings, the distribution of angles tells us about the dynamics of a single ring through time. This conceptual extrapolation is due to the fact that we can treat the frequency of an observed angle, α, also as the relative amount of time any single ring spends in that state. For instance, if we observe 10% of rings tilted by an angle α, we can say that any given ring spends 10% of its time tilted at an angle α. Being able to 'watch' a ring tilt by making this logical leap common to statistical mechanics gives us insight into the mobility of the ring on the surface of the microtubule and tells us whether it is capable of diffusion. If the ring can tilt with a low energy barrier, that is, if tilting is relatively easy, this implies that moving along the microtubule lattice is also easy, since both processes involve making and breaking bonds with tubulin.

The measured histogram of Dam1 ring tilt angles along a MT shows that the Dam1 ring tilts quite evenly with respect to the normal direction of MT surface (from approximately -30 to +30 degrees). There is no obvious preferred angle for which the ring aligns itself to maximize contacts with the helical microtubule lattice. This observation suggests that the Dam1 ring does not “see” the helical arrangement of the tubulin subunits along the MT. Orientations that maximize direct contacts between cannonical motor-binding sites on tubulin (like that of kinesin (Kikkawa et al., 1995; Mizuno et al., 2004; Sindelar and Downing, 2010) and the Dam1 protrusion, such as pointing the Dam1 binding element into the interface between alpha and beta tubulin, are not favored over others. This argues against a previous model of Dam1 binding to the microtubule with a distinct footprint on the lattice (Efremov et al., 2007). In this previous «footprint» model, the ring would jump between specific angles that optimize the number of binding events between Dam1 and the microtubule. This behavior is incompatible with our present observations.

From the distribution of ring tilt angles it also follows that the energy barrier for the MT-bound ring to move between different postures on the helical lattice of tubulin subunits should be equal or less than the thermal noise energy of ~ 1 k_BT. This is essentially stating, in energetic terms, what we observed qualitatively above. The preference for following the helical pattern of the microtubule, if there is such a preference, is so small that it is on the same scale as the thermal energy of the bath in which the reaction sits. This result is significant because it implies that the energy barrier for jumping between adjacent tubulin dimers is also low, since the helical pattern is made of repeating dimers. This parameter, the energy barrier for moving from one dimer to the next, is at the heart of the question of whether the ring can diffuse, with a low energy barrier allowing diffusion and a high barrier requiring large forces for movement. Through a collaboration with theoretical chemist Jian Liu we were able to show using statistical mechanics methods that the ring angles observed do in fact point to a small barrier between adjacent dimer, or monomers, and that in principle the ring should be able to diffuse easily along the microtubule (Ramey et al., 2011).

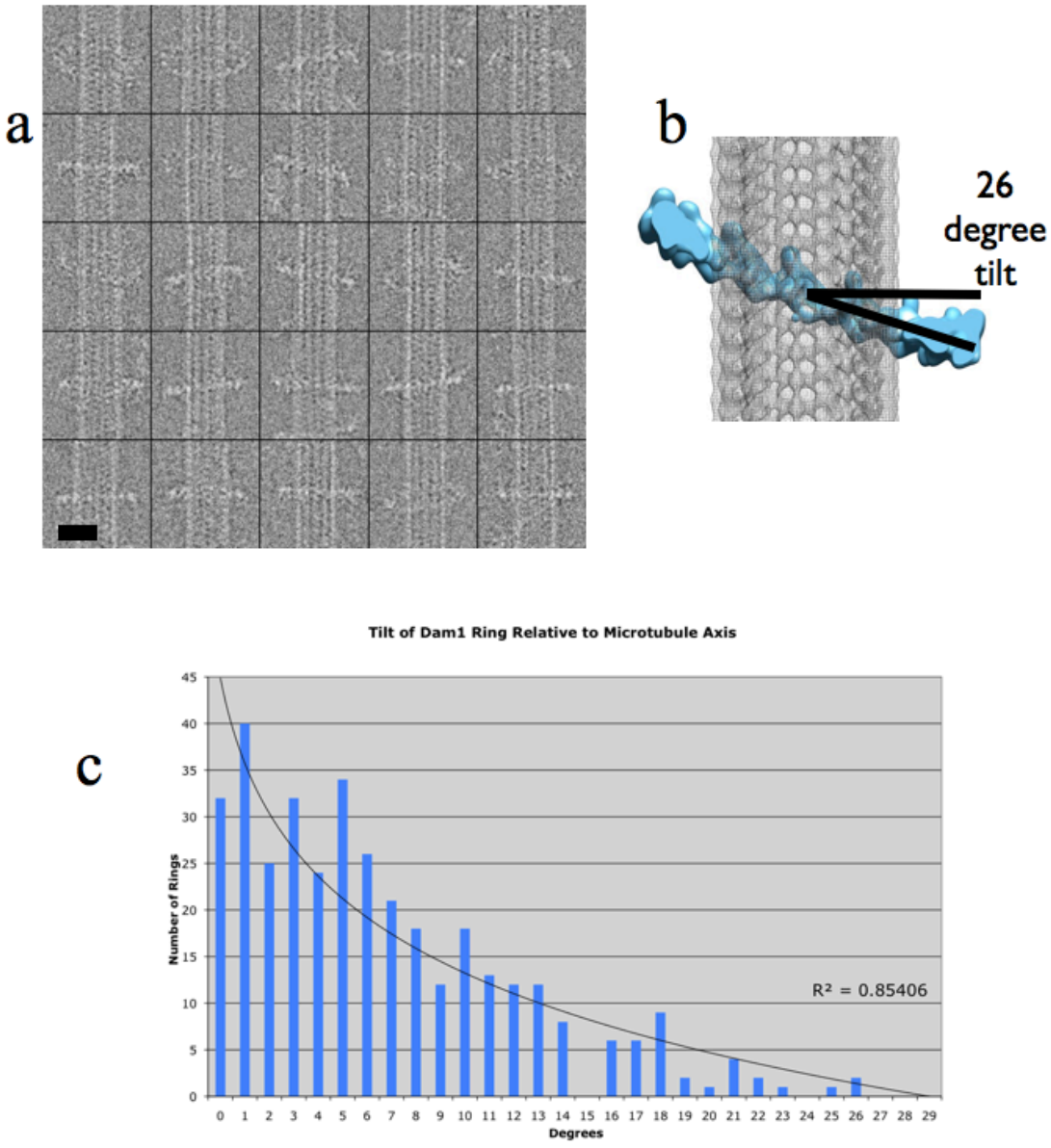

Figure 25 - Calculation of tilt angles of single rings relative to the microtubule axis. a) Gallery of single rings decorating microtubules. Each has a different tilt relative to the microtubule. b) Model of the highest tilt observed in this dataset. A 26 degree tilt would bring the arms extending toward the microtubule wall to within 1 nm. Further tilts are presumably impossible due to steric clash. c) Histogram of tilt angles between the microtubule axis and the plane of each ring. The distribution is wide and is fit well by an exponential. Therefore the ring does not 'see' the helical pattern of the microtubule and can in principle diffuse freely along the microtubule.

Spacing of Rings on Microtubules

Further evidence for a diffusive ring comes from micrographs of Dam1 assembled on microtubules at concentrations ~10 fold higher than those used for the ring tilt data. When imaged under cryo-EM conditions these microtubules show dense but subsaturating decoration by Dam1 rings (Fig 26). What is immediately striking about these micrographs is that rings exhibit a narrow range of distances between them and have a smaller range of tilts, with most being near zero degrees. Distances between neighboring rings were measured based on the location of the center of each ring, as shown in the schematic in Fig. 26b.

If we assume that the ring is not able to diffuse along the microtubule, then it should become anchored wherever it assembles. That is, the MT would provide a periodic energy barrier, and the tubulin subunit length would define its period. In order to hold the ring and keep it from getting across to the neighboring tubulin subunit under the influence of thermal fluctuations, such an energy barrier would have to be higher than 10 kT. Under this assumption, calculation of the equilibrium distribution of the neighboring ring distance can be translated into a well-defined statistics problem: N particles are put on a straight line with M equally spaced binding sites, in which the spacing is defined by the microtubule periodicity (8 nm). Each binding site can accommodate no more than one particle. In collaboration with Jian Liu, we then calculated the statistical distribution of particles along with the resulting neighboring distance between particles if they are placed randomly. A combinatorial calculation shows that $P(j)$, the probability for a neighboring ring distance of j is:

$$P(j) = \frac{(M-j)\binom{M-j-1}{N-2}}{(N-1)\binom{M}{N}} \qquad \text{Eq. [1]}$$

A numerical calculation shows that the equilibrium distribution is a strict decreasing function of the neighboring distance, starting at the distance of 8 nm. This result is very different from the measured histogram, in which there is a well-defined peak at ~ 20 nm (Ramey et al., 2011)(Fig. 26c).

If Dam1 rings do not diffuse, what would be the repulsive forces that could cause this distribution? Under the present experimental conditions, the system is in a solution with a salt concentration equivalent to 75 mM of NaCl. At this salt concentration the electrostatic screening length (Debye length) is 1-2 nm. Although Dam1 rings are positively charged, their electrostatic interaction is thus largely truncated into a short-range repulsion. Therefore, the effective range of electrostatic repulsion between neighboring rings is much shorter than the MT periodicity (8 nm) and, hence, such repulsion will not change the calculated distribution of neighboring ring distance.

Alternatively, the ongoing tilting of the ring while sitting in place could preclude close binding. The tilt angle histogram demonstrates that most of the rings do not tilt very far, with few rings tilting more than 20 degrees. In fact, under the conditions of our

measurements of neighboring ring distance, Dam1 rings tilt significantly less than in the conditions under which we obtained the tilt angle histogram. The half height of the histogram, corresponding to a tilt angle of ~ 10 degrees, would exclude neighboring rings only by 8 nm, given that the outer diameter of the ring is ~ 50 nm. Although this exclusion effect could be at play, it still cannot explain why the observed peak value of the neighboring ring distance is 20 nm.

One could explain our experimental results by invoking a repulsive force that acts to keep the non-diffusing rings from assembling within ~20 nm of each other in a non-diffusive model. However, we cannot envision any such repulsive forces under our experimental conditions that act over such a long range. Our data, on the other hand, can be explained by a model in which Dam1 rings can diffuse rapidly and freely along the microtubule, bouncing off one another and excluding each other from close proximity by steric clash.

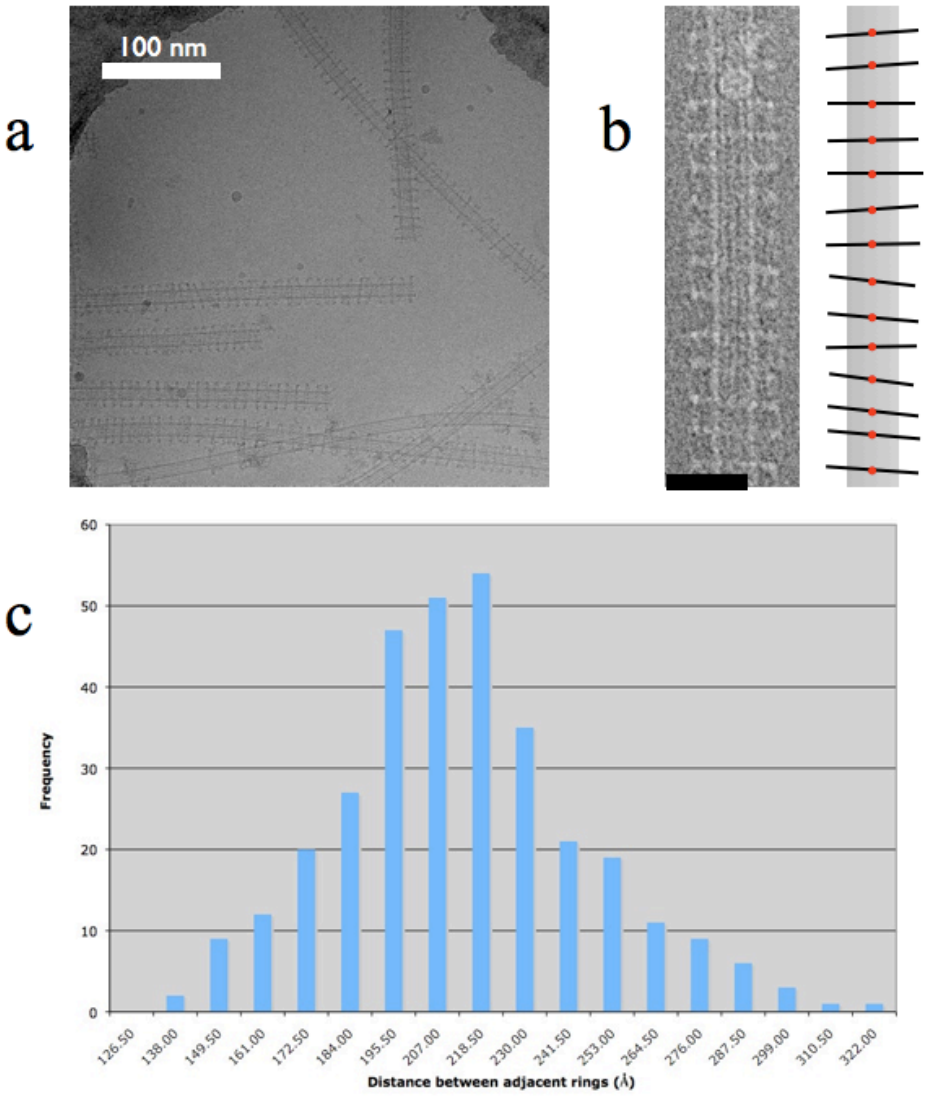

Figure 26 - Analysis of Dam1 rings assembled at high density on microtubules. a) Cryo-EM image of Dam1 rings around microtubules at a higher density than those used in figures 20 and 25. b) Left, image of a densely Dam1 ring-decorated microtubule. Right, schematic of the image. The red dots are the points selected for measuring the distance between rings. The schematic also illustrates the limited range of angles the Dam1 rings adopt when they are close together. We attribute this to steric clash during ring "wobbling". c) Histogram of distances between adjacent rings for "dense" ring decoration. The most common distance is ~210 Å, far outside the range of apparent direct interaction between Dam1 rings. Scale bars are 50 nm unless marked otherwise.

Ring is Insensitive to Microtubule Polarity

We have previously proposed, based on the observation that Dam1 forms antiparallel, double spirals (Wang et al., 2007), that the Dam1 ring should be insensitive to the polarity of the underlying microtubule, as the two spiral strands face the microtubule in opposite directions. In our analysis of ring-decorated microtubules, unedited segments such as those shown in the top of Fig 25a were also refined against a microtubule model to determine if the Dam1 ring had any preference for microtubule polarity. After sorting segments based on the microtubule protofilament number, they were aligned to a previously calculated 3D reconstruction of a microtubule using a projection matching scheme. The microtubule signal dominated the alignment of these segments due to its much larger mass and repeating pattern. The resulting structures were microtubules with a diffuse cloud of noisy density around them corresponding to the Dam1 ring, reflecting the different symmetries of the microtubule and the ring. By docking in the tubulin atomic structure (PDB: 1JFF), the polarity of the microtubule in the reconstruction and therefore the polarity in each image was determined. Combining this information with the orientation parameters of the ring in each segment showed that the Dam1 ring has no preference for facing either the plus or minus end of the microtubule. This confirms our previous predictions and strongly argues for an interaction between the Dam1 complex and the microtubule that is mediated by flexible regions originating from one or both sides of the interaction interface. A Dam1 ring at the kinetochore would presumably have a preferred orientation determined by its interaction with other kinetochore components, such as Ndc80 (Lampert et al., 2010; Tien et al., 2010; Wong et al., 2007).

Conclusion and Future Directions

When this project started essentially nothing was known structurally about the Dam1 complex and sequence bioinformatics showed no homology to any known protein fold. The qualitative observation that Dam1 complex can bind microtubules and assemble into rings captured the imagination of kinetochore biologists and satisfied a prediction made two decades earlier that an encircling coupler could tether chromosomes to microtubules (Hill, 1985; Miranda et al., 2005; Westermann et al., 2005). Functional, *in vitro* studies followed, showing that Dam1 could recapitulate many essential functions of the kinetochore: it tracked the plus end of the microtubule, was a highly processive attachment, and could utilize the energy released by microtubule depolymerization to drag a load polewards. The field had uncovered a central driver of the budding yeast kinetochore.

We now know a great deal about the low-resolution structure and architecture of the Dam1 complex and its oligomerization around microtubules. Because electron microscopy has been ideally suited to studying the complex, both alone and with microtubules, the qualitative observation that Dam1 forms rings around microtubules has been replaced by a quantitative structure. Through labeling experiments, both with deletion mutants and MBP fusion constructs, five of the ten proteins in the complex have been localized within the monomer. This information, combined with protein-protein interaction studies, has generated a model of the layout of the complex. Statistical analysis of ring tilt angles have also resulted in models of the Dam1 ring's movement on the microtubule. It appears to diffuse freely along the microtubule lattice and would therefore be predicted to carry a load poleward through biased diffusion since the depolymerizing end would create a moving barrier.

However, much is yet to be done to discover how Dam1 does its essential job in the budding yeast kinetochore. Because we now know which proteins sit in each arm of the complex we can predict which domains may sit at the two inter-complex interfaces created during oligomerization. The N-termini of Ask1p and Spc34p and the C-terminal domain of Dam1p are all at or near these interfaces. Each is also post-translationally modified during mitosis by regulatory kinases and/or methyltransferases, suggesting that these interactions may be modulated by the spindle checkpoint in order to ensure correct chromosome capture. Mutational studies, either abolishing or mimicking modification, could be used to tease about the effects these chemical changes have on Dam1 function.

Previous structural data had led us to conclude that Dam1 underwent a large conformational change upon binding the microtubule (Wang et al., 2007). This was due to the ambiguous docking of the Dam1 dimer into the spiral reconstruction and supported by evidence that the C-terminus of Dam1p was on the interior of the spiral contributing to the arm that binds the microtubule. Later discoveries, including the structure of the ring and class averages of rings formed in the absence of microtubules, have showed convincingly that in fact there is not a large conformational change upon binding and that the inter-complex interfaces seen in the dimer are preserved in the assembled state. This now leaves the open question of what domains are interacting

with the microtubule. Both dam1p and duo1p have been reported to be microtubule binders and now that the C-terminus of Dam1p is mapped to the outer arms of the ring it seems likely that the N-terminal regions of Dam1p and some or all of Duo1p are contributing to the extremely flexible domains seen extending inward towards the microtubule (Fig 8). Limited proteolysis experiments found Dam1p, Ask1p, and Duo1p digested after a two hour treatment with elastase, both with or without microtubules. Interestingly, the N-terminal portion of Duo1p seemed to be cleaved specifically. This suggests that the C-terminal domain of Duo1p and the N-terminal domain of Dam1p make up the microtubule-binding interface. Ask1p may be a flexible attachment to other elements in the kinetochore or the microtubule, although no microtubule binding activity has been attributed to it.

With the complex defined at the resolution of 3 nm in several different forms, much could be learned from an atomic structure of either the full complex or any of the subcomplexes that have been shown to be stable. While this seems to have been the goal of at least one group, no Dam1 component structures have been published. The labeling data and unique shape of the complex would allow for a unambiguous fit of an atomic structure into both the assembled and unassembled structures. This would lead to a mechanistic understanding of Dam1 function and would undoubtedly suggest many further experiments.

A final future direction, and perhaps the most pressingly interesting biologically, is work to discover how the Dam1 complex works in the context of the other components of the kinetochore. Ndc80 and Dam1 have been imaged recently *in vitro* on microtubules (Lampert et al., 2010; Tien et al., 2010). There is also evidence that Spc34p, a compentent of the Dam1 complex which has been localized with MBP labeling during this project, binds to Ndc80p and that this interaction is modulated by a phospho-site on its N-terminus (Shang et al., 2003). It should be possible to image the same Ndc80-Dam1-microtubule assembly used in these studies and generate a structural model of the outer kinetochore. In the best-case scenario, Ndc80 would bind to Dam1 at a specific site which causes it to follow Dam1's symmetry. This hypothetical sample would allow for their 3-D reconstruction, docking of crystal structures, and would provide a wealth of information about the outer kinetochore in budding yeast.

References

Amos, L.A., and Hirose, K. (1997). The structure of microtubule-motor complexes. Curr Opin Cell Biol *9*, 4-11.

Asbury, C.L., Gestaut, D.R., Powers, A.F., Franck, A.D., and Davis, T.N. (2006). The Dam1 kinetochore complex harnesses microtubule dynamics to produce force and movement. Proc Natl Acad Sci U S A *103*, 9873-9878.

Cheeseman, I.M., Anderson, S., Jwa, M., Green, E.M., Kang, J., Yates, J.R., 3rd, Chan, C.S., Drubin, D.G., and Barnes, G. (2002). Phospho-regulation of kinetochore-microtubule attachments by the Aurora kinase Ipl1p. Cell *111*, 163-172.

Cheeseman, I.M., Brew, C., Wolyniak, M., Desai, A., Anderson, S., Muster, N., Yates, J.R., Huffaker, T.C., Drubin, D.G., and Barnes, G. (2001a). Implication of a novel multiprotein Dam1p complex in outer kinetochore function. J Cell Biol *155*, 1137-1145.

Cheeseman, I.M., Chappie, J.S., Wilson-Kubalek, E.M., and Desai, A. (2006). The conserved KMN network constitutes the core microtubule-binding site of the kinetochore. Cell *127*, 983-997.

Cheeseman, I.M., and Desai, A. (2008). Molecular architecture of the kinetochore-microtubule interface. Nat Rev Mol Cell Biol *9*, 33-46.

Cheeseman, I.M., Enquist-Newman, M., Muller-Reichert, T., Drubin, D.G., and Barnes, G. (2001b). Mitotic spindle integrity and kinetochore function linked by the Duo1p/Dam1p complex. J Cell Biol *152*, 197-212.

Chen, Y.J., Zhang, P., Egelman, E.H., and Hinshaw, J.E. (2004). The stalk region of dynamin drives the constriction of dynamin tubes. Nat Struct Mol Biol *11*, 574-575.

De Carlo, S., and Stark, H. (2010). Cryonegative staining of macromolecular assemblies. Methods Enzymol *481*, 127-145.

DeRosier, D.J., and Klug, A. (1968). Reconstruction of Three Dimensional Structures from Electron Micrographs. Nature *217*, 130-134.

DeRosier, D.J., and Moore, P.B. (1970). Reconstruction of three-dimensional images from electron micrographs of structures with helical symmetry. J Mol Biol *52*, 355-369.

Efremov, A., Grishchuk, E.L., McIntosh, J.R., and Ataullakhanov, F.I. (2007). In search of an optimal ring to couple microtubule depolymerization to processive chromosome motions. Proc Natl Acad Sci U S A *104*, 19017-19022.

Egelman, E.H. (2000). A robust algorithm for the reconstruction of helical filaments using single-particle methods. Ultramicroscopy *85*, 225-234.

Egelman, E.H. (2007). The iterative helical real space reconstruction method: surmounting the problems posed by real polymers. J Struct Biol *157*, 83-94.

Enquist-Newman, M., Cheeseman, I.M., Van Goor, D., Drubin, D.G., Meluh, P.B., and Barnes, G. (2001). Dad1p, third component of the Duo1p/Dam1p complex involved in kinetochore function and mitotic spindle integrity. Mol Biol Cell *12*, 2601-2613.

Franck, A.D., Powers, A.F., Gestaut, D.R., Gonen, T., Davis, T.N., and Asbury, C.L. (2007). Tension applied through the Dam1 complex promotes microtubule elongation providing a direct mechanism for length control in mitosis. Nat Cell Biol *9*, 832-837.

Frank, J., Radermacher, M., Penczek, P., Zhu, J., Li, Y., Ladjadj, M., and Leith, A. (1996). SPIDER and WEB: processing and visualization of images in 3D electron microscopy and related fields. J Struct Biol *116*, 190-199.

Frost, A., Perera, R., Roux, A., Spasov, K., Destaing, O., Egelman, E.H., De Camilli, P., and Unger, V.M. (2008). Structural basis of membrane invagination by F-BAR domains. Cell *132*, 807-817.

Gaitanos, T.N., Santamaria, A., Jeyaprakash, A.A., Wang, B., Conti, E., and Nigg, E.A. (2009). Stable kinetochore-microtubule interactions depend on the Ska complex and its new component Ska3/C13Orf3. EMBO J *28*, 1442-1452.

Galkin, V.E., Orlova, A., Brieher, W., Kueh, H.Y., Mitchison, T.J., and Egelman, E.H. (2008a). Coronin-1A stabilizes F-actin by bridging adjacent actin protomers and stapling opposite strands of the actin filament. J Mol Biol *376*, 607-613.

Galkin, V.E., Orlova, A., Cherepanova, O., Lebart, M.C., and Egelman, E.H. (2008b). High-resolution cryo-EM structure of the F-actin-fimbrin/plastin ABD2 complex. Proc Natl Acad Sci U S A *105*, 1494-1498.

Galkin, V.E., Wu, Y., Zhang, X.P., Qian, X., He, Y., Yu, X., Heyer, W.D., Luo, Y., and Egelman, E.H. (2006). The Rad51/RadA N-terminal domain activates nucleoprotein filament ATPase activity. Structure *14*, 983-992.

Gardner, M.K., and Odde, D.J. (2008). Dam1 complexes go it alone on disassembling microtubules. Nat Cell Biol *10*, 379-381.

Gestaut, D.R., Graczyk, B., Cooper, J., Widlund, P.O., Zelter, A., Wordeman, L., Asbury, C.L., and Davis, T.N. (2008). Phosphoregulation and depolymerization-driven movement of the Dam1 complex do not require ring formation. Nat Cell Biol *10*, 407-414.

Glaeser, R.M., Downing, K.H., DeRosier, D.J., Chiu, W., and Frank, J. (2007). Electron Crystallography of Biological Macromolecules (New York, NY, Oxford University Press).

Grishchuk, E.L., Efremov, A.K., Volkov, V.A., Spiridonov, I.S., Gudimchuk, N., Westermann, S., Drubin, D., Barnes, G., McIntosh, J.R., and Ataullakhanov, F.I. (2008a). The Dam1 ring binds microtubules strongly enough to be a processive as well as energy-efficient coupler for chromosome motion. Proc Natl Acad Sci U S A *105*, 15423-15428.

Grishchuk, E.L., Molodtsov, M.I., Ataullakhanov, F.I., and McIntosh, J.R. (2005). Force production by disassembling microtubules. Nature *438*, 384-388.

Grishchuk, E.L., Spiridonov, I.S., Volkov, V.A., Efremov, A., Westermann, S., Drubin, D., Barnes, G., Ataullakhanov, F.I., and McIntosh, J.R. (2008b). Different assemblies of the DAM1 complex follow shortening microtubules by distinct mechanisms. Proc Natl Acad Sci U S A *105*, 6918-6923.

Hanisch, A., Sillje, H.H., and Nigg, E.A. (2006). Timely anaphase onset requires a novel spindle and kinetochore complex comprising Ska1 and Ska2. EMBO J *25*, 5504-5515.

Hill, T.L. (1985). Theoretical problems related to the attachment of microtubules to kinetochores. Proc Natl Acad Sci U S A *82*, 4404-4408.

Hirose, K., Amos, W.B., Lockhart, A., Cross, R.A., and Amos, L.A. (1997). Three-dimensional cryoelectron microscopy of 16-protofilament microtubules: structure, polarity, and interaction with motor proteins. J Struct Biol *118*, 140-148.

Hofmann, C., Cheeseman, I.M., Goode, B.L., McDonald, K.L., Barnes, G., and Drubin, D.G. (1998). Saccharomyces cerevisiae Duo1p and Dam1p, novel proteins involved in mitotic spindle function. J Cell Biol *143*, 1029-1040.

Holmes, K.C., Angert, I., Kull, F.J., Jahn, W., and Schroder, R.R. (2003). Electron cryo-microscopy shows how strong binding of myosin to actin releases nucleotide. Nature *425*, 423-427.

Ikeuchi, A., Nakano, H., Kamiya, T., Yamane, T., and Kawarasaki, Y. (2010). A method for reverse interactome analysis: High-resolution mapping of interdomain interaction network in Dam1 complex and its specific disorganization based on the interaction domain expression. Biotechnol Prog *26*, 945-953.

Indiani, C., and O'Donnell, M. (2006). The replication clamp-loading machine at work in the three domains of life. Nat Rev Mol Cell Biol *7*, 751-761.

Janke, C., Ortiz, J., Tanaka, T.U., Lechner, J., and Schiebel, E. (2002). Four new subunits of the Dam1-Duo1 complex reveal novel functions in sister kinetochore biorientation. Embo J *21*, 181-193.

Jensen, G. (2010). Methods in Enzymology, Vol 481 (Academic Press).

Joglekar, A.P., Bloom, K.S., and Salmon, E.D. (2010). Mechanisms of force generation by end-on kinetochore-microtubule attachments. Curr Opin Cell Biol *22*, 57-67.

Joglekar, A.P., Bouck, D.C., Molk, J.N., Bloom, K.S., and Salmon, E.D. (2006). Molecular architecture of a kinetochore-microtubule attachment site. Nat Cell Biol *8*, 581-585.

Jones, M.H., Bachant, J.B., Castillo, A.R., Giddings, T.H., Jr., and Winey, M. (1999). Yeast Dam1p is required to maintain spindle integrity during mitosis and interacts with the Mps1p kinase. Mol Biol Cell *10*, 2377-2391.

Jung-seog Kang, I.M.C., George Kallstrom, Soundarapandian Velmurugan, Georjana Barnes, and Clarence S.M. Chan. (2001). Functional cooperation of Dam1, Ipl1, and the inner centromere protein (INCENP) related protein Sli15 during chromosome segregation. J Cell Biol *155*, 763-774.

Kang, J., Cheeseman, I.M., Kallstrom, G., Velmurugan, S., Barnes, G., and Chan, C.S. (2001). Functional cooperation of Dam1, Ipl1, and the inner centromere protein (INCENP)-related protein Sli15 during chromosome segregation. J Cell Biol *155*, 763-774.

Kikkawa, M., Ishikawa, T., Wakabayashi, T., and Hirokawa, N. (1995). Three-dimensional structure of the kinesin head-microtubule complex. Nature *376*, 274-277.

King, R.W. (2008). When 2+2=5: the origins and fates of aneuploid and tetraploid cells. Biochim Biophys Acta *1786*, 4-14.

Koshland, D.E., Mitchison, T.J., and Kirschner, M.W. (1988). Polewards chromosome movement driven by microtubule depolymerization in vitro. Nature *331*, 499-504.

Lampert, F., Hornung, P., and Westermann, S. (2010). The Dam1 complex confers microtubule plus end-tracking activity to the Ndc80 kinetochore complex. J Cell Biol *189*, 641-649.

Leschziner, A.E., and Nogales, E. (2006). The orthogonal tilt reconstruction method: an approach to generating single-class volumes with no missing cone for ab initio reconstruction of asymmetric particles. J Struct Biol *153*, 284-299.

Li, H., DeRosier, D.J., Nicholson, W.V., Nogales, E., and Downing, K.H. (2002). Microtubule structure at 8 A resolution. Structure *10*, 1317-1328.

Li, X., and Nicklas, R.B. (1995). Mitotic forces control a cell-cycle checkpoint. Nature *373*, 630-632.

Li, Y., and Elledge, S.J. (2003). The DASH complex component Ask1 is a cell cycle-regulated Cdk substrate in Saccharomyces cerevisiae. Cell Cycle *2*, 143-148.

Liu, J., and Onuchic, J.N. (2006). A driving and coupling "Pac-Man" mechanism for chromosome poleward translocation in anaphase A. Proc Natl Acad Sci U S A *103*, 18432-18437.

Ludtke, S.J., Baldwin, P.R., and Chiu, W. (1999). EMAN: semiautomated software for high-resolution single-particle reconstructions. J Struct Biol *128*, 82-97.

Maresca, T.J., and Salmon, E.D. (2009). Intrakinetochore stretch is associated with changes in kinetochore phosphorylation and spindle assembly checkpoint activity. J Cell Biol *184*, 373-381.

Maure, J.F., Komoto, S., Oku, Y., Mino, A., Pasqualato, S., Natsume, K., Clayton, L., Musacchio, A., and Tanaka, T.U. (2011). The Ndc80 loop region facilitates formation of kinetochore attachment to the dynamic microtubule plus end. Curr Biol *21*, 207-213.

McIntosh, J.R., Grishchuk, E.L., Morphew, M.K., Efremov, A.K., Zhudenkov, K., Volkov, V.A., Cheeseman, I.M., Desai, A., Mastronarde, D.N., and Ataullakhanov, F.I. (2008). Fibrils connect microtubule tips with kinetochores: a mechanism to couple tubulin dynamics to chromosome motion. Cell *135*, 322-333.

Metoz, F., Arnal, I., and Wade, R.H. (1997). Tomography without tilt: three-dimensional imaging of microtubule/motor complexes. J Struct Biol *118*, 159-168.

Miranda, J.J., De Wulf, P., Sorger, P.K., and Harrison, S.C. (2005). The yeast DASH complex forms closed rings on microtubules. Nat Struct Mol Biol *12*, 138-143.

Miranda, J.J., King, D.S., and Harrison, S.C. (2007). Protein arms in the kinetochore-microtubule interface of the yeast DASH complex. Mol Biol Cell *18*, 2503-2510.

Miyazawa, A., Fujiyoshi, Y., and Unwin, N. (2003). Structure and gating mechanism of the acetylcholine receptor pore. Nature *423*, 949-955.

Mizuno, N., Toba, S., Edamatsu, M., Watai-Nishii, J., Hirokawa, N., Toyoshima, Y.Y., and Kikkawa, M. (2004). Dynein and kinesin share an overlapping microtubule-binding site. EMBO J *23*, 2459-2467.

Narita, A., Mizuno, N., Kikkawa, M., and Maeda, Y. (2007). Molecular determination by electron microscopy of the dynein-microtubule complex structure. J Mol Biol *372*, 1320-1336.

Nezi, L., and Musacchio, A. (2009). Sister chromatid tension and the spindle assembly checkpoint. Curr Opin Cell Biol *21*, 785-795.

Nogales, E., and Wang, H.W. (2006). Structural intermediates in microtubule assembly and disassembly: how and why? Curr Opin Cell Biol *18*, 179-184.

Ogura, T., Iwasaki, K., and Sato, C. (2003). Topology representing network enables highly accurate classification of protein images taken by cryo electron-microscope without masking. J Struct Biol *143*, 185-200.

Orlova, A., Garner, E.C., Galkin, V.E., Heuser, J., Mullins, R.D., and Egelman, E.H. (2007). The structure of bacterial ParM filaments. Nat Struct Mol Biol *14*, 921-926.

Orlova, E.V., Rahman, M.A., Gowen, B., Volynski, K.E., Ashton, A.C., Manser, C., van Heel, M., and Ushkaryov, Y.A. (2000). Structure of alpha-latrotoxin oligomers reveals that divalent cation-dependent tetramers form membrane pores. Nat Struct Biol *7*, 48-53.

Pinsky, B.A., Kung, C., Shokat, K.M., and Biggins, S. (2006). The Ipl1-Aurora protein kinase activates the spindle checkpoint by creating unattached kinetochores. Nat Cell Biol *8*, 78-83.

Pomfret, A.J., Rice, W.J., and Stokes, D.L. (2007). Application of the iterative helical real-space reconstruction method to large membranous tubular crystals of P-type ATPases. J Struct Biol *157*, 106-116.

Powers, A.F., Franck, A.D., Gestaut, D.R., Cooper, J., Gracyzk, B., Wei, R.R., Wordeman, L., Davis, T.N., and Asbury, C.L. (2009). The Ndc80 kinetochore complex forms load-bearing attachments to dynamic microtubule tips via biased diffusion. Cell *136*, 865-875.

Radermacher, M., Wagenknecht, T., Verschoor, A., and Frank, J. (1987). Three-dimensional reconstruction from a single-exposure, random conical tilt series applied to the 50S ribosomal subunit of Escherichia coli. J Microsc *146*, 113-136.

Ramey, V.H., Wang, H.W., Nakajima, Y., Wong, A., Liu, J., Drubin, D., Barnes, G., and Nogales, E. (2011). The Dam1 ring binds to the E-hook of tubulin and diffuses along the microtubule. Mol Biol Cell *22*, 457-466.

Ramey, V.H., Wang, H.W., and Nogales, E. (2009). Ab initio reconstruction of helical samples with heterogeneity, disorder and coexisting symmetries. J Struct Biol *167*, 97-105.

Ruchaud, S., Carmena, M., and Earnshaw, W.C. (2007). Chromosomal passengers: conducting cell division. Nat Rev Mol Cell Biol *8*, 798-812.

Sachse, C., Chen, J.Z., Coureux, P.D., Stroupe, M.E., Fandrich, M., and Grigorieff, N. (2007). High-resolution electron microscopy of helical specimens: a fresh look at tobacco mosaic virus. J Mol Biol *371*, 812-835.

Salmon, E.D. (2005). Microtubules: a ring for the depolymerization motor. Curr Biol *15*, R299-302.

Sanchez-Perez, I., Renwick, S.J., Crawley, K., Karig, I., Buck, V., Meadows, J.C., Franco-Sanchez, A., Fleig, U., Toda, T., and Millar, J.B. (2005). The DASH complex and Klp5/Klp6 kinesin coordinate bipolar chromosome attachment in fission yeast. Embo J *24*, 2931-2943.

Shang, C., Hazbun, T.R., Cheeseman, I.M., Aranda, J., Fields, S., Drubin, D.G., and Barnes, G. (2003). Kinetochore protein interactions and their regulation by the Aurora kinase Ipl1p. Mol Biol Cell *14*, 3342-3355.

Shannon, K.B., Canman, J.C., and Salmon, E.D. (2002). Mad2 and BubR1 function in a single checkpoint pathway that responds to a loss of tension. Mol Biol Cell *13*, 3706-3719.

Shimogawa, M.M., Graczyk, B., Gardner, M.K., Francis, S.E., White, E.A., Ess, M., Molk, J.N., Ruse, C., Niessen, S., Yates, J.R., 3rd*, et al.* (2006). Mps1 phosphorylation of Dam1 couples kinetochores to microtubule plus ends at metaphase. Curr Biol *16*, 1489-1501.

Sindelar, C.V., and Downing, K.H. (2010). An atomic-level mechanism for activation of the kinesin molecular motors. Proc Natl Acad Sci U S A *107*, 4111-4116.

Sosa, H., and Milligan, R.A. (1996). Three-dimensional structure of ncd-decorated microtubules obtained by a back-projection method. J Mol Biol *260*, 743-755.

Tanaka, K., Kitamura, E., Kitamura, Y., and Tanaka, T.U. (2007). Molecular mechanisms of microtubule-dependent kinetochore transport toward spindle poles. J Cell Biol *178*, 269-281.

Tien, J.F., Umbreit, N.T., Gestaut, D.R., Franck, A.D., Cooper, J., Wordeman, L., Gonen, T., Asbury, C.L., and Davis, T.N. (2010). Cooperation of the Dam1 and Ndc80 kinetochore complexes enhances microtubule coupling and is regulated by aurora B. J Cell Biol *189*, 713-723.

Trachtenberg, S., Galkin, V.E., and Egelman, E.H. (2005). Refining the structure of the Halobacterium salinarum flagellar filament using the iterative helical real space reconstruction method: insights into polymorphism. J Mol Biol *346*, 665-676.

Uchida, K.S., Takagaki, K., Kumada, K., Hirayama, Y., Noda, T., and Hirota, T. (2009). Kinetochore stretching inactivates the spindle assembly checkpoint. J Cell Biol *184*, 383-390.

Van Heel, M. (1987). Angular reconstitution: a posteriori assignment of projection directions for 3D reconstruction. Ultramicroscopy *21*, 111-123.

van Heel, M., and Frank, J. (1981). Use of multivariate statistics in analysing the images of biological macromolecules. Ultramicroscopy *6*, 187-194.

van Heel, M., Harauz, G., Orlova, E.V., Schmidt, R., and Schatz, M. (1996). A new generation of the IMAGIC image processing system. J Struct Biol *116*, 17-24.

Wang, H.W., Ramey, V.H., Westermann, S., Leschziner, A.E., Welburn, J.P., Nakajima, Y., Drubin, D.G., Barnes, G., and Nogales, E. (2007). Architecture of the Dam1 kinetochore ring complex and implications for microtubule-driven assembly and force-coupling mechanisms. Nat Struct Mol Biol *14*, 721-726.

Wang, Y.A., Yu, X., Ng, S.Y., Jarrell, K.F., and Egelman, E.H. (2008). The structure of an archaeal pilus. J Mol Biol *381*, 456-466.

Welburn, J.P., Grishchuk, E.L., Backer, C.B., Wilson-Kubalek, E.M., Yates, J.R., 3rd, and Cheeseman, I.M. (2009). The human kinetochore Ska1 complex facilitates microtubule depolymerization-coupled motility. Dev Cell *16*, 374-385.

Westermann, S., Avila-Sakar, A., Wang, H.W., Niederstrasser, H., Wong, J., Drubin, D.G., Nogales, E., and Barnes, G. (2005). Formation of a dynamic kinetochore-microtubule interface through assembly of the Dam1 ring complex. Mol Cell *17*, 277-290.

Westermann, S., Drubin, D.G., and Barnes, G. (2007). Structures and functions of yeast kinetochore complexes. Annu Rev Biochem *76*, 563-591.

Westermann, S., Wang, H.W., Avila-Sakar, A., Drubin, D.G., Nogales, E., and Barnes, G. (2006). The Dam1 kinetochore ring complex moves processively on depolymerizing microtubule ends. Nature *440*, 565-569.

White, H.E., Saibil, H.R., Ignatiou, A., and Orlova, E.V. (2004). Recognition and separation of single particles with size variation by statistical analysis of their images. J Mol Biol *336*, 453-460.

Wong, J., Nakajima, Y., Westermann, S., Shang, C., Kang, J.S., Goodner, C., Houshmand, P., Fields, S., Chan, C.S., Drubin, D.*, et al.* (2007). A protein interaction map of the mitotic spindle. Mol Biol Cell *18*, 3800-3809.

Yonekura, K., Maki-Yonekura, S., and Namba, K. (2003). Complete atomic model of the bacterial flagellar filament by electron cryomicroscopy. Nature *424*, 643-650.

Zhang, K., Lin, W., Latham, J.A., Riefler, G.M., Schumacher, J.M., Chan, C., Tatchell, K., Hawke, D.H., Kobayashi, R., and Dent, S.Y. (2005). The Set1 methyltransferase opposes Ipl1 aurora kinase functions in chromosome segregation. Cell *122*, 723-734.

Zhang, P., and Hinshaw, J.E. (2001). Three-dimensional reconstruction of dynamin in the constricted state. Nat Cell Biol *3*, 922-926.

Materials, Methods and Protocols

Purification of recombinant Dam1 complex from bacteria:

Streak out BL21Rosetta cells containing the Dam1 plasmid on LB-amp plates. Next day, inoculate small 3 ml overnight cultures (LB + 100 mg/ml Ampicillin and 34 mg/ml Chloramphenicol (cam)). The following day, inoculate a large pre-culture (50 ml LB-amp, cam in 250 ml flask) with 200 ul of the small culture. Prepare and autoclave 2.5 l LB medium split in two 2.5 l baffled flasks. In the morning inoculate each flask containing 1.25 l LB-amp-cam with 21 ml of the overnight pre-culture (1:60 dilution). Grow to OD_{600} = 0.4 – 0.5 at 37°C (takes about 3-4 hours. Induce expression by adding IPTG (1 M stock) to a final concentration of 1 mM. Harvest bacteria after 4 hours, by centrifuging in Sorvall SLA1500 rotor, 6000 rpm, 10 min. Wash pellet by resuspending in PBS, centrifuge and store Pellet at –80°C.

1) Thaw and resupend Pellet in 100 ml 20 mM Na_2HPO_4/NaH_2PO_4, 500 mM NaCl, 20 mM imidazole, pH 6.6 (**Buffer A**). Add PMSF and 1 tablet of complete MINI protease inhibitor cocktail. Add Lysozyme to 0.1 mg/ml and sonicate slurry in Corex glass tubes for 5 x 30 seconds.

2) Add Triton X-100 (10% v/v stock) to a final of 0.5% and stir 15 min at 4°C to complete lysis.

3) Centrifuge in SA-300 rotor, 20 min, 10,000 rpm, 4°C, decant supernatant into 2 x 50ml Falcon-Tubes.

4) Wash 1.5 ml Ni-NTA Agarose slurry (Qiagen) in 15 ml Falcon-Tube 3 x with Buffer A. Add Ni-beads to the Falcon-Tubes with the bacterial lysate and rotate at 4°C for at least 3 hours.

5) Spin down beads by centrifuging the Falcon Tubes in clinical centrifuge (2.5 K, 4 min, RT), resuspend beads in Buffer A and transfer into 15 ml Falcon – Tubes. Wash 3 more times with Buffer A.

6) Aspirate as much liquid as possible from the beads and resuspend them in 6 ml elution buffer (Buffer A + 200 mM imdazole. To prepate elution buffer, I simply add 2.5 ml of I M Imidazole to 10 ml Buffer, I don't adjust the pH at this point).

7) Rotate for at least 1 hour at 4°C to elute proteins. Retrieve supernatant into new 15 ml Falcon-tube (keep protein sample for gel).

8) Dialyze overnight against 2 liter 25 mM Na_2HPO_4/NaH_2PO_4 150 mM NaCl, 1 mM EDTA, pH 6.6 **(Buffer B**). I use Snakeskin dialysis tubing (Pierce) with a 10,000 MW cutoff.

Cation exchange chromatography (on AKTA FPLC)

Equilibrate 1 ml HiTRAP SP column with Buffer B. Using the 2 ml sample loop I inject 3 x 2 ml of dialysed Dam1 eluate (clear the eluate by spinning it briefly in the clinical centrifuge). Develop column with program “Stefan HighTrapS”, which uses a 10 ml linear gradient from 150 mM NaCl to 1 M NaCl . Collect 1 ml fractions, the complex will elute as a single peak at about 600 mM NaCl (Fractions 11 and 12 are usually the peak fractions). Check fractions on gel, aliquot and snap freeze peak fractions in liquid N_2.

Size exclusion chromatography

If desired, the complex can be further purified on a Superose 6 column. Equilibrate the column with 20 mM Na_2HPO_4/NaH_2PO_4 500 mM NaCl, 1 mM EDTA, pH 6.6.(Buffer C) Inject up to 400 ul of HiTRAP S purified complex and develop with program “Stefan Superose6 (0.3 ml/min flow rate), ”. Collect 1 ml Fractions. The complex elutes after about 11 ml (Fractions 11-13).

Run Fraction on protein gel and snap-freeze in small aliquots.

Buffers:

Buffer A

	250ml
20mM NaPO4	5ml of 1M NaPO4
500mM NaCl	25ml of 5M NaCl
20mM Imidazole	5ml of 1M Imidazole

pH to 6.6
DDH_2O to 250ml
Add Complete tablet and PMSF (0.5mM) before use.

Elution Buffer

10ml buffer A + 2.5ml of 1M Imidazol

Buffer B

	2L
25mM NaPO4	50ml of 1M NaPO4
150mM NaCl	60ml of 5M NaCl
1mM EDTA	4ml of 0.5M EDTA

pH to 6.6
DDH_2O to 2L.

Buffer C

500ml

20mM NaPO4	10ml of 1M NaPO4
500mM NaCl	50ml of 5M NaCl
1mM EDTA	1ml of 0.5M EDTA
pH to 6.6	
DDH_2O to 500ml.	

BRB80 Buffer:

80 mM PIPES pH 6.9
1 mM EGTA
1 mM $MgCl_2$
10% glycerol

Single Rings on Microtubules

141 μl BRB80 buffer with 2 μM taxol and at least 2 mM DTT (more is OK) and 0.05% NP40

8 μl microtubules @ 1 mg/ml

1 μl Dam1 complex @ 1 mg/ml

Add components in order. My observation has been that diluting Dam1 into a buffer without microtubules causes poor decoration later on. This is why there is such a large reaction volume: to avoid diluting the purified Dam1 sample. Wait several minutes before adding to sample grid. After more than an hour microtubules may start to aggregate. As with all reactions involving microtubules, keep at room temperature or up to 37 degrees C.

Stacked Rings on Microtubules

97 μl Stack Buffer (40 mM BisTris @ pH 5.8, 1 mM EGTA, 1 mM $MgCl_2$) + 2 μM taxol + 2 mM DTT + 0.05% NP40

2 μl microtubules @ 1 mg/ml

1 μl Dam1 complex @ 10 mg/ml

Add components in order. Incubate overnight at room temperature. Incubation at 37 degrees C causes microtubules to denature. Leaving the tube overnight seems to increase order, however, stacked rings can be seen within hours. In negative stain they appear as rafts of ~10-20 rings closely packed separated by breaks between one raft and the next. In cryo-EM the microtubule is completely covered with no obvious breaks.

Spirals on Microtubules

96 μl BRB80 buffer with 2 μM taxol and at least 2 mM DTT (more is OK) and 0.05% NP40

2 μl microtubules @ 1 mg/ml

2 μl Dam1 @ 10 mg/ml that has been dialyzed in BRB80

Add components in order. The most important step to making spirals is dialyzing Dam1 at high concentration, ideally 10 mg/ml or higher, in BRB80 for an hour at room temperature before adding it to microtubules. Dam1 must be incubated in this condition prior to binding to microtubules in order to form long oligomers. These oligomers can then assemble around microtubules as spirals. Without this step the protocol above generates microtubules saturated with disordered, fluffy-looking rings.